UNIVERSITÉ DE MONTRÉAL

MICROSCOPIC STUDIES OF NEUROVASCULAR COUPLING DURING EPILEPSY IN THE MOUSE BRAIN

CONG ZHANG

INSTITUT DE GÉNIE BIOMÉDICAL

ÉCOLE POLYTECHNIQUE DE MONTRÉAL

THÈSE PRÉSENTÉE EN VUE DE L'OBTENTION

DU DIPLÔME DE PHILOSOPHIAE DOCTOR

(GÉNIE BIOMÉDICAL)

DÉCEMBRE 2016

UNIVERSITÉ DE MONTRÉAL

ÉCOLE POLYTECHNIQUE DE MONTRÉAL

Cette thèse intitulée:

MICROSCOPIC STUDIES OF NEUROVASCULAR COUPLING DURING EPILEPSY IN THE MOUSE BRAIN

présentée par : ZHANG Cong

en vue de l'obtention du diplôme de : Philosophiae Doctor

a été dûment acceptée par le jury d'examen constitué de :

M. LEBLOND Frédéric, Ph. D., président

M. LESAGE Frédéric, Ph. D., membre et directeur de recherche

M. STIKOV Nikola, Ph. D., membre

M. GROVA Christophe, Ph. D., membre externe

DEDICATION

To my family

ACKNOWLEDGEMENTS

First and for most I would like to express my thanks to my supervisor, Professor Frédéric Lesage, for giving me this wonderful opportunity as a Ph. D. student in his research group, and mostly for his careful guidance, administration, and support through my entire Ph. D. study. A talk with Prof. Lesage is always inspiring and enjoyable, thanks to his profound knowledge in optical brain imaging, as well as his great patience at all times. His confidence and immense knowledge in my work and prompt corrections contributed enormously to finish this thesis.

I would like to sincerely thank Dr. Philippe Pouliot, who instructed me from time to time as if I were his own student. From the talk with him, I gained much knowledge about the analyzing data.

I also would like to thank all staffs from the Montreal Heart Institute animal facility, in particular Marc-Antoine Gillis and Natacha Duquette, whose assistance in animal preparation, animal monitoring and animal administration undoubtedly promoted my research.

I am also grateful to thank coauthors of my three papers, Maryam Tabatabaei, Hélène Girouard and Mohammad Moeini, who spent quite a lot of their time to discuss my research. I would like to thank Samuel Bélanger for his suggestions to improve the quality of the French text in this thesis and for useful discussion on my research. I thank all past and current members of the laboratory of molecular and optical imaging at Polytechnique of Montreal who shared many pleasant moments and supplied much help through my studies: Clément Bonnéry, Michèle Desjardins, Baoqiang Li, Edgar Guevara, Mahnoush Amiri, Maxime Abran, Alexandre Castonguay, Hanieh Mohammadi, Joël Lefebvre, Parikshat Sirpal, Yuankang Lv, Ghada Jerbi, Xuecong Lv, Maryam Tabatabaei, Pier-Luc Tardif, Luis Akakpo, Azadeh Naderian.

Next, it was very grateful to know kind friends in Montreal, with whom I took many of our holidays and week-ends to find new and interesting aspects in here. This provided a lot of fun in my studies.

In the end, I gratefully acknowledge the China Scholarship Council (CSC) that supplied a scholarship from the “Chinese government graduate student overseas study program”, and my supervisor for providing me with financial support through my doctorate. I would like to express my endless thankfulness to my parents and my family, who left everything behind to accompany

me on this work; without their encouragement and support this work would not have been finished at all.

RÉSUMÉ

Les mécanismes liant l'activité neuronale au changement local du flot sanguin sont regroupés dans un ensemble nommé couplage neurovasculaire. Ce lien neurovasculaire, qui est à la base de plusieurs principes d'imagerie fonctionnelle du cerveau, est altéré par l'épilepsie. Ces dernières années, des techniques d'imagerie tel l'IRMf, IOS et la NIRS ont été utilisées pour l'étude de cette maladie, montrant une forte corrélation entre l'activité épileptique et le signal mesuré. Par contre, la plupart de ces travaux se sont concentrés sur les changements d'hémoglobine, qui peuvent être liés à des phénomènes non-linéaires et qui ne renseignent pas directement sur la quantification de l'oxygène délivré localement. Le but de cette thèse est d'investiguer l'utilisation de la microscopie avec de nouvelles sondes moléculaires permettant l'imagerie de l'oxygénation des tissus durant les évènements épileptiques dans le cortex sensori-moteur de la souris.

Dans un premier temps, une méthode de mesure de la pression partielle d'oxygène (PO_2) en microscopie confocale du temps de vie de phosphorescence fut développée. Ce système permet une mesure minimalement invasive du PO_2 dans les tissus corticaux à haute fréquences spatiale et temporelle lorsqu'il est utilisé conjointement avec la sonde phosphorescente OxyphorG4. Les mesures réalisées durant les crises épileptiques, induites avec l'agent 4-aminopyridine (4-AP), montrent des changements significatifs de l'oxygénation tissulaire. De plus, la distribution spatio-temporelle de la chute initiale de la réserve en oxygène, à proximité du point d'injection et le long des artérioles, a été caractérisé durant ces mêmes épisodes épileptiques. Une corrélation positive entre la variation du PO_2 durant cette première phase et la durée de la crise épileptique a aussi été mesurée. Cette mesure pourrait s'avérer utile dans la localisation des foyers épileptique et dans la prédiction de la durée des crises.

La deuxième étude présentée dans cette thèse se concentre sur le possible rôle joué par les astrocytes, qui sont un des acteurs importants dans le couplage neurovasculaire, dans la propagation des crises épileptiques. La concentration en ions calciques libres à la base axonale des astrocytes, conjointement avec le diamètre des artérioles adjacentes a été mesuré in-vivo en simultané sur des souris durant les épisodes épileptiques. Pour la mesure du calcium, la sonde fluorescente OregonGreen BAPTA-1 AM (OGB-1) a été utilisée en imagerie du temps de demie-vie de fluorescence avec un microscope 2-photons. Les résultats montrent que l'augmentation de calcium induirait une vasodilatation à chaque ictus dans la région du foyer épileptique. Dans les

régions plus éloignées, cette même mesure corrèlerait plutôt avec une vasoconstriction dans les premiers moments de la crise, suivi par une vasodilatation selon la durée de l'épisode. De plus, une augmentation lente du niveau absolu de la concentration calcique a été observé lors de longues séquences d'évènements. Cette tendance à la hausse semble induire à son tour une constriction des artérioles dans les régions adjacentes. Ces observations confirment le rôle des astrocytes dans le contrôle local de la microcirculation et suggèrent un second rôle de modulation du niveau de la concentration calcique autour de leur base axonale.

Puisqu'il n'a pas été possible de mesurer le PO_2 en profondeur dans le cerveau ou de pouvoir imager adéquatement les réseaux de capillaires en microscopie confocale, et suivant le développement d'une sonde sensible aux ions d'oxygène en microscopie 2-photons, il a donc été possible, dans le cadre de la dernière étude de cette thèse, d'acquérir cette mesure en profondeur durant des épisodes épileptiques. Des changements significatifs du PO_2 dans les tissus et les vaisseaux ont pu être observés. La distribution spatiale de la chute initiale de ce paramètre autour des artérioles, des capillaires, des veinules et du tissu près du foyer a pu être caractérisée. Les résultats obtenus pourraient avoir des implications profondes dans notre compréhension des mécanismes de livraison de l'oxygène dans les tissus en profondeur et leur capacité à supporter le cortex adéquatement dans les situations pathologiques. Le potentiel de la microscopie dans l'étude du couplage neurovasculaire et des changements liés à des pathologies a pu être pleinement démontré par les travaux de cette thèse.

ABSTRACT

Neurovascular coupling (NVC) is the mechanism that links a transient neural activity to the corresponding increase of cerebral blood flow (CBF). It underlies the local increase in blood flow during neural activity, forms the basis of functional brain imaging and is altered in epilepsy. For the last decades, functional imaging using BOLD fMRI, IOS and fNIRS and others have been applied to epilepsy, and yielded good correlation between epileptic activity and the measured signal. However, most previous work on epilepsy focused on the measurement of hemoglobin changes which sometimes leads to non-linear phenomena and does not quantify oxygen delivery in tissue. The aim of this thesis is to study oxygen delivery using microscopy with new oxygen sensitive molecular probes during epileptic events in the mouse somatosensory cortex.

First, a confocal phosphorescence lifetime microscopy system for measuring brain oxygen partial pressure (PO_2) was developed. This system enabled minimally invasive measurements of oxygen partial pressure in cerebral tissue with high spatial and temporal resolution using a dendritic phosphorescent probe, Oxyphor G4. Significant changes of PO_2 in tissue were found at the epileptic focus and in remote areas during 4-aminopyridine (4-AP) induced epilepsy. The spatio-temporal distribution of the "initial dip" in PO_2 near the injection site and along nearby arterioles was characterized by investigating epileptic events. A positive correlation between the percent change in the PO_2 signal during the "initial dip" and the duration of seizure-like activity was revealed in this work, which may help localize the epileptic focus and predict the length of seizures. Because astrocytic calcium signalling is involved in neurovascular coupling, the second study investigated the role of this pathway in epilepsy. The free calcium concentration in astrocytic endfeet and diameter of adjacent arterioles were simultaneously monitored with the calcium-sensitive indicator OGB-1 by two-photon fluorescence lifetime measurements following 4-AP injection. Our results revealed that, increases in calcium concentration induced vasodilation for each ictal event in the focus. In the remote area, increases in calcium concentration correlated with vasoconstriction at the onset of seizure and vasodilation during the later part of the seizures. Furthermore, a slow increase in absolute calcium concentration following multiple seizures was observed, which in turn, caused a trend of arteriolar constriction both at the epileptic focus and remote areas. These observations confirmed the role of astrocytes in the control of local microcirculation and suggest a modulating role for baseline absolute calcium concentration in

astrocytic endfeet. Since the confocal phosphorescence microscopy system was not able to measure PO_2 deep in the cortex or resolve capillaries, two-photon phosphorescence microscopy was then used in the last project to study the PO_2 delivery during epilepsy in deep tissue and vessels. Significant changes of PO_2 in tissue and vasculature were observed during epileptic events. The spatial landscape of "initial dip" in PO_2 signals around arterioles, veins and tissue near the injection site was characterized. These results may have profound implications for evaluating microvascular oxygen delivery capacity to support cerebral tissue in disease. The results of this thesis confirmed the potential of using microscopy to study neurovascular coupling during epilepsy.

TABLE OF CONTENTS

LIST OF TABLES

LIST OF FIGURES

LIST OF SYMBOLS AND ABBREVIATIONS

CBF	Cerebral blood flow
fMRI	Functional magnetic resonance imaging
PET	Position emission tomography
BOLD	Blood oxygenation level dependent
$CMRO_2$	Cerebral metabolic rate of oxygen
IOI	Intrinsic optical imaging
PO_2	Partial oxygen pressure
MRI	Magnetic resonance imaging
IOZ	Ictal onset zone
IISs	Interictal spikes
SPECT	Single-photon-emission computer emission tomography
NVC	Neurovascular coupling
CBV	Cerebral blood volume
NADH	Nicotinamide adenine dinucleotide
rCBF	Regional cerebral blood flow
[99mTc]-HMPAO	Tc-99m Hexamethyl-propylene Amine Oxime
[99mTC]-ECD	Tc-99m Ethyl Cysteinate Dimer
EEG	Electroencephalography
^{18}F-FDG	Fluorine-18 fluorodeoxyglucose
TLE	Temporal lobe epilepsy
SISCOM	Subtraction ictal SPECT coregistered to MRI
IGE	Idiopathic generalized epilepsy
GSWDs	Generalized spike wave discharges

fNIRS	Functional near-infrared spectroscopy
HbO	Oxygenated hemoglobin
HbR	Deoxygenated hemoglobin
HbT	Total hemoglobin
SO_2	Saturation of oxygen
CW	Continuous wave
TD	Time domain
FD	Frequent domain
OIIS	Optical imaging of intrinsic signal
IOS	Intrinsic optical signal
CCD	Charge-coupled device
SNR	Signal to noise ratio
TPM	Two-photon microscopy
DAQ	Data acquisition
APD	Avalanche photodiode
4-AP	4-Aminopyridine
F_iO_2	Fraction of inspired oxygen
SE	Standard error
LFP	Local field potential
FLIM	Fluorescence lifetime imaging
OGB-1	Oregon Green 488 BATPA-1
$[Ca^{2+}]_i$	Calcium concentration
Ca_{2+}	Calcium
SD	Standard deviation

EETs	Epoxyeicosatrienoic acids
20-HETE	20-hydroxyeicosatetraenoic
VPR	Volume-pressure recording
PMT	Photomultiplier tube
AODs	Acousto-optic deflectors
MEG	Magnetoencephalography
HR-EEG	High-resolution electroencephalogram
EcoG	Electrocorticography

CHAPTER 1 INTRODUCTION

1.1 Overview

While neuron functioning consumes energy, the brain itself does not keep a reserve of energy substrates such as glucose or oxygen (Lecrux and Hamel, 2011). Instead, it relies on a constant supply of blood flow to provide these substrates, particularly during neural hyperactivity (Siesjö and Plum, 1971), and to remove metabolites, e.g. lactic acid. There is a tight coupling between the cerebral blood flow (CBF) and neural activity (Lecrux and Hamel, 2011). In the cortex, the adequate supply of blood during neural activation is ensured by the complex interactions among neurons, astrocytes and microvessels (Hamel, 2006). This mechanism is the basis of neuroimaging techniques that infer neural activity from the observation of the associated vascular responses, for example, variations in local blood volume or blood oxygenation levels. Currently there are various imaging techniques that indirectly record metabolic changes of neural activity in the central nervous system. In functional neuroimaging, participants are often asked to perform a task (e.g. finger-tapping) while their neural activity is measured non-invasively. Since the difference in neural activity between the task period and the resting period is believed to reflect the mental capacities of the subjects, the imaging of brain function can be used to observe human psychological state (Kosslyn, 1999).

Human functional brain imaging techniques play a prominent role in neuroscience and physiological research nowadays. From the 1990s, functional magnetic resonance imaging (fMRI) has been used to detect blood-oxygenation-level-dependent (BOLD) signals associated with neuronal activity, based on the different paramagnetic properties of oxygenated and deoxygenated hemoglobin (Ogawa et al., 1990a).Using a surrogate marker of oxygen, positron emission tomography (PET) is another method that has been widely applied in brain imaging. With the application of these techniques, researchers invested substantial effort in improving our understanding of neuronal activity and brain functioning.

The neurovascular coupling describes the relationship between neural activity and triggered hemodynamic changes (i.e. cerebral blood volume (CBV), oxygenation levels, and cerebral blood flow (CBF)), which are measurable with neuroimaging techniques. Important insights have been obtained by using animal models, in which researchers can use functional brain imaging and/or

neuronal and hemodynamic events to specifically underpin them (Berwick et al., 2005; Boorman et al., 2010; Mathiesen et al., 2000; Vazquez et al., 2012). Using animal models enables the exploration of neuroimaging signal changes of each component in the complex brain system. With such models, the general validity of BOLD signal changes obtained from fMRI as indicators of varied neuronal activity has been established: increased neuronal activity in healthy cortical structures is reflected by increases in BOLD signals in those structures (Logothetis et al., 2001). However, the generalizability of this broad statement is becoming increasing important with brain studies now performed in both health and disease models.

1.2 Epilepsy

Epilepsy represents a chronic neurological disordered state that is characterized by recurrent, spontaneous seizures. Unlike normal neural processing, epileptic seizures consist of abnormal, excessive neuronal discharges, and therefore require supernormal energy to meet the demand of increased neural activity (Folbergrová et al., 1981; Zhao et al., 2009). Therefore, the neurovascular coupling in the normal brain processing state may not be applied to epileptic conditions. Between these ictal events (i.e. seizures), brief short-duration events may occur, and are thus called interictal spikes (de Curtis and Avanzini, 2001). Previous work studying neurovascular coupling in epilepsy has presented contradictory results both in humans and animals, using neuroimaging techniques such as PET, fMRI and intrinsic optical imaging (IOI). For example, although a local increase in blood perfusion associated with ictal events is generally observed in those studies, some showed that the increase in blood perfusion oversupplied the consumption of oxygen due to increased metabolism (Bénar et al., 2002; Lemieux et al., 2001; Nersesyan et al., 2004; Tenney et al., 2004), while other studies discovered the opposite, i.e. the blood hyperperfusion was inadequate to compensate for the oxygen loss(Ingvar, 1986; Kreisman et al., 1991; Tanaka et al., 1990). Therefore, the explicit relationship between oxygenation and perfusion during epileptiform events remains elusive. Given that perfusion is necessary for oxygen delivery and that brain tissue might be damaged in hypoxic conditions, understanding potential un-couplings in epilepsy is essential.

The goal of this thesis is to study the neurovascular coupling during epilepsy using novel optical imaging techniques such as two-photon fluorescence lifetime microscopy and confocal phosphorescence microscopy. Phosphorescence lifetime imaging provides a measurement of the

partial oxygen pressure (PO_2) in tissue and vessels, which leads to estimations of oxygen metabolism and therefore is considered to be more directly related to neural activity than hemoglobin concentration (Brieu et al., 2010). The recent emergence of this technique in two-photon microscopy allows for direct measures of the oxygen in three-dimension with sufficient temporal and spatial resolution, providing access to deeper layers of the brain (Sakadzić et al., 2010).

1.3 Organization of the thesis by objectives

Three objectives were defined in this thesis and each is associated with different hypotheses.

Objective #1: Develop a confocal phosphorescence lifetime microscopy system and use the system to investigate the change of PO_2 during epileptic events in the mouse brain in conjunction with a dendritic phosphorescence molecular probe, Oxyphor G4.

Hypothesis #1-1: The confocal microscopy system in conjunction with Oxyphor G4 can provide a measurement of PO_2 *in-vivo* in mice.

Hypothesis #1-2: The PO_2 changes associated with epileptic events can be reliably monitored in the mouse brain with the confocal phosphorescence lifetime microscopy system.

The article that addressed this objective is:

Article 1: **Cong Zhang**, Samuel Bélanger, Philippe Pouliot and Frédéric Lesage, "Measurement of local partial pressure of oxygen in the brain tissue under normoxia and epilepsy with phosphorescence lifetime microscopy," PLOS One, 10, e0135536. doi:10.1371/journal.pone.0135536 (Aug 25, 2015).

Objective #2: Simultaneously monitor the changes of absolute calcium signals in astrocytic endfeet and diameter changes of encased arterioles with two-photon microscopy during seizures in the mouse brain.

Hypothesis #2-1: The two-photon microscopy system and specific scanning techniques can be used to simultaneously measure the absolute calcium signal in astrocytic endfeet and arteriolar diameter.

Hypothesis #2-2: The calcium signal in astrocytic endfeet and arteriolar diameter correlate during epileptic seizures in the mouse brain.

Article 2: **Cong Zhang**, Maryam Tabatabaei, Samuel Bélanger, Hélène Girouard and Frédéric Lesage, "Astrocytic endfoot Ca^{2+} modulates arteriolar responses during epilepsy: an *in vivo* two-photon lifetime microscopy study" was submitted to the journal of Cerebral Blood Flow & metabolism and is in revision.

Objective #3: Measure the PO_2 changes in tissue near arterioles and in cerebral vasculature in microdomains during epileptic seizures in mouse brain with a two-photon phosphorescence microscopy system.

Hypothesis #3-1: Using two-photon phosphorescence microscopy, PO_2 changes can be measured in 3D with an oxygen-sensitive dye (PtP-C343).

Hypothesis #3-2: The PO_2 changes in tissue are different around various size arterioles during epileptic events in the mouse brain.

Hypothesis #3-3: The PO_2 changes in vessels correlate with their size during epileptic seizures in the mouse cortex.

Article 3: **Cong Zhang**, Mohammad Moeini and Frédéric Lesage, "Spatial landscape of oxygen in and around microvasculature during epileptic events" Neurophotonics 4, 010501-010501. doi:10.1117/1.NPh.4.1.010501

This thesis is organized as follows. The second chapter gives a brief literature review of various techniques used in neurovascular coupling studies. The third chapter describes a basic theory of confocal phosphorescence lifetime system and two-photon microscopy. From the fourth chapter to the sixth chapter, three published papers are fully included to address the three objectives above. In the seventh chapter, a discussion of the advantages as well as limitations of the proposed methods is provided. Finally, the thesis is concluded in the eighth chapter.

CHAPTER 2 LITERATURE REVIEW

2.1 Brief literature review

Epilepsy is a most common human neurological disorder, impacting 1.2% of the word population (Hauser et al., 1991). The pharmacological treatment of epilepsy with one or several drugs achieves effective seizure control in 60-70% of the cases (Callaghan et al., 2007). The treatment of the remaining drug-resistant epilepsy cases relies upon identifying and surgically removing the epileptogenic zone. For example in temporal lobe epilepsy (TLE), surgically removing the epileptogenic zone was reported to lead to seizure freedom up to 70-80% of the patients (Engel, 2003, 1993). In another study, neocortical resections yielded a successful treatment rate of 25% ~ 40% (Rasmussen, 1991). There are several factors that may affect the outcome of surgical treatment in nonlesional neocortical epilepsy, most importantly, an accurate localization of the epileptic focus area. It is usually more difficult and variable to localize the epileptic region in neocortical epilepsy. Hardware and sequences in magnetic resonance imaging (MRI) have been improved, however, MRI remains unable to reveal the focus localization in up to 50% of drug-resistant patients with focal epilepsy (Berg et al., 2003; Bernasconi et al., 2011; McGonigal et al., 2007). For humans with longstanding seizures, there is an independent epileptogenic area in surrounding cortices (Berger et al., 1993; Cascino et al., 1994). Hence, in many patients, it is usually quite challenging to achieve an accurate localization of the epileptic region.

Traditional localization of the ictal onset zone (IOZ) in neocortical epilepsy requires a surgical intervention to implant electrodes directly onto the exposed surface of the cortex, a technique called electrocorticography (ECoG), which may put the patients under the risk of clinical complications such as bleeding or infection (Shariff et al., 2006). Therefore, it is extremely useful to exploit new methods that are able to localize epileptic region in a noninvasive manner, e,g, using single-photon-emission computed emission tomography (SPECT), PET or fMRI. These techniques monitor neural activity indirectly by measuring associated hemodynamic variations, i.e. changes in CBF, glucose metabolism or BOLD signals. Based on the current understanding of neurovascular coupling, these techniques have been used to localize the IOZ by observing the temporal and spatial changes of the hemodynamic signals during epileptic events. However, these techniques are not suitable to be used to study the neurovascular coupling during epilepsy at a

more fundamental level, due to the limited temporal or spatial resolution Here we provide a review of the current understanding of neurovascular coupling during normal cortical processing and epilepsy, as well as the previous applications of the above described neuroimaging technique in the study of neurovascular coupling and EOZ localization in epilepsy.

2.1.1 Neurovascular coupling in the brain during normal cortical processing and epilepsy

Elevated neural activity leads to increased energy consumption of neurons and astrocytes. The increased consumption of energy imposes extra demands on the supply of two energy substrates, oxygen and glucose, from blood flow. Previous investigations have shown that blood vessels could be controlled to match the need of blood flow delivery (Attwell and Laughlin, 2001; Iadecola and Nedergaard, 2007). As a response to transient neural activity, local vessels dilate, which leads to a substantial increase in CBF. This mechanism, termed functional hyperemia, has its origin in a complex mechanism involving different vasoactive agents (Attwell et al., 2010; Iadecola and Nedergaard, 2007).

Neurovascular coupling (NVC) is the phenomenon describing the activation of neuron to the associated increase of CBF (Huneau et al., 2015). The study of the neurovascular coupling focuses on examining the relationships among neuronal activity, tissue oxygenation, blood oxygenation, blood flow and metabolism. It has been widely accepted that the cerebral metabolic rate of oxygen ($CMRO_2$) increases simultaneously with increasing neuronal activity, which leads to a subsequent increase in CBF and CBV to compensate the consumption of local oxygen (Roy and Sherrington, 1890). Several functional neuroimaging techniques rely on the NVC to infer cerebral functions. For example, the BOLD contrast measured by fMRI has been widely applied to study brain response to neural stimulations in human and animal (Buxton, 2013; Ogawa et al., 1990a). Near-infrared spectroscopy (NIRS) can also be applied to detect hemoglobin changes in blood following the neural activity (Strangman et al., 2002). These techniques are based on the concentration changes of oxygenated or deoxygenated hemoglobin, and therefore they can only provide an indirect measure of the functional hyperemia (Figure 2-1). On the other hand, optical techniques, such as laser Speckle or laser Doppler flowmetry are able to measure blood flow and velocity variations in superficial cortical layers with a depth up to ~500 μm in animal (Fukuda et al., 1995). Although there are still debates on the physiology mechanisms underlying local blood

flow and oxygenation variation in response to the focal neural activation, these optical imaging techniques have been widely accepted as useful tools to study brain functions (Attwell et al., 2010; Hillman, 2014).

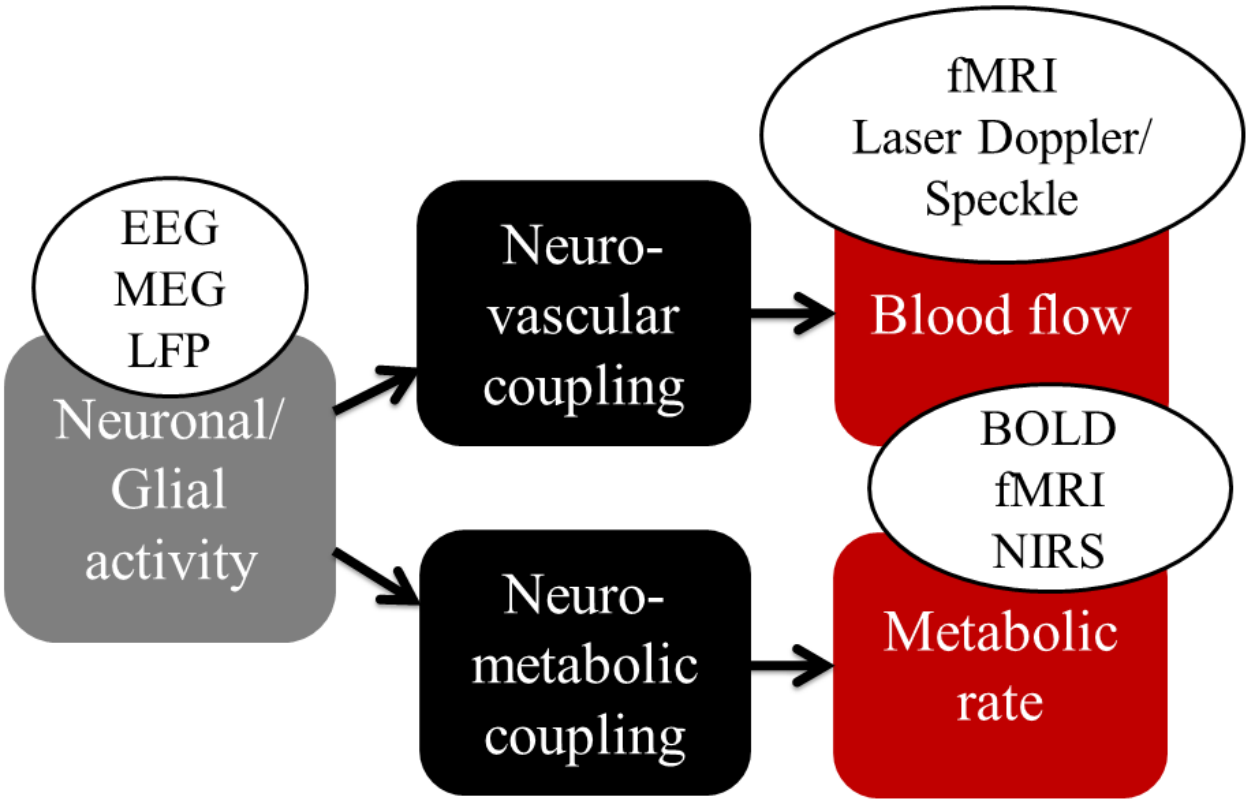

Figure 2-1: Physiological signal detected with classical functional neuroimaging techniques (Huneau et al., 2015).

Unlike normal brain processing, epileptic seizures (i.e. the ictal events) consist of excessive neural activity which causes an enormous increase of the metabolic rate of oxygen (Sheth et al., 2004b). Therefore, the neurovascular coupling mechanism during normal brain functioning may not be applied to seizures. For example, there is a long-standing debate on whether or not the increase in CBF is enough to compensate the consumption of oxygen due to increased metabolism during epilepsy. Early studies proposed the hypoxia-hypoperfusion hypothesis where they assumed that tissue damage during epilepsy was a result of cerebral anoxia (Meldrum, 2002; Plum et al., 1968; Simon, 1985). However, later studies presented results that were discordant with this hypothesis e.g. these studies have shown that the relative increase in CBF was more than the relative increase in cerebral metabolism (Zhao et al., 2009); that the tissue damage

during epilepsy was not identical to hypoxia (Siesjö and Wieloch, 1986); that seizures might produce increases in venous oxygenation (Pinard et al., 1984; Plum et al., 1968); that seizures induced increases in tissue oxygen partial pressure (PO_2) (Kreisman et al., 1984, 1983); that tissue injury were caused in the absence of cerebral anoxia (Meldrum, 2002; Pinard et al., 1984); and that epileptic activity might be associated with oxidation in cytochrome oxidase, mitochondrial transport chain and nicotinamide adenine dinucleotide (NADH) (Jöbsis et al., 1971; Mayevsky and Chance, 1975). All these observations contributed to our current understanding of the neurovascular relationship in epilepsy, but they have been insufficient to make sense of the observations. In epilepsy, the supranormal demand on the brain modifies autoregulatory mechanisms leading to various confounding factors, e.g. the abnormal vascular coupling, peculiar features of interictal activity and increased oxygen consumption during seizures (Folbergrová et al., 1981), which are factors that may modulate the neurovascular coupling (Osharina et al., 2010).

2.2 Review of observations from functional neuroimaging during epilepsy

2.2.1 Single-photon emission computed tomography (SPECT)

SPECT is a neuroimaging technique that images regional cerebral blood flow (rCBF). In the SPECT scan, gamma ray emitting radiotracers (such as Tc-99m Hexamethyl-propylene Amine Oxime ([99mTc]-HMPAO) or Tc-99m Ethyl Cysteinate Dimer ([99mTc]-ECD) (Niels A. Lassen, 1989; Walovitch et al., 1989)) are first injected to measure the blood flow of the subject. These radiotracers cross the blood brain barrier rapidly and are then trapped in tissue compartments seconds after the injection (~ 40s). The distribution of the radiotracers is able to be kept for a long time (up to four or five hours), which allows for subsequent imaging procedures. Therefore, SPECT images reflect an integration of CBF changes in the tissue during the first 40s following the injection (d'Asseler et al., 1997).

The first clinical observation of an increase in local cortical blood flow induced by a seizure was made more than a century ago (Horsley, 1892), and was supported by more recent studies on animal models(Sierra-Marcos et al., 2016; Wang et al., 2014; Zeng et al., 2013). Based on these observations, SPECT can be applied to monitor the CBF distribution in the ictal state (named ictal SPECT) as a method to localize the EOZ. However, due to the time delay between the

seizure onset and tracer administration, brain regions showing increased CBF on ictal SPECT images are likely to include both the brain areas initiating the seizure and receiving propagated activity (So and O'Brien, 2012). Moreover, the initial hyperperfusion in the seizure onset zone and the propagated areas have been observed to be rapidly followed by a hypoperfusion in the same areas in temporal lobe epilepsy, presumably due to autoregulatory mechanisms limiting excitotoxic damage (Rowe et al., 1991). Therefore, it has been reported the radiotracer injection needs to be performed within 20s after the seizure onset time in order to yield a reasonable sensitivity and specificity in localizing the seizure onset region (Lee et al., 2006; Patil et al., 2007).

SPECT is also routinely performed in the interictal period as a way to provide the baseline comparison for images taken in the ictal period to increase the localization accuracy. Limitations of the conventional interpretation of ictal SPECT images include the difficulty in distinguishing subtle changes resulting from different baseline patterns, the dose of injected medicine and the injection time (Kim and Mountz, 2011; Lee et al., 2000). Moreover, if the IOZ is hypoperfused during baseline (i.e. in the interictal period), the increase in CBF in the ictal period may appear to be obscure despite the presence of relative hyperperfusion (O'Brien et al., 1998). To overcome these limitations in ictal SPECT interpretation, subtraction methods have been proposed where SPECT images are also taken in the interictal periods to be subtracted from the ictal images(Kim and Mountz, 2011; Zubal et al., 1995). Compared to the conventional side by side visual analysis, the subtraction analysis was reported to yield a more favorable concordance rate between the localization results and the EOZ (Gaillard et al., 1995b; Lavy et al., 1976). Another subtraction method that was widely applied in ictal SPECT analysis is named subtraction ictal SPECT coregistered to MRI (SISCOM), which allows visualization of ictal activities in the brain by mapping abnormal neural perfusion onto surrounding neural structures. Similar to other subtraction methods, SISCOM was also shown to be able to significantly improve the localization accuracy over conventional visual analysis (O'Brien et al., 1998). Several previous studies reported that resecting the potential epileptogenic region identified by SISCOM could lead to good surgical outcome (G. D. Cascino et al., 2004; Gregory D. Cascino et al., 2004; O'Brien et al., 2004; Wichert-Ana et al., 2008). While these results seem to be encouraging, further work is still needed to determine the accuracy of SISCOM in surgical decision-making, and its predictive power for surgical outcomes.

2.2.2 Positron emission tomography (PET)

PET is another minimally invasive nuclear medicine imaging technique that applies short-lived radiopharmaceuticals to measure and assess perfusion and metabolic activities in various organ systems (Tarkin et al., 2014). It provides information on the functional and metabolic conditions in the brain that is complementary to the anatomical information (Prvulovich and Bomanji, 1998). Various PET tracers exist, serving different purposes, e.g. in the measurement of glucose metabolism (^{18}F-FDG-PET) or cerebral blood flow perfusion (^{15}O-H_2O-PET). The most widely used PET tracer in epilepsy studies is fluorine-18 fluorodeoxyglucose (^{18}F-FDG), which is used to measure glucose metabolism as a reflection of neuronal activity. As an analog of glucose, FDG is transported to brain tissues and is phosphorylated by hexokinase in the same manner as glucose. However, unlike glucose, FDG cannot be consumed through metabolism and thus accumulates in the cell compartments. As proton-rich isotopes such as FDG decay, positrons are emitted. The positrons annihilate rapidly with nearby electrons. Each annihilation generates two photons traveling in opposite directions which can then be captured by multiple pairs of oppositely situated detectors surrounding the subject to produce images (Juhász et al., 2005).

FDG-PET images are normally co-registered with MR images to combine functional and structural information. In epilepsy, PET scans are usually operated in the interictal phase as a result of a much longer tracer uptake time (from thirty to forty-five minutes), which is much longer than the lasting of most seizures (Sarikaya, 2015). FDG-PET localizes the epileptogenic zone based on the fact that the epileptogenic zone usually shows hypometabolism in the interictal period (Liu et al., 2001). Plenty of work have approved the feasibility of using FDG-PET in the presurgical localization of the epileptic focus in subjects with refractory partial seizures which have no contribution in EEG and MRI (Hikima et al., 2004). The localization sensitivity of FDG-PET in TLE were first reported to be 84% in a meta-analysis research conducted in 1994 (Spencer, 1994), while other studies presented a higher sensitivity of PET for TLE cases (87-90%) in the following years (Drzezga et al., 1999; Gaillard et al., 1995a; Kim et al., 2002; Knowlton et al., 1997). Previous studies reported a comparable localization accuracy using interictal FDG-PET and ictal SPECT (Bouilleret et al., 2002; Ho et al., 1995; Hwang et al., 2001; Won et al., 1999) or SISCOM (Desai et al., 2013; Perissinotti et al., 2014). For example, in 117 subjects with intractable epilepsy undergoing surgery, ictal SPECT and interical PET correctly localized the epileptic focus region in 70.3% and 77.7% of the subjects respectively (Hwang et al., 2001). In

another study, the correct lateralization rate was reported to be 85% and 73% using interictal PET and ictal SPECT respectively (Won et al., 1999). These results revealed the potential of using interictal FDG-PET as a routine procedure in the presurgical localization of epilepsy area in subjects with normal MR and no contribution of EEG. However, FDG-PET has a limitation, which is usually not able to precisely delineate the surgical margins of the resection area, as the region showing hypometabolism in the interictal period usually extends beyond the epileptogenic zone (Sarikaya, 2015).

2.2.3 Combined EEG-fMRI

Functional magnetic resonance imaging (fMRI) is another invasive functional neuroimaging technique and monitors neural activity with MRI technology. It depends upon the property of differential magnetic susceptibilities of deoxygenated and oxygenated hemoglobin. EEG-fMRI is a special application of fMRI incorporating information from EEG and was developed in 1992 by John Ives *et al* (Ives et al., 1993). EEG-fMRI strives to merge the temporal resolution of EEG and the structural resolution of fMRI (Stern, 2006). The epileptic events in the brain comprise synchronous firing from multiple neurons, which generate the local field potential. It can be measured by EEG as seizures or interictal epileptiform discharges. The fMRI recorded hemodynamic signal is the result of coupling between neural activity and the response of interest as hemodynamic fluctuation, which specifically is measured by exploiting the magnetic properties of blood (the BOLD) (Kwong et al., 1992; Ogawa et al., 1990b).

The activation is an increased BOLD signal that is caused by increases in CBF outstripping changes in oxygen consumption (reduced HbR). Conversely, the deactivation is a decreased BOLD signal that is induced by decreases in CBF outstripping changes in oxygen consumption (increase HbR). Although the BOLD signal has the low temporal resolution (Vulliemoz et al., 2010) and problems on the exact nature in relation to neural activity (Ekstrom, 2010; Logothetis and Wandell, 2004), BOLD fMRI has been used to study the cognitive and epileptic phenomena.

During the past 10 years, several studies have revealed increases of BOLD signal in areas that were coupled with the area generating epilepsy (Bénar et al., 2002). Similar studies have approved that there were some BOLD signal changes in areas far away from presumed epileptic foci but no apparent EEG changes in these regions (Kobayashi et al., 2006a). In these surrounding areas increase in BOLD is most often observed but sometimes a decrease of BOLD

signal is obtained. These results indicate that BOLD signal can show the distance impact of interictal spikes. These areas of BOLD signal changes were verified with intracerebral electrodes (Bénar et al., 2006). There was the hope of supplying useful clinical information in patients when the location of epilepsy was evaluated before surgery. For localization of epileptic focus, EEG-fMRI studies have shown it can supply complementary information in evaluation of patients with intractable epilepsy (Zijlmans et al., 2007). It was possible to localize epileptic focus in nonlesional frontal lobe epilepsy that was subsequently confirmed by other imaging techniques or pathologic analysis (Moeller et al., 2009). Some studies have shown that a good postsurgical outcome happens after the area of BOLD activation was removed surgically (An et al., 2013; Thornton et al., 2010). However, some studies have observed a paradoxical response and do not explain it: instead of an increase in BOLD signals, a decrease in BOLD signal was found during some spikes (Jacobs et al., 2009; Kobayashi et al., 2006b; Rathakrishnan et al., 2010). One limitation of understanding of EEG-fMRI signal is the low temporal resolution (around several seconds) (Heers et al., 2014).

Unlike focal epilepsy, idiopathic generalized epilepsy (IGE) is described by an EEG signal with generalized spike wave discharges (GSWDs). Early EEG-fMRI studies observed short GSWDs in the EEG signal, which revealed that there was an activation in thalamus during GSWDs, but a deactivation was also found in lateral parietal and frontal cortex (Aghakhani et al., 2004; Gotman et al., 2005; Hamandi et al., 2006). Study with absence epilepsy indicated increased synchronous activity in the orbitofrontal cortex (Bai et al., 2011). During the period of GWSDs the increased synchronous connectivity was more widely observed (Luo et al., 2012). However, several studies showed decreased functional connectivity in the thalamus (Masterton et al., 2012; Wang et al., 2012) and the attention network with absence seizures (Killory et al., 2011). Such studies on functional connectivity are needed to replicate further. In summary, EEG-fMRI was useful in investigating the temporal changes of paroxysms and provided novel insights into the mechanism of IGE.

2.2.4 Functional near-infrared spectroscopy (fNIRS)

FNIRS is an emerging technique that can continuous, non-invasive monitor the deoxygenated, oxygenated and total hemoglobin (Jöbsis, 1977). FNIRS uses optical emitters to send near-infrared light with the wavelength of 650 ~ 900 nm onto the scalp and the hemoglobin in tissue

mainly absorbs the light. The scattered light can be collected by the sensors positioned near the emitters (a few centimeters). Local blood oxygenation changes on the cortex can be recorded in terms of deoxygenated hemoglobin (HbR) and oxygenated hemoglobin (HbO) (Delpy and Cope, 1997; Irani et al., 2007). Compared to fMRI, fNIRS has some distinct advantages, such as portability, lower cost and long term recordings. It can also separate the concentrations of saturation of oxygen (SO_2), HbO, HbR and total hemoglobin (HbT) when several wavelengths are applied simultaneously. There are several methods developed for fNIRS technique, involving the (1) frequency domain (FD) (2) continuous wave (CW), and (3) time domain (TD) methods, which have been used in brain imaging (Khan et al., 2011; Mesquita et al., 2010; Zhang et al., 2005).

In recent years, fNIRS has been widely used in study of epilepsy. fNIRS combined with continuous EEG has been applied to investigate the hemodynamic changes before, during and after epileptic seizures (Irani et al., 2007; Steinhoff et al., 1996; Villringer et al., 1994). In past decades, different groups have used EEG-fNIRS as an complementary method of epilepsy diagnosis (Adelson et al., 1999; Arca Diaz et al., 2006; Buchheim et al., 2004; Cooper et al., 2011; Rizki et al., 2015; Seyal, 2014; Sokoloff et al., 2015). In most cases, there is an increase in CBV and HbO during partial seizures, which lasts beyond the seizure (Villringer et al., 1994). Some investigations have found an increase of CBV with 10 subjects with TLE in the lesion territories, which confirms earlier studies of partial epilepsy (Watanabe et al., 2002). The hemodynamic response of absence seizures shows a deoxygenation (increase in HbR, decrease in CBV and HbO), which is delayed by several seconds from the first spike (Buchheim et al., 2004; Roche-Labarbe et al., 2008). Two different groups have found preictal oxygenation changes in the frontal lobe with EEG-fNIRS (Seyal, 2014; Slone et al., 2012).

Overall, EEG-fNIRS is a promising technique for study of epilepsy and preliminary work have confirmed its usefulness and clinical potential (Machado et al., 2014; Pellegrino et al., 2016; Peng et al., 2014; Vinette et al., 2015; Yücel et al., 2014). It may become a primary tool to manage epileptic patients (particularly neonates and children) in clinical routine, (Wallois et al., 2010).

2.2.5 Optical imaging of intrinsic signals

Intrinsic optical signal (IOS) was first applied to measure the neuronal response with stimulation in tissue by Hill and Keynes (Hill and Keynes, 1949). Optical imaging of intrinsic signals (OIIS) is a method for detecting hemodynamic changes in the brain, according to the absorption of neural tissue with enhanced light, which is induced by focal increases in HbO and CBF (Frostig et al., 1990; Malonek and Grinvald, 1996; Prakash et al., 2009). These changes in reflectance can be detected by a camera with various wavelengths, which can measure the hemodynamic changes with temporal resolution of millisecond and micrometer spatial resolution. Since OIIS requires brain surgery to show the cortex it is widely known as an "invasive" imaging. However, compared to the electrophysiological methods that insert electrodes directly into the human brain, the OIIS is non-invasive because the intraoperative IOS is operated in the operating room by adding a camera to the operating scope (Prakash et al., 2009).

When the light illuminates the cerebral cortex, the active cortex and its corresponding vasculature have changes in reflective light compared to the inactive areas (Prakash et al., 2009; Zepeda et al., 2004). Until now three sources of intrinsic signals are mostly used based on the spectral composition of measured light (Mayhew et al., 2000; Sheth et al., 2004a). Using the light with the wavelength ~500-599 nm, both HbO and HbR directly correlating with HbT or CBV can be measured since they reflect light equally (Mayhew et al., 2000; Nemoto et al., 2004). Using the light with the wavelength ~ 600-699 nm, deoxy-hemoglobin absorbs most of light, as HbR has three times of the absorption coefficient than HbO. Hence, an increase in reflection at these wavelengths implies a decrease in HbR. Finally, using the near infrared light (~700-800 nm), variations in cellular swelling are the main component of the intrinsic signal since hemoglobin minimally absorbs light (Malonek and Grinvald, 1996). Therefore, the OIIS can be applied to detect changes of HbO and CBV in the brain cortex. OIIS is a little bit different from fNIRS. For example, the whole surface of the cortex is illuminated and cameras that are sensitive to certain wavelengths are used to collect changes of hemoglobin concentration and CBV. OIIS also requires the exposure of the brain cortex and has high spatial resolution.

OIIS has been used to study epileptic events *in vitro* using slices of cortex in rat brain (Borbély et al., 2014; Mané and Müller, 2012) and *in vivo* in rat (Chen et al., 2000; Schwartz and Bonhoeffer, 2001; Suh et al., 2005), ferret (Schwartz, 2005, 2003; Schwartz and Bonhoeffer, 2001) and

mouse (Guevara et al., 2013). These work revealed that OIIS can localize the area of an interictal spikes as well as the site of surrounding (Schwartz, 2003; Schwartz and Bonhoeffer, 2001). OIIS could also be applied in preictal seizure that can be used to predict epileptic onset (Chen et al., 2000). Besides, the relationship between epileptic events and HbR or CBV could be studied by OIIS (Bahar et al., 2006, 2005; Suh et al., 2005).

OIIS has also been used to image epileptic focus and brain function activity during the surgery in human (Haglund et al., 1992; Sato et al., 2002; Schwartz et al., 2004; Zhao et al., 2007). Beyond localizing human physiological and pathological activity and studying hemodynamic response, it was also used to predict the pre-ictal changes in human epilepsy. Overall, OIIS measurements of hemodynamic response and CBF may become increasingly important for localizing and predicting epileptic seizures.

2.2.6 Confocal and two-photon microscopy

Confocal microscopy is an inestimable technique for high-resolution microscopy. The principle based on the confocal imaging is depicted by Marvin Minsky in 1957 (Prasad et al., 2007). It increases optical resolution and contrast using a confocal mechanism. In the conventional microscope, the image is obtained from some light that is out of focus, which has limitations on thickness and contrast of the sample (Prasad et al., 2007; Rudd et al., 2005). Confocal laser scanning microscopy scans the sample with a focused spot of laser and a small pinhole at the confocal plane, which only allows the light generating from the focus to pass (Rajadhyaksha et al., 1999, 1995). The photomultiplier tube (PMT) or an avalanche photodiode (APD) can detect the emitted light mapping the image, which is a function of the location of the scanning spot. Compared to the conventional microscopy, the confocal laser scanning microscopy has a better resolution. The pinhole needs to be near an extent in practice so that it can discard most of the light (Heintzmann et al., 2003). Confocal microscopy enables the reconstruction of three-dimensional structures by stacking individual 2D images at different depths.

In the past few years, there is remarkable progress in confocal microscopy, which includes using new optical methods to study ultrastructural issues and using other methods to study cellular dynamic in animals. The advancement in image analysis is propelling the availability of large-scale anatomical reconstruction (Wilt et al., 2009). However, it is also important for advancements in complementary fields that involve animal preparation and strategies of labelling

fluorescence. In vivo, it can be used to obtain high resolution images in the superficial cortex (first 150um) because of the light diffusion of tissue.

There is an approach for deep imaging into tissue that includes two-photon fluorescence microscopy (Denk et al., 1990) and other nonlinear optical techniques. Two-photon microscopy provides high-resolution (submicron) imaging with lower phototoxicity and deeper tissue penetration than single-photon microscopy. In two-photon excitation, two photons with a doubled wavelength are absorbed by the fluorophore, which then releases the energy to the ground state. To achieve reasonable excitation/collection efficiency, typical two-photon microscopy system focuses the excitation photons into a very tiny volume using a high numerical aperture objective lens and delivers them in a very short period of time (femtosecond pulse). The first practical two-photon microscopy system was developed in 1990 (Denk et al., 1990). TPM uses longer wavelength light for excitation; therefore it can provide deeper penetration than single-photon microscopy. Because TPM requires two photons to arrive at the same time and same location to excite the molecule, the fluorescence signal depends upon the square of the illumination intensity. TPM can perform “optical sectioning” without using the physical pinhole that is used in confocal microscopy. As a result, TPM can collect signals more efficiently than confocal microscopy (So et al., 2000; Zipfel et al., 2003).

Traditional TPM image technique uses 2D raster scanning (line-by-line scanning), which is slow for applications demanding high temporal resolution. Hence, other imaging approaches have been developed, including random-access scanning with acousto-optic deflectors (AODs), a device that can change beam deflection angle with tuning input electric frequency (Salomé et al., 2006), and parallel scanning with multiple beams (Kim et al., 2007). More recently, alternative scanless TPM using temporal focus has been developed (Oron et al., 2005). Moreover, typical TPM systems use an excitation wavelength at ~800 nm. To further improve the penetration depth of TPM, longer wavelength excitation at ~1300 nm can be used (Kobat et al., 2009). The achieved resolution ultimately depends on the excitation wavelength of the light (Hell, 2007), but the excitation light can be seriously degraded by optical scattering.

The application of TPM *in vivo* has started to shed light in the field of neuronal function (Zhang et al., 2017). Since the TPM can study the cortex with a depth of several hundred micrometres *in vivo* (Denk et al., 1994). TPM was applied to image the activity of single neuron in dendrites *in*

vivo, which were loaded with a calcium indicator by a recording electrode (Svoboda et al., 1997). A number of laboratories have used TPM to study the activity of neurons with other bulk-loading methods that were previously applied in wild-field microscopy (Friedrich and Korsching, 1998, 1997). These studies were operated in the somatosensory cortex in mice and rats (Kerr et al., 2007; Sato et al., 2007), the cerebellum in rats (Sullivan et al., 2005), the visual cortex in rats, cats (Ohki et al., 2006, 2005) and mice (Mrsic-Flogel et al., 2007), the tectum in zebrafish (Niell and Smith, 2005) and the olfactory bulb in mice (Wachowiak et al., 2004) and zebrafish (Li et al., 2005; Yaksi et al., 2007). In recent years time-lapse imaging becomes available in the mammalian brain with TPM conjunction with cellular labeling and transgenetically introduced protein-based fluorophores (Feng et al., 2000).

Confocal and two-photon microscopy techniques have shown great promise for imaging biological structures at the cellular and molecular level. In the past few years, most studies were focused on the exploitation of new microscopy techniques. Major breakthroughs have been obtained in multiple technological fronts, imaging cellular properties and reconstruction large-scale tissue in live animals. These new findings will expand the role of confocal microscopy in neuroscience research.

2.2.7 High-resolution electroencephalogram (HR-EEG) and MEG

The high-resolution electroencephalogram (HR-EEG) is an EEG recording with high spatial and temporal resolution (millisecond scale). MEG uses a magnetoencephalography platform to record the magnetic fields induced by the cerebral activity. These two techniques are entirely non-invasive and apply the same mathematical tools to localize the sources of electromagnetic activities. MEG and EEG signals are converted into knowledge of localizing epileptic generators along cortical surface by these two techniques with solving an ill-posed inverse problem. HR-EEG and MEG can help identify epileptic zones with the localization signals recorded during interictal spikes or seizures (Gadhoumi et al., 2015; Grova et al., 2006; Pellegrino et al., 2016). Some studies use the sensitivity and specificity of EEG and MEG to localize the irritative and epileptic zones. Recent studies showed a specificity of 88% and a sensitivity of 84% with recorded spikes (Brodbeck et al., 2011). Several studies have revealed that these two techniques supplied additional information relative to other presurgical research (Jung et al., 2013; Knowlton et al., 2008, 2006) .

For some lesional epilepsy, localization of interictal spikes using HR-EEG and/ or MEG correlates the presurgical evaluation since the irritative or epileptic zones can be identified by an overlap (Chassoux et al., 2000; Gambardella et al., 1996). Overall, these two techniques cannot be solely used to identify the exact surgical zone of interest. When the epileptic discharges have a high enough signal-to-noise ratio and are not disturbed by major artifacts, HR-EEG and MEG can be applied to localize the epileptic zone by ictal recording (Eliashiv et al., 2002; Koessler et al., 2010).

In summary, preliminary work of other groups has measured hemoglobin providing an indirect way to study the mechanism of neurovascular coupling during epileptic events with various optical imaging techniques. However, there was no technique that could measure oxygen changes directly in tissue with high resolution in multiple locations during epilepsy. In this study, we investigate tissue oxygen delivery using a novel molecular probe based on phosphorescence and sensitive to oxygen to evaluate whether hypoxia plays a role in epilepsy.

CHAPTER 3 THEORY AND METHODOLOGY

This chapter first gives a brief introduction of confocal phosphorescence lifetime microscopy and the hardware setup that was built for the first study. Then the principle and application of an extension to two-photon laser scanning microscopy are described. The rest of this chapter covers the theory of the Krogh-Erlang model used to simulate oxygen delivery in tissue.

3.1 Confocal microscopy

Confocal microscopy is nowadays widely used in biological imaging and can generate three-dimensional images of nonbiological and biological specimens. Compared to the conventional wide-field microscopy the superior spatial resolution of confocal microscopy is beyond question. It has been shown that it is useful to study the neural function in small animal. This optical technique, combined with phosphorescence lifetime imaging can measure oxygen changes, providing direct measures of oxygen delivery to neural tissue with the perspective of linking oxygen to neural activity. Prior to our novel investigation in epilepsy, this method has been successfully used to study neural activity from the exposed cortex in the small animal (Golub and Pittman, 2008; Sakadžić et al., 2009; Yaseen et al., 2009).

3.1.1 Principle and application of confocal microscopy

Confocal microscopy is an optical technique that places a spatial pinhole at the confocal plane to eliminate out-of-focus light, which leads to a high optical resolution and contrast image. It can operate the three-dimensional reconstruction using sets of images from different depths. The principle of confocal laser scanning microscopy was patented in 1957 by Marvin Minsky (Minsky, 1988, 1961) and is diagrammatically shown in Figure 3-1. The laser system (light source) emits coherent light, which travels through the pinhole aperture and is focused on the specimen. The collected light reflected by the dichroic mirror passes through the second pinhole aperture located in front of the detector and is focused at the detector (Paddock, 2000). Compared to the conventional microscopy, confocal microscopy has several advantages as follows: (1) it can control the depth of the field. (2) it reduces or eliminates the background noise from the focal plane. (3) it has the ability to image successive optical sections of the thick specimen. In confocal microscopy, the illuminating light and the detecting signals are focused on the same point in the specimen. Unlike conventional microscopy, the confocal microscopy technique only

measures one point of the objective lens rather than the whole field view each time (P. N. Dean, 2001). The complete image is built point by point with moving the spot over the specimen. The most important advantage of the confocal microscopy is that applying spatial filtering methods can eliminate out-of-focus light and it can image the thick specimen (Graham et al., 2013).

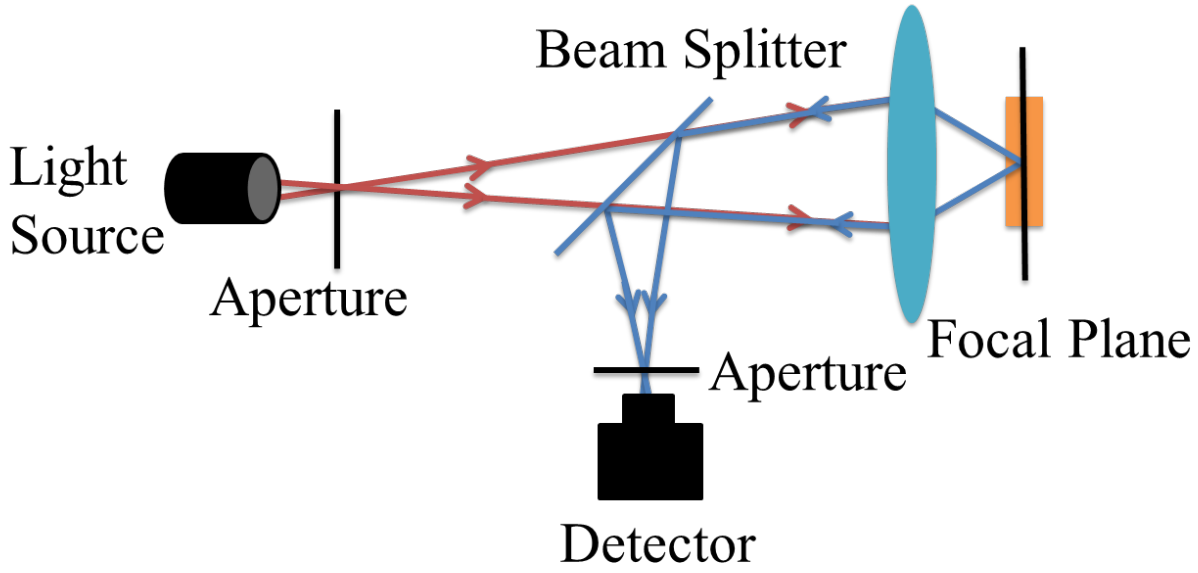

Figure 3-1: The principle of confocal microscopy.

Confocal microscopy offers a way to obtain thin slice images with minimum interference from out-of-focus area of the specimen. This technique has been widely applied in biological science (Gourdie, 1994). The major application of confocal microscopy is in the optical sectioning, where the process is similar to apply a microtome to obtain brain slices except that it is operated optically (Phillip N. Dean, 2001). This procedure starts with an image taken at the top of the cell, followed progressively by more images taken in deeper layers. These steps are repeated until the whole cell is imaged.

The crucial application of confocal microscopy in the biomedical field is to image the tissue with labeled fluorescent probes *in vivo* or *in vitro*. Using conventional light microscope to image these samples, the thickness of the slice in focus is usually more than 2μm or so. However, the confocal microscopy technique has the ability to exclude "out-of-focus" signal from thick labeled samples that has caused the explosion in its popularity (Paddock, 2000), therefore improving the resolution of the images.

3.2 Oxygen dependent phosphorescence imaging

3.2.1 Principle of oxygen dependent phosphorescence imaging

Oxygen dependent phosphorescence imaging provides a very sensitive measurement of oxygen partial pressure surrounding phosphorescent molecules. The intersystem crossing of Pd-porphyrins can quantitatively convert the excited singlet state to the triplet state. A singlet state is an electronic state that all electron spins lack net angular momentum and are paired. The triplet state is the excited electrons that all electron spins are not paired. Hence, these compounds have little or no fluorescence, and therefore the quantum efficiency of phosphorescence is high. The phosphorescence lifetime can be rapidly measured by intensified video cameras and photomultipliers. The intensified video cameras apply arrays of detectors and each of the arrays must obtain sufficient light energy to measure the light intensity. Photomultipliers are single light detectors, which concentrate all phosphorescence light from the specimen on one detector (Diaspro, 2001; Wilson, 1992).

For molecules capable of phosphorescence emission, an electronic transition from the excited triplet state to the singlet ground state generates a phosphorescent photon (Figure 3-2). When a large number of these molecules are excited simultaneously into the triplet state, the resulting emission can be empirically characterized by an exponential decay function (Shonat and Kight, 2003).

$$I(t) = I_0 \exp\left(-\frac{t}{\tau}\right) \tag{3-1}$$

where I(t) is the intensity of phosphorescence at time t, I_0 is the maximum phosphorescence intensity at time t=0, and τ (μs) is the apparent lifetime of the decay. In the presence of a quenching agent, the reduction in phosphorescence manifests itself experimentally as a shortening of the lifetime τ. This diffusion-controlled quenching is described by the Stern-Volmer relationship:

$$\frac{I_0}{I} = \frac{\tau_0}{\tau} = 1 + K_Q \tau_0 PO_2 \tag{3-2}$$

where I_0 and τ_0 are unquenched intensity of phosphorescence and lifetime at PO_2 = 0, respectively. I and τ are intensity of phosphorescence and lifetime at specified oxygen pressure. K_Q is the quencher rate coefficient, and PO_2 is the partial oxygen pressure, which is proportional

to the oxygen concentration in the solution (Diaspro, 2001). The calibration is used to determine the variables of τ_0 and K_Q as temperature and pH under reproducible experimental conditions. Phosphorescence lifetime is an accurate technique to measure oxygen partial pressure since the lifetime measurements do not depend on the probe concentration and the intensity of illumination light. Moreover, lifetime measurements are not affected by variations of other chromophores absorption in tissue, such as hemoglobin and myoglobin.

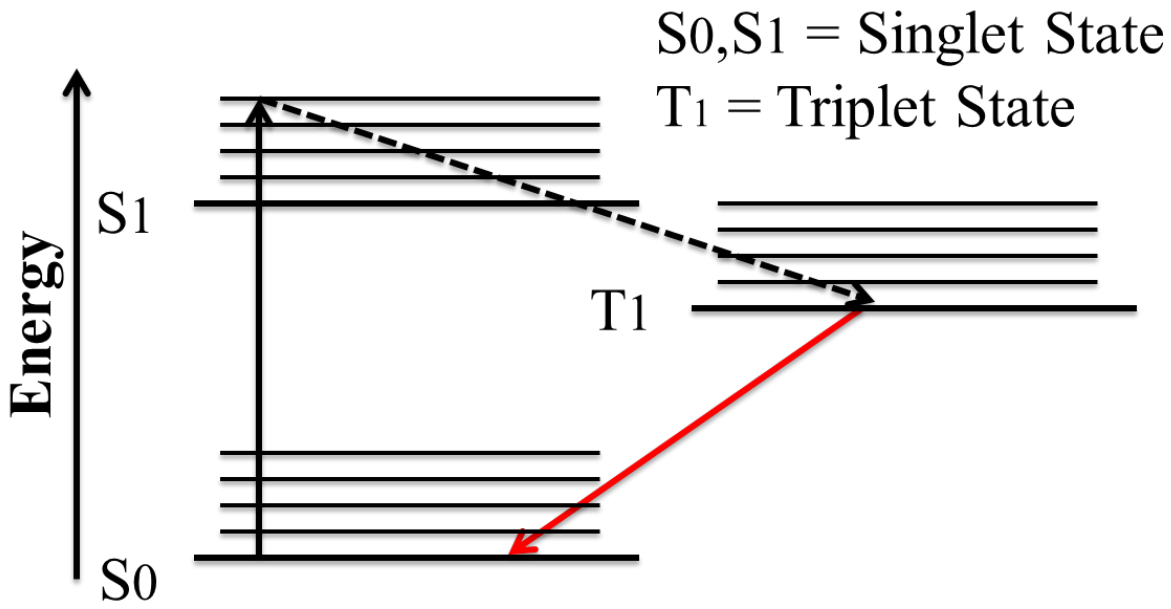

Figure 3-2: Simplified Jablonski energy diagram of phosphorescence progress

3.2.2 Phosphors for measuring oxygen by oxygen-dependent quenching of phosphorescence

Several oxygen sensing molecules have been applied for different modes of phosphorescence-based oximetry over the years. Generally, nanoparticle-based molecules are mainly used for oxygen measurements in cell culture, however, bio-distributions and aqueous solubility are specifically important for measurements in intact organisms (Palmer et al., 2010). Previously, the phosphorescent probes according to simple Pd porphyrins (Papkovsky and O'Riordan, 2005; Vanderkooi et al., 1987), required prebinding of macromolecular carriers (such as albumin) in order to enhance their aqueous solubility and brought their quenching parameters (τ_0 and K_Q) into a range compatible with physiological oxygen concentration. But foreign albumin potentially

offered immunogenic and toxicity responses. The presence of polyglutmatic dendritic porphyrins (such as Oxyphor R_2 and G_2) (Dunphy et al., 2002) supplied a way to solve this question. Poly-glutmatic probes have the high aqueous solubility, which can be used into the vasculature directly without aggregation of albumin. However, R_2 and G_2 have the limitation in albumin-rich environments because of forming complexes with endogenous albumin, such as blood plasma. Recently, a general way to protect molecular oxygen probes that do not require supporting macromolecular carriers or albumin was discovered (Finikova et al., 2008; Lebedev et al., 2009). For such probes, phosphorescent metalloporphyrins are encapsulated inside the hydrophobic dendrimers, which protect shells and regulate the method's sensitivity (Esipova et al., 2011). Oxyphor R_4 and G_4 were two new oxyphors, which were presented and widely applied in biological study. These probes are obtained based on the above general process. Besides, their components are optimized for better chemical stability (such as lack of prebinding albumin in aqueous solution and higher mono-dispersity) (Esipova et al., 2011).

3.2.3 Principle of the calibration for phosphors

The oxygen quenching properties can be detected as functions of pH, temperature and concentration. For calibration, solutions with controlled amounts of oxygen are manufactured. The easiest way is to prepare a solution with air, which is done by diluting phosphorescence molecules in deionized water. The obtained value of lifetime corresponds to an oxygen pressure of 160mmHg because of 21% of pressure in normal atmosphere. Using a completely deoxygenated solution, the lifetime of the probe in the absence of oxygen can be measured. With the glucose oxidase, each glucose molecule consumes one oxygen molecule, which is described by the reaction:

$$2G + 2O_2 + 2H_2O \xrightarrow{glucose\ oxidase} 2GO + 2H_2O_2 \quad (3\text{-}3)$$

where G represents the glucose molecule and GO represents the gluconic acid. As the reaction produces hydrogen peroxide (H_2O_2), catalase is used to decompose H_2O_2, for which the reaction is:

$$2H_2O_2 \xrightarrow{catalase} 2H_2O + O_2 \quad (3\text{-}4)$$

If the reaction (3-3) and (3-4) are added, we obtain the reaction:

$$2G + 2O_2 + 2H_2O \xrightarrow{glucose\ oxidase\ and\ catalase} 2GO + 2H_2O + O_2 \quad (3\text{-}5)$$

This reaction products approach zero amount of oxygen (0 mmHg) when properly dosed. For a completely deoxygenated probe, samples include catalase (12.5µg/ml), glucose oxidase (75µg/ml) and 0.3% glucose are required during phosphorescence measurement under anaerobic conditions (Vanderkooi et al., 1987). We followed this procedure to calibrate our probes below.

A system combining the confocal microscopy and phosphorescence lifetime imaging was developed (see below), which can measure partial oxygen pressure in tissue and vessels with high transverse and axial resolution, avoiding phosphorescence signal contamination from neighboring voxels. To determine parameters (τ_0 and K_Q) in the Stern-Volmer equation, two oxygen pressures (0 mmHg and 160 mmHg) were measured under experimental conditions. At 0 mmHg partial oxygen pressure, the τ_0 was obtained from the lifetime. The Stern-Volmer equation was then applied to calculate K_Q with τ_0 at 160 mmHg oxygen pressure. All measures were done at 37C and 7.4pH to reproduce *in vivo* conditions.

3.2.4 Overview of the confocal phosphorescence lifetime microscopy system and experiment

A standard confocal microscope was built, integrating time-domain readout measures for lifetime estimates. A Matlab interface was developed to control the whole system consisting of a confocal scanner, camera and photon counting detection arm. From the interface of confocal phosphorescence microscopy system (Figure 3-3), we can adjust the laser power and the length of the pulse. Quality of images from the camera was controlled by adjusting the exposure time of the camera. High concentration areas of the probe can be found by fitting the histogram while scanning at equal laser power. Points of interest can be scanned along a line or spiral. When the measurement started, all acquisition parameters on the interface were saved in a text file.

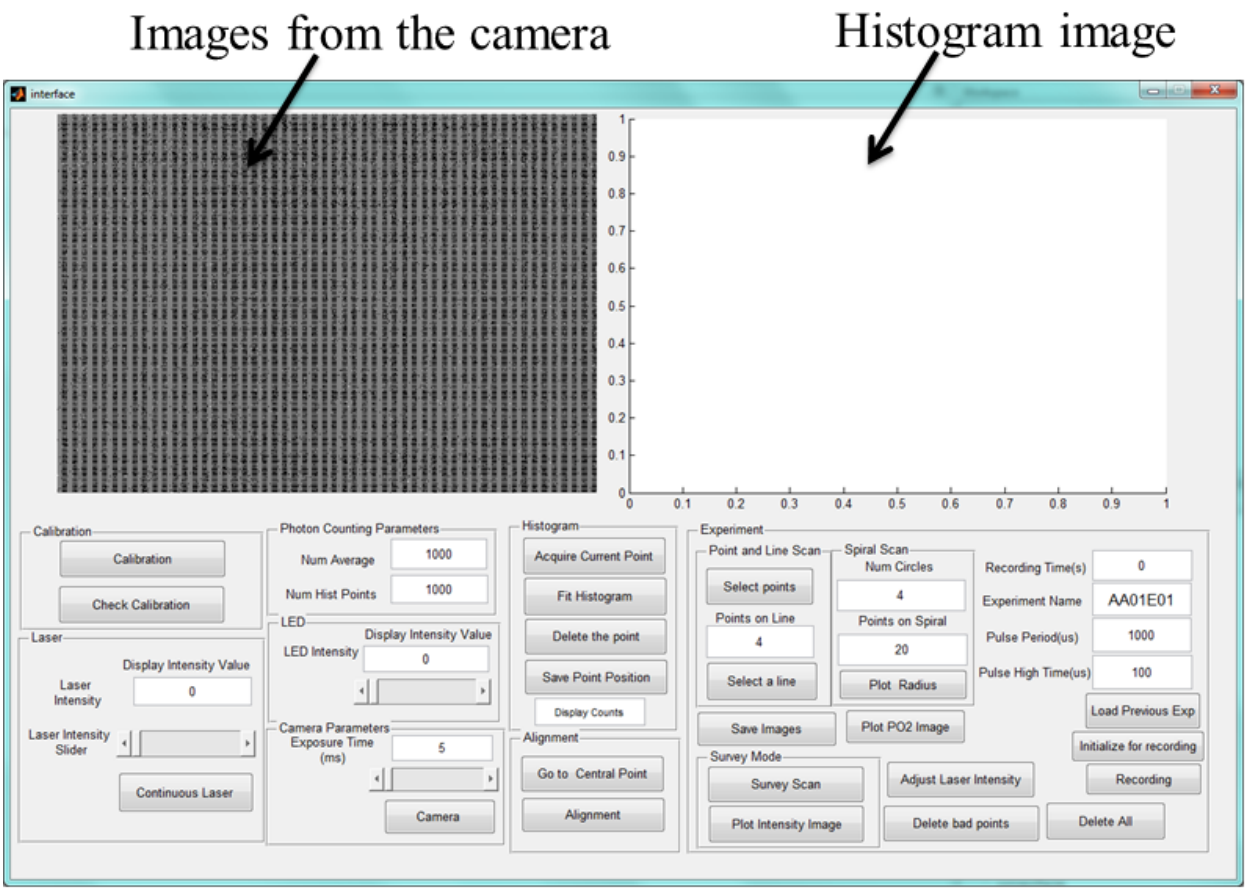

Figure 3-3: The interface of the confocal phosphorescence microscopy system

Before the measurement started, the mouse was moved on the lab platform. A tungsten electrode was inserted in the cortex and reference electrodes as well as ground electrodes were put on the mouse brain to reduce the noise during local field potential measures. The imaging focus was achieved through images obtained by the camera, which was displayed in the interface (Figure 3-3 and Figure 3-4). A spatial calibration was done by building an interpolation matrix between voltage sent to the galvanometer and positions of laser spot in the image. The calibration was checked manually in each experiment to ensure the points of interest were recorded.

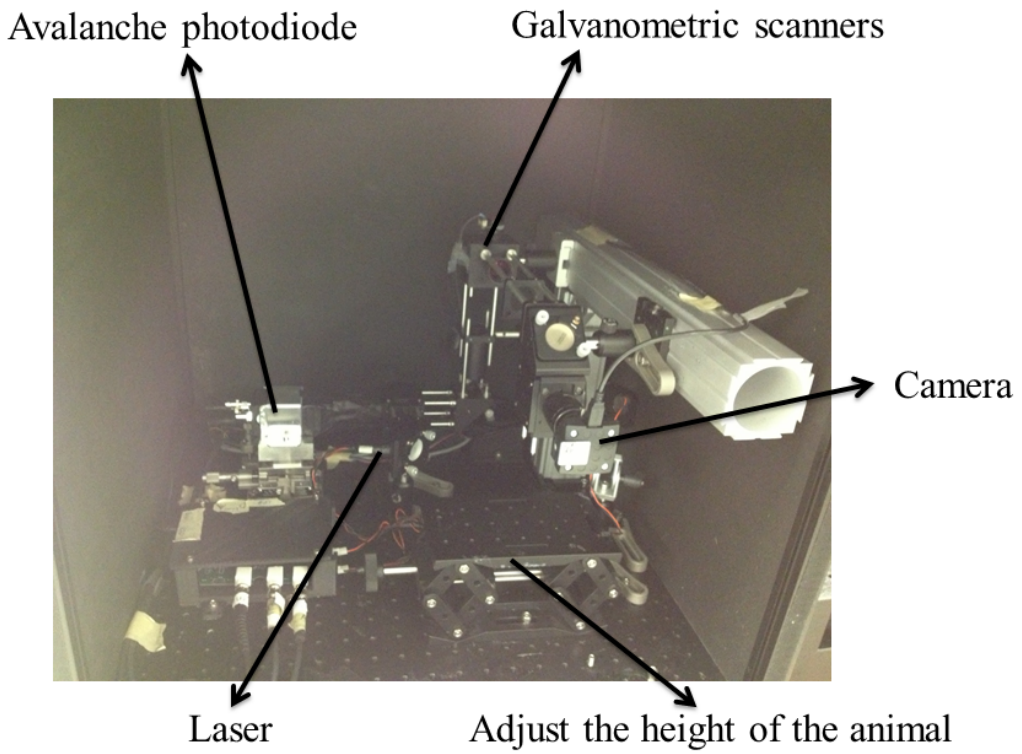

Figure 3-4: Overview of the confocal phosphorescence microscopy system.

Two steps were performed during the experiment. Initially, points of interest were selected for measuring PO_2. Survey scan were obtained by scanning these points and summing photon counts at each point using an excitation pulse duration and phosphorescence detection window of 100 µs and 500µs respectively. From the survey scan counts of these points, the power of laser diode for each point was adjusted to minimize the photo-oxidative damage to tissue and limit consumption during the measurement based on the number of recorded counts in the survey. Following the survey scan, the same points were measured while averaging 100 times to increase the signal-to-noise ratio at varying laser power. All experiments were recorded around 3 hours until the mouse did not have epileptic events.

3.2.5 Characterization of confocal phosphorescence lifetime microscopy

The signal to noise ratio (SNR) was calculated to characterize the system. The lifetime was obtained by fitting measured data with the exponential decay, which depends on the noise level and the stability of the signal. The SNR of lifetime is defined by the average of lifetime from the same condition over its standard deviation. These two parameters are shown in Table 2-1 for

equilibrium measurements with different concentration of the Oxyphor G4 and various duration of the pulse. The SNR of the lifetime decreases with the concentration of probe but remains relatively constant regardless of the pulse duration. This is explained by the fact that the noise is correlated with the intensity of the signal due to Poisson statistics.

Table 3-1. The SNR of various measurements in equilibrium with air

Concentration of the probe, pulse duration	Lifetime SNR
50 μM, 100μs	50.4
25 μM, 100μs	34.0
10 μM, 100μs	28.5
50 μM, 50μs	52.7
50 μM, 10μs	50.2

The field of view of the confocal system in object plane is calculated by the following formula:

$$\Delta x = f_1 \cdot \tan\left(\frac{f_2}{f_3}\beta\right) \tag{3-6}$$

where the f_1 is the effective focal length of the objective used, which is 18 mm. β is the largest angle that galvanometer system can turn, which is 15.5° in axis x and 18.8° in axis y (measured from the system). f_1 and f_2 are the focal lengths of two lenses used in the system as a telescope to map the galvo mirrors on the objective pupil. In here, f_2 and f_3 are 50 mm and 125 mm separately. From this formula we could obtain the field of view in x was 1.96 mm and the field of view in y was 2.38 mm. The resolution of the camera was 1024 × 1280. Hence, the pixel size in x and y were both 1.9 μm. The resolution is improved by a higher magnification objective with a large numerical aperture but this could result in decreasing the field of view.

3.3 Two-photon microscopy

The theoretical basis of two-photon excitation was discovered by Maria Goeppert-Maye in 1931. This technique was first applied in experimental research by Kaiser and Garret in 1963 (Palikaras and Tavernarakis, 2001). Based on the nonlinear excitation of fluorophores, Webb Denk and colleagues developed a two-photon fluorescence microscopy system, which represents a revolutionary progress in the 3D imaging of cells and tissue *in vivo* (Denk et al., 1990). Two-photon microscopy (TPM) has four unique capabilities, which are considered to be advantageous over the traditional biological imaging techniques (Nemoto et al., 2015). First, TPM can image living specimens because of great reduction of photodamage. Second, the wavelength of the light used to excite fluorophores in TPM is much larger, usually within the deep red and near infrared wavelength range. This means that the light is able to penetrate more deeply due to less scattering and absorption by endogenous chromophores, therefore leading to a considerably deeper imaging depth of TPM. TPM can image with depth of a few hundred micrometers (Yaroslavsky et al., 2002). Third, TPM eliminates the contamination of fluorescence signal from the excitation light, allowing high-sensitivity imaging (Centonze and White, 1998). Fourth, TPM initiates photochemical reaction with a sub-femtoliter volume inside cells. Thanks to these advantages, two-photon fluorescence microscopy has now become a useful tool in studying biological function *in vivo*.

3.3.1 Principle of two-photon excitation microscopy

Photobleaching and phototoxicity are unavoidable issues in imaging of biological samples that are labeled with fluorophores. Photodamage (such as photobleaching and phototoxicity) limits the application of fluorescence microscopy *in vivo*. Each excitation event has the risk of photodamage. In order to minimize photodamage, two-photon fluorescence microscopy maximizes the measure of a signal photon in every excitation event. Compared to other methods, TPM dramatically improves the detection of photons especially in deep imaging (Svoboda and Yasuda, 2006).

Two-photon microscopy is a nonlinear process that the absorption of two photons is adequate to provide enough energy to elicit a molecular to an excited state. In Figure 3-5 we show a comparison between the two-photon absorption and the more conventional single-photon

excitation (So et al., 2000). In the single-photon excitation event, the fluorescent molecules of interest are excited by ultraviolet or visible light. The excitation occurs when the absorbed photon energy is enough to fill the gap of the energy between the excited electronic state and singlet ground state. The two-photon excitation process shares a similar basis, except that two less energetic photons are absorbed simultaneously. More explicitly, the molecule is excited to a virtual intermediate state with the absorbed energy of the first photon, while the absorption of the second photon eventually brings the molecule to the final excited state.

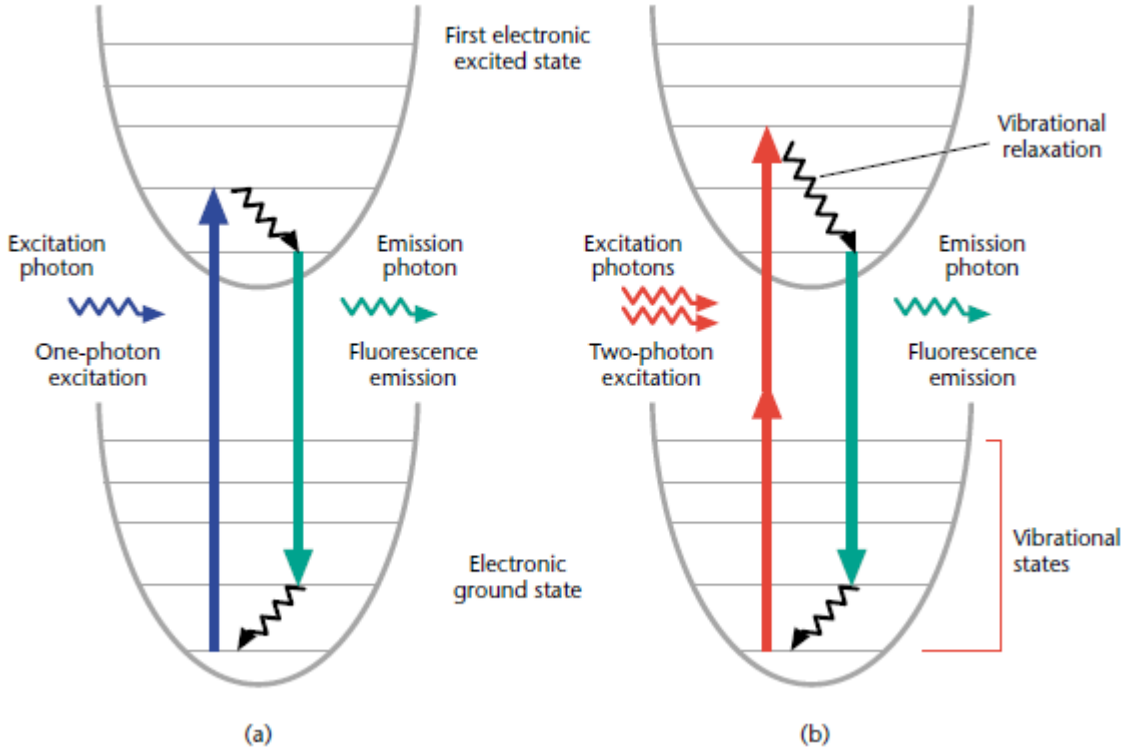

Figure 3-5: Simplified Jablonski diagram of one-photon excitation (a) and two-photon excitation (b) (So et al., 2000).

Two-photon fluorescence lifetime microscopy is a fluorescence process in which a dye molecule is excited by simultaneously absorbed two photons with approximately a doubled wavelength as that of the photon in the single-photon excitation. There are several additional constrictions with regard to the light source used in the two-photon excitation process. For example, the source needs to output a high intensity of light. This is because that the fluorescence can absorb two photons only when they hit the molecule simultaneously. With a high-power laser source, the possibility of having two photons hit simultaneously is much higher. However, continuous

lighting of lasers with a high average power may cause severe damage to the biological tissue. Therefore, in two-photon excitation microscopy, pulse-emitting lasers with low average power and high peak powers are usually applied. The high peak power is obtained by short light pulses at high repetition rates ~80Mhz (Rubart, 2004; Williams et al., 1994).

In a focused laser spot, the intensity of the light is the highest at the center and decays with increasing distance from the center in a quadratic manner. Hence, fluorophores are excited in a diffraction-limited focal volume. With a high numerical aperture objective, the majority of fluorophores are excited in a focal volume that can be up to ~0.1 μm^3 (Zipfel et al., 2003). All fluorescence photons from the focal volume are captured by the objective to produce an image of that volume. The laser then moves to another location and starts a same imaging procedure. This process is repeated until all the regions of interest in the specimen are scanned.

3.3.2 Application of two-photon excitation microscopy

Two-photon microscopy has been widely applied to detect physiological signals in many tissue types, such as salamander retina (Denk and Detwiler, 1999), the corneal structure in rabbit eyes (Buehler et al., 1999), human mucosa (Riegler et al., 1999), as well as the human and mouse dermal structures (So et al., 1998). Besides, TPM has also seen its application in embryology and neurobiology. In embryology field, TPM has been successfully used to study the calcium passage (Golshani and Portera-Cailliau, 2008; Russell, 2011). In neurobiology, TPM has been applied to study neuronal and cellular morphological changes in the neocortex (Helmchen, 2009; Kretschmer et al., 2016), the neuronal function in brain with slices (Girouard et al., 2010), the calcium signal changes in dendritic spine function (Rochefort and Konnerth, 2012; Takasaki and Sabatini, 2014), and hemodynamic changes in the rat brain neocortex (Driscoll et al., 2013; Lindvere et al., 2010), etc. However, several limitations exist when TPM is applied in tissue measures. First, on different types of specimens, the imaging depth of TPM can vary dramatically. Moreover, for deep tissue there is a major technical challenge in fluorescence labelling. Currently there is no standard method to label fluorescence in deep tissue, which is considered as the major obstacle of TPM in such applications (So et al., 2000).

A promising direction of TPM is in clinical diagnosis and treatment. In clinical diagnosis, optical biopsy is a new technique. The removal and fixation of tissue are required in conventional biopsy. When these steps are prepared the histological procedure is poorly preserved in tissue

biochemical information. TPM has been successfully used to study the skin structure in clinical diagnosis (Masters et al., 1997). TPM has also been used in clinical treatment. Photodynamic therapy is a technique, which destructs specific tissue (such as tumor) with a photosensitizer. With laser illumination photosensitizer-loaded tissue is destroyed. Unfortunately, the normal tissue is often non-negligible taken because of the higher of photosensitizer uptake in tumorous tissue. The destruction of healthy tissue in photodynamic therapy is a common issue. The attractive opinion is that tumor is localized by TPM first and then photodynamic action is initiated at the selected site.

3.4 Krogh-Erlang Model for oxygen diffusion in tissue

The Krogh_Erlang model that depicts the oxygen diffusion in any cross-section of a cylinder near a vessel is mostly applied to model of oxygen transport (Krogh, 1919). The diffusion equation was described in a Krogh cylinder (Foster et al., 1991; Okunieff et al., 2006):

$$\frac{1}{r}\frac{\partial}{\partial r}\left(r\frac{\partial U}{\partial r}\right)+\frac{\partial^2 U}{\partial z^2}-\frac{Q}{D}=0 \tag{3-6}$$

boundary conditions in tissue $r_0 \le r \le R, 0 \le z \le L$:

$$z=0,\frac{\partial U}{\partial r}=0;\ z=L,\frac{\partial U}{\partial z}=0; \tag{3-7a}$$

$$r=R,\frac{\partial U}{\partial r}=0; r=r_0, U_c=U|_{r0} \tag{3-7b}$$

and boundary conditions in the vessel $0<r<r_0, 0 \le z \le L$:

$$\pi r_0^2 V\frac{dU_c}{dz}=2\pi r_0 D\frac{\partial U}{\partial r}|_{r0}, U_c(0)=U_0 \tag{3-8}$$

where $U=U(r,z), Uc=U(r,z)$ are oxygen concentrations in tissue and vessel, respectively, R is the radius of Krogh cylinder,L is the length of Krogh cylinder, Q is the rate of oxygen consumption which is the product of $CMRO_2$ and the density of brain tissue, D is oxygen diffusion coefficient, r_0 is radius of the vessel, V is speed of flow in the vessel, and U_0 is concentration of oxygen in the vessel at the arterial end (Grinberg et al., 2005).

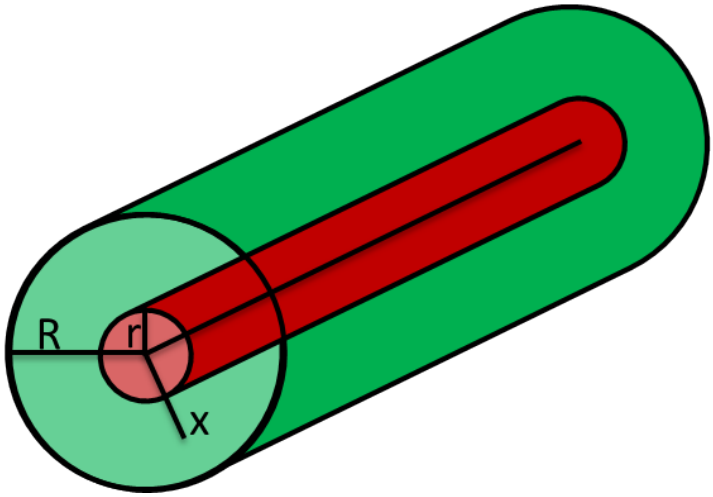

Figure 3-6: Sketch of the Krogh cylinder model where the blood vessel (radius r) provides oxygen with a tissue cylinder (radius R) by diffusion.

The discrete oxygen distribution in the same level that is perpendicular to the vessel at any point z_i (the diffusion distance r_j) of the vessel can be depicted with the classical Krogh equation:

$$PO_2(z_i, r_j) = PO_2^{VES}(z_i) - \frac{Q}{4\alpha D}\left(2R^2 \ln\left(\frac{r_j}{r_0}\right) - (r_j^2 - r_0^2)\right) \quad (3\text{-}9)$$

When r_j is equal to R (the secondary boundary condition), the simplified Krogh-Erlang formula is applied to supply oxygen in the vasculature.

$$PO_2(z_i, R) = PO_2^{VES}(z_i) - \frac{Q}{4\alpha D}\left(2R^2 \ln\left(\frac{R}{r_0}\right) - (R^2 - r_0^2)\right) \quad (3\text{-}10)$$

By definition, we can obtain that the microregional oxygen pressure $PO_2(z_i, R)$ at the cylinder boundary is rate limiting. Where $PO_2^{VES}(z_i)$ is the oxygen concentration in the vessel at the point z_i, $\alpha = 1.3\times10^{-3} cm^3/(cm^3\times760 mmHg)$ is oxygen solubility. $D = 1.5\times10^3 \mu m^2/s$ is oxygen diffusion coefficient, Q is oxygen consumption rate, r_0 is capillary radius, r_j is radial coordinate and $r_0 \geq r_j \geq R$. We used literature values for Q, i.e. 2.6 μmol/g/min at baseline (Cui et al., 2013) and an increase of ~12% during epileptic seizures (Zhao et al., 2011). In my work, the tissue PO_2 and artery diameter are measured with two-photon phosphorescence lifetime microscopy. The Krogh model is used to simulate the relationship between PO_2 in tissue and perpendicular distance from an artery.

CHAPTER 4 ARTICLE 1: MEASUREMENT OF LOCAL PARTIAL PRESSURE OF OXYGEN IN THE BRAIN TISSUE UNDER NORMOXIA AND EPILEPSY WITH PHOSPHORESCENCE LIFETIME MICROSCOPY

Cong Zhang,[1] Samuel Bélanger,[1] Philippe Pouliot,[1,2] Frédéric Lesage,[1,2]

1 École Polytechnique de Montréal, Department of Electrical Engineering, C.P. 6079 succ.Centre-ville, Montreal, Quebec, Canada, H3C 3A7

2 Montreal Heart Institute, 5000 Bélanger street, Montreal, Quebec, Canada, H1T 1C8

Correspondance: Dr. Frédéric Lesage, École Polytechnique de Montréal, Department of Electrical Engineering, C.P. 6079 succ.Centre-ville, Montreal, Quebec, H3C 3A7; Tel: +1 514-340-4711x7542; Fax: +1 514-340-4611; E-mail: frederic.lesage@polymtl.ca

This article addresses the first objective of this thesis which is to provide an invasive measurement of oxygen partial pressure in tissue during epileptic seizures in mouse brain by confocal phosphorescence lifetime microscopy. This article has been published in PLOS ONE in 2015 (Zhang et al., 2015).

4.1 Abstract

In this work a method for measuring brain oxygen partial pressure with confocal phosphorescence lifetime microscopy system is reported. When used in conjunction with a dendritic phosphorescent probe, Oxyphor G4, this system enabled minimally invasive measurements of oxygen partial pressure (PO_2) in cerebral tissue with high spatial and temporal resolution during 4-aminopyridine (4-AP) induced epileptic seizures. Investigating epileptic events, we characterized the spatio-temporal distribution of the "initial dip" in PO_2 near the probe injection site and along nearby arterioles. Our results reveal a correlation between the percent change in the PO_2 signal during the "initial dip" and the duration of seizure-like activity, which can help localize the epileptic focus and predict the length of seizure.

Keywords: Confocal microscopy, phosphorescence lifetime system, oxygen partial pressure, epilepsy.

4.2 Introduction

The nature of coupling between neuronal activity and the associated metabolic response is a subject of great debate (Arthurs et al., 2000; Lauritzen, 2001; Norup Nielsen and Lauritzen, 2001). Evaluating tissue oxygen changes and quantifying oxidative metabolism is crucial for the understanding of neuropathologies in the brain, such as Parkinson's disease, stroke, epilepsy, Alzheimer's disease (Bahar et al., 2006; Cheng et al., 2014; Ferris et al., 2013; Nagata et al., 2002) and developing effective therapies. While blood oxymetry provides a proxy for tissue oxygenation, under conditions of large metabolic demand and/or non-linear hemodynamic response (Pouliot et al., 2012a), such as in epilepsy, measuring blood oxygenation alone is not sufficient. In order to investigate such conditions, monitoring of the spatio-temporal characteristics of oxygen changes in cerebral tissue is crucial.

Several techniques have been developed to measure cerebral oxygenation in vivo, including positron emission tomography (PET), near-infrared spectroscopy (NIRS), blood-oxygenation level dependent functional magnetic resonance imaging (BOLD-fMRI) and oxygen polarimetric electrodes (Ances et al., 2001; Hyder et al., 2002; Mintun et al., 2001; Osharina et al., 2010). BOLD-fMRI and NIRS are noninvasive, while PET is minimally invasive (requires an exogenous marker), and all three are utilized widely in clinical research. However, each of these techniques has limitations. BOLD-fMRI measures oxygen consumption indirectly through a complex combination of flow, volume and deoxyhemoglobin concentration. PET provides measurements of oxygen by monitoring short-lived positron emitting radionuclides, such as ^{15}O, and can thus be carried out only nearby a cyclotron. Thus, both PET and BOLD-fMRI require expensive and bulky instrumentation. NIRS, on the other hand, has the advantage of portability, low cost and excellent temporal resolution; however, it measures oxygen saturation of hemoglobin, which is a proxy of oxygen concentration in blood as opposed to partial pressure (PO_2) in tissue. Moreover, the above techniques suffer from low spatial resolution, ranging from millimeters to centimeters. Measurements by oxygen sensitive electrodes – the gold standard of oximetry, are capable of fast assessment of PO_2, but these are invasive by nature and confined to discrete locations.

Among optical approaches, oxygen-dependent quenching of phosphorescence stands out in its ability to provide fast absolute measurements of PO_2, which are not affected by optical

parameters of the tissue (Vanderkooi et al., 1987). Oxygen-dependent quenching phosphorescence is an optical method for oxygen sensing in biological systems, which offers excellent specificity, high sensitivity and relative simplicity of implementation (Papkovsky and Dmitriev, 2013; Quaranta et al., 2012; Vinogradov et al., 2011). One implementation of the technique is based on lifetime imaging in combination with microscopy and O_2-sensitive phosphorescent probes (Golub and Pittman, 2008; Hogan, 1999; Shonat et al., 1997; Smith et al., 2002). With the emergence of phosphorescent probes that are water-soluble and nontoxic (Vinogradov et al., 2011) the spatio-temporal evolution of oxygen in tissue can be investigated in greater details. Two distinct approaches have been used to experimentally determine the phosphorescence lifetime. A time-domain approach, whereby the phosphorescent probe is excited by a light pulse, and a frequency-domain approach whereby the probe is excited continuously by sinusoidally modulated light (Shonat and Kight, 2003). For imaging applications, the time-domain approach has been the most common in vivo. Several examples of microscopic measurements of phosphorescence have been reported (Golub and Pittman, 2008; Plant and Burns, 1993; Torres Filho et al., 1994; Wilson et al., 2005), including recent improvements using new probes tailored for multiphoton excitation (Estrada et al., 2008; Finikova et al., 2008; Sakadzić et al., 2010).

In this work we developed a confocal system to measure PO_2 in tissue and vessels with high transverse and axial resolution, avoiding phosphorescence signal contamination from neighboring voxels. We optimized the recording conditions to reduce the prospect of measurement errors induced by photo-consumptive effects of the probe. The system allows fast data collection, avoiding excessively long data averaging, enabling us to perform PO_2 measurement at multiple locations. We then exploited this system to investigate tissue oxygenation in a model of epilepsy.

4.3 Materials and Methods

4.3.1 Principle of phosphorescence quenching imaging

Our methodology is based on oxygen-dependent quenching of phosphorescence of metallo-porphyrins, whereby the phosphorescence decay rate is directly related to the concentration of O_2 molecules in the medium either in vitro or in vivo. Dynamical quenching of phosphorescence involves collisions between the quencher molecules and the probe (metalloporphyrin) in its

excited triplet state, resulting in radiationless deactivation and return to the ground state. Phosphorescence quenching by O_2 is a function of the probability of collisions between the excited state probe and molecular oxygen, which is appropriately described by the Stern-Volmer equation (Vanderkooi et al., 1987)

$$\frac{\tau_0}{\tau} = 1 + K_q \cdot \tau_0 \cdot pO_2 \quad (4\text{-}1)$$

where τ_0 and τ represent the phosphorescence lifetimes in the absence of oxygen and at a given PO_2, while K_q represents the quenching constant, both factors being dependent on the temperature. The phosphorescence decay time τ is a robust and quantitative indicator of oxygen in the environment, as it is not affected by the probe concentration, and/or absorption of light by endogenous biological chromophores, such as myoglobin, hemoglobin, or cytochromes.

4.3.2 Phosphorescent probe Oxyphor G4

Phosphorescence lifetime microscopy has been used previously to measure PO_2 changes through phosphorescence of exogenous probes. Early phosphorescent probes, based on Pd porphyrins (Rumsey et al., 1988; Vanderkooi et al., 1987), required pre-binding to a macromolecular carrier (e.g. albumin) in order to enhance their aqueous solubility and bring their quenching parameters into the range compatible with physiological oxygen concentration (Dunphy et al., 2002; Vanderkooi et al., 1987). Moreover, the albumin was a potential source of toxicity. Recently, Esipova et al. (Esipova et al., 2011) developed a new probe, Oxyphor G4, which is free of these limitations. Oxyphor G4 is derived from Pd-meso-tetra-(3, 5-dicarboxyphenyl)-tetrabenzoporphyrin (PdTBP) and belongs to the group of dendritic oxygen probe (Lebedev et al., 2009). It is highly soluble in aqueous environments and does not permeate biological membranes. It can operate in either albumin-rich (blood plasma) or albumin-free (interstitial space) environments at all physiological oxygen concentrations, from normoxic to deep hypoxic conditions. Oxyphor G4 used in these studies was obtained from Oxygen Enterprises Ltd (University of Pennsylvania, Philadelphia, PA 19104-6059, USA). Received Oxyphor G4 was calibrated before the experiments, first equilibrated with room air (21% O_2) and then with a completely deoxygenated solution at various temperatures (results of calibration are shown in Figure 4-1). In vivo the measured parameters (Kq and $\tau 0$) were selected at temperature ~37℃.

The phosphorescence lifetimes of Oxyphor G4 range from ~23 to ~215 µs in the physiological PO_2 range (160 mmHg-0 mmHg).

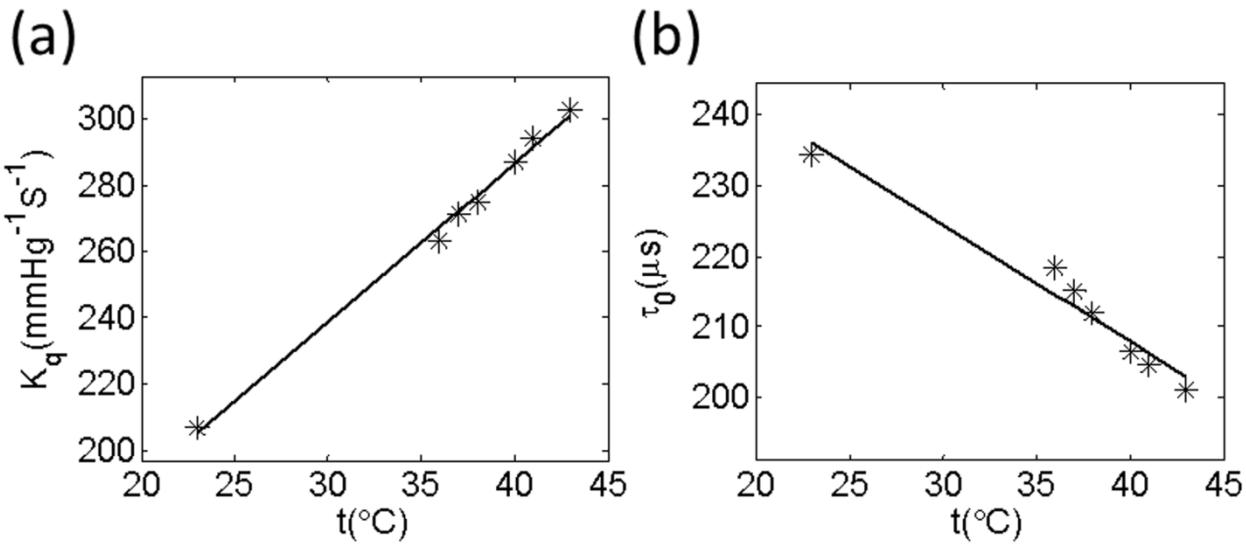

Figure 4-1: Temperature dependencies of oxygen quenching constants (Kq) and lifetimes (τ0) for G4 (a and b). The measurements were performed using 50 µM solutions of the probes, pH 7.23.

4.3.3 Animal preparation

Animals were used according to the recommendations of the Canadian Council on Animal Care, and all procedures were approved by Animal Research Ethics Committee of the Montreal Heart Institute (Permit Number: 2013-32-01). Eight male C57BL/6 mice (8 weeks old, 20-25g weight) were anesthetized by injection of urethane (2 mg/g body weight) in a 10% (wt/vol) saline solution. Body temperature was maintained at 37 °C with controlled heating blanket. Mice were ventilated via a tracheotomy using ambient air. After positioning mice on a stereotactic frame, the scalp was retracted, and 5 × 5mm sections of the skin were removed over the coronal suture around bregma. The somatosensory cortex was exposed and the bone was removed over a region along the coronal suture closer to the bregma (AP: -1.5 mm DV: +1.5 mm). Following brain exposure, 500nL of 50µM solution of Oxyphor G4 was injected in the tissue via a 34G bevelled syringe with a microsyringe pump controller (uMC4, World Precision Instruments, Sarasota, FL) over a period of 10 min. The syringe was lowered to a depth ~300µm for injections. A glass coverslip window (5mm in diameter) was then installed using agarose gel and fixed with dental acrylic cement.

For epilepsy experiments, epileptiform activity was induced in 6 mice by injecting of 500nL of the K^+-channel blocking agent 4-AP (A78403, Sigma-Aldrich, St. Louis, MO) solution (100mM), mixed with Oxyphor G4, through a syringe pump controller, similar to the injection of Oxyphor G4 alone described above. A higher concentration of 4-AP was required in this study to generate regular seizures, mixing with G4 may reduce the potency of 4-AP thus requiring these higher dosages. Following injection, a tungsten microelectrode (0.5-2 MΩ) was placed around the glass coverslip and inserted ~500μm into the cortex with an angle ~30° (leading to a depth of 250μm) in order to record extracellular local field potential (LFP). At the end of experiments, animals were sacrificed by cervical dislocation while under anesthesia.

4.3.4 Phosphorescence lifetime microscopy setup and PO_2 estimation

The confocal lifetime system is depicted in Figure 4-2. The excitation light is provided by a laser diode at 637 nm (Thorlabs: HL63133DG), controlled by a data acquisition (DAQ) board (National Instruments USB-6343). A galvanometer mirror positioning system (Thorlabs: GVS002) guides the excitation beam to selected points in the focal plane with a telescope consisting of two convex lens (f1 = 50 mm and f2 = 125 mm). The response time of galvanometric scanners was 3ms. A 10×magnification objective lens (Olympus PLN10x NA = 0.25) is used to focus the light onto the sample. The phosphorescence light travels back through the telescope to be separated by a beam splitter (BS2, Semrock: FF685-DI02-25×36) and a band-pass filter (Semrock: FF02-809/81-25, 768.5 nm ~ 849.5 nm), so that only the emitted phosphorescence signal is collected by a photon-counting avalanche photodiode (APD) (Micro Photon Devices: PDM series), whose active area (50 μm in diameter) functions as a pinhole. The APD amplifier outputs a TTL pulse for each detected photon and the pulsed are counted by the DAQ board. A second beam splitter (BS1, Semrock: FF520-DI02-25×36) is placed between the objective lens and the telescope to be used in combination with a camera (Thorlabs: DCC1545M) to gather anatomic references during experiments using LED illumination. The system is controlled by a computer running custom-designed software written in Matlab (The MathWorks, Natick, MA). The software allows adjustment of the length of the excitation pulse (temporal gate), and selection of points at which PO_2 values are measured. The in-plane resolution of the system in non-diffusive media is ~1.9 μm and axial resolution ~20.1μm. Assuming a Gaussian beam, the

radius of each measured region is ~1.5 μm. In all experiments below, the excitation power of laser diode after the objective was kept below 6.5mW.

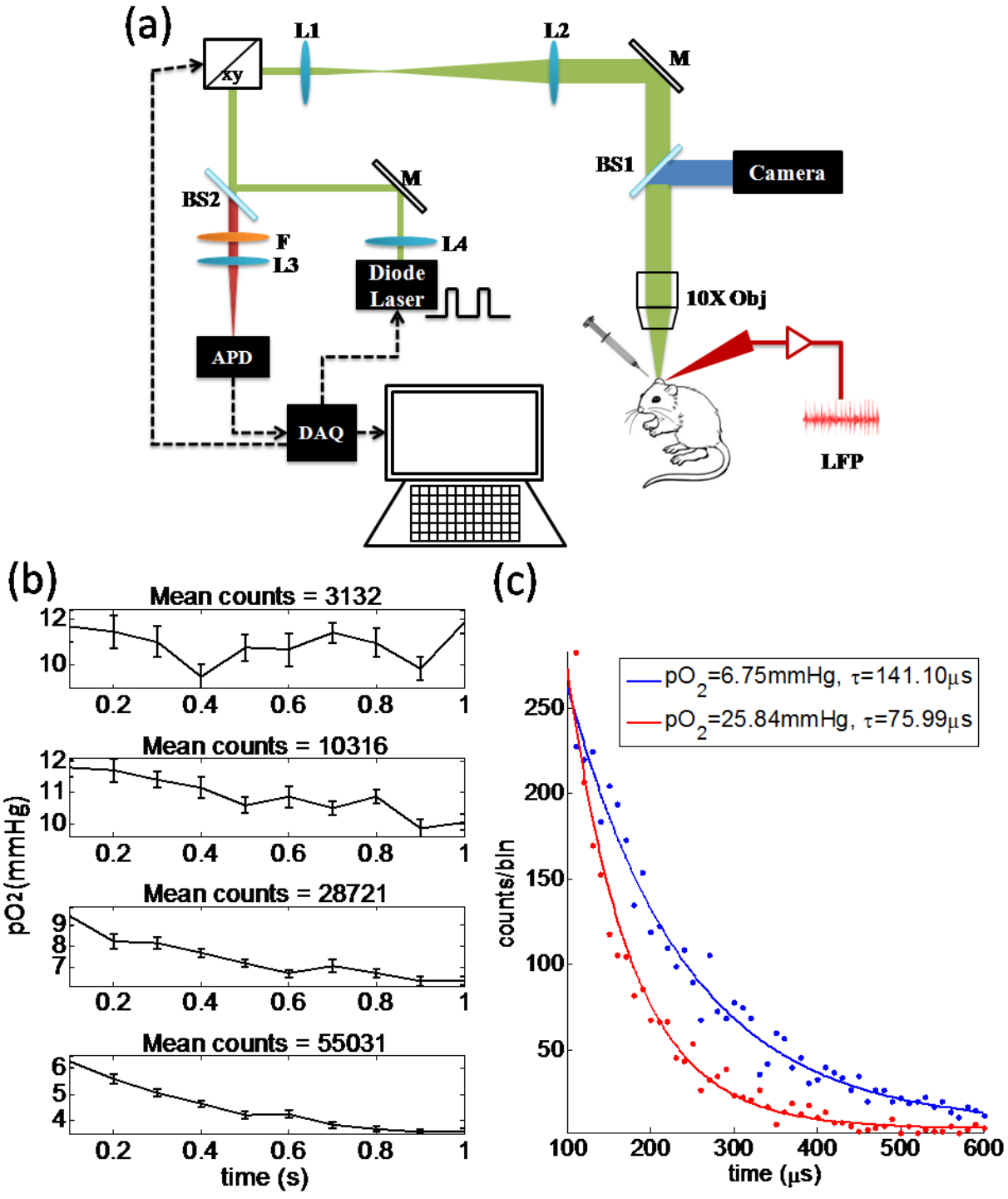

Figure 4-2: (a) Schematic of the confocal lifetime imaging system. Excitation light is provided by a laser diode (λ=637nm, 170 mW maximum power, which is collimated by a convex lens (L_1)

and travels through the objective for illumination. It is focused onto the cranial window by a 10×magnification objective (Obj), which is directed to the specific points using galvanometric scanners (xy). Emitted phosphorescence light is separated from excitation light using a beam splitter (BS_2) and filter (F) and detected with an avalanche photodiode (APD). The system is controlled by a computer through a data acquisition card (DAQ). (b) In vivo measurements of PO_2 vs mean counts per millisecond as controlled by the diode laser power. Higher laser powers correlate with higher consumption of O_2 leading to a significant decrease of PO_2 estimates over time (seen in the first point when average counts exceed 10000). When limiting to 3000 average counts, no significant decrease in PO_2 could be measured over time. (c) Example of phosphorescence decay profiles under conditions where photo-consumption is negligible. Higher O_2 concentration causes more quenching of phosphorescence signal, and consequently a faster decay (red profile).

Experiments are performed in two steps. Focus is first achieved on the cortex and the animal is moved towards the objective to measure tissue at a depth of ~100 μm. Initially, a few points of interest are selected for measuring PO_2. Survey scan phosphorescence recordings are obtained by scanning these points and summing photon counts at each point using an excitation pulse duration and phosphorescence detection window of 100 μs and 500 μs respectively. From the survey scan counts of these points, the power of the laser diode for each point is adjusted for ensuing scans to minimize the photo-oxidative damage to tissue and limit consumption according to the number of measured counts in the survey. A value of counts around 3000 was sought based on Figure 4-2(b). Thus following survey scans, the same points are measured while averaging 100 times to increase the signal-to-noise ratio at varying laser power. Representative excitation and decay profiles are provided in Figure 4-2(c). Consequently, each PO_2 measurement at a given location required around 250 ms.

All data was processed using software custom-written in Matlab. Using a weighted least squares fitting routine, the resulting time decay curves at each point are fit with a single-exponential function:

$$I(t) = I_0 \exp\left(-\frac{t}{\tau}\right) + c \tag{4-2}$$

where I(t) represents the light intensity at time t and I_0 is the initial value of light intensity at time t=0. Here τ is the phosphorescence lifetime at the point being measured and c is the magnitude of

the baseline I_0. Following the estimated parameter τ, the Stern-Volmer formula was applied to calculate the PO_2 values.

4.3.5 Normal and variable F_iO_2 experiments

The system was first tested in vivo by monitoring PO_2 in cortical tissue near an artery and by varying the fraction of inspired oxygen (F_iO_2). In the first mouse, PO_2 values were measured in cortical tissue near the artery during the normal atmospheric gas fraction, which the F_iO_2 is 21%. In a second mouse, the inspired gas fractions was changed from normal to higher F_iO_2 from 21% to 40% for 10 minutes at t=260s. During each experiment, PO_2 values were measured at multiple selected positions.

4.3.6 PO_2 values and LFP data analysis in 4-AP injected mice

The LFP data was obtained from the tungsten electrode, which was filtered by a band-pass filter between 10 and 5000Hz, amplified 1000 times with a microelectrode AC amplifier (model 1800, A-M systems, Sequim, WA), and digitized at 10kHz. In post-processing the LFP data was filtered using a Butterworth digital filter between 0.2 and 130Hz. LFP data were acquired simultaneously to PO_2 to measure the onset-time of seizures and their duration. Since all measures were started a few minutes following 4-AP injection, identifying a baseline value PO_2 value was difficult. Therefore, the tissue PO_2 data were converted to percent change by subtracting then dividing the average value obtained over a 15s block of time before the onset of the epileptic events by the formula:

$$V_{\%} = \frac{V_{raw} - V_{mean}}{V_{mean}} \times 100\% \quad (4\text{-}3)$$

where V% is the final value of PO_2, V_{raw} is the raw value and V_{mean} is the average value over 15s block of PO_2 before onset. All data were expressed as means ± SE of mean (SE).

4.4 Results

4.4.1 PO_2 in normoxia and during variable F_iO_2

The spatial PO_2 profiles of tissue near an artery at 38 locations were measured in the somatosensory cortex of an anesthetized mouse during normoxia (Figure 4-3). Obtained PO_2

values were within the range of 6-25mmHg, in concordance with previously established cortical PO_2 levels by two-photon phosphorescence quenching technique (Sakadzić et al., 2010). Relatively high PO_2 values were measured close to a large artery, with a rapid PO_2 decrease at locations slightly further away from it reflecting values from the capillary bed. These results were in concordance with the fact that tissue PO_2 gradients exist at the cortical surface near arteries (Sharan et al., 2008).

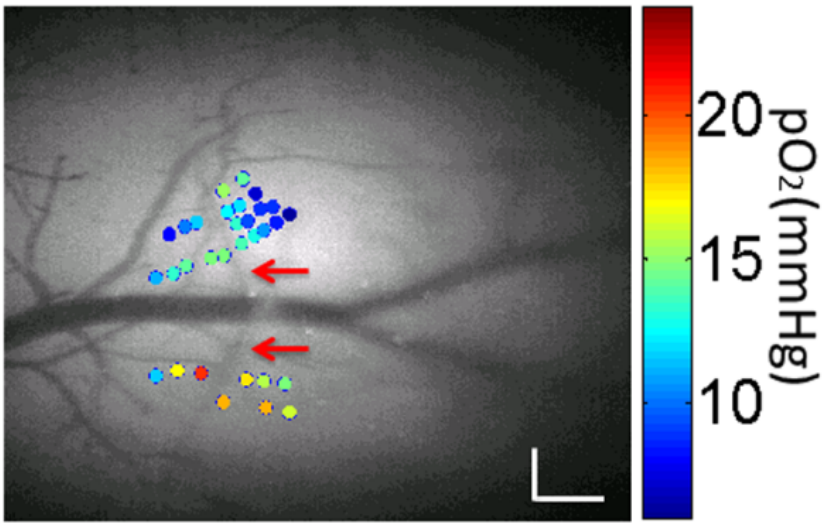

Figure 4-3: Measured PO_2 values during normoxia (color dots), overlaid with a grayscale angiogram of cortical pial tissue from an exposed window (with an artery shown by the red arrows) The size of scale bar is 0.2mm.

Confocal lifetime measurements have the capability of simultaneously monitoring tissue PO_2 at multiple locations. In a second animal, we obtained temporal PO_2 profiles at selected tissue locations as the F_iO_2 was altered from 21% to 40% (Figure 4-4). During the first few minutes at 21% F_iO_2, the surplus O_2 in the tissue met the metabolic demand. Our measurements (13.9±4.1 in tissue during the first few minutes) were found within the range of 5 to 25mmHg. Upon increasing the F_iO_2 from 21% to 40%, PO_2 increased greatly and then saturated. An increase of 13.1 ± 3.1 mmHg in tissue from normoxic to hyperoxia was observed. Following this change in F_iO_2, PO_2 values reached their peak after 191.5 ± 27.0 s in tissue.

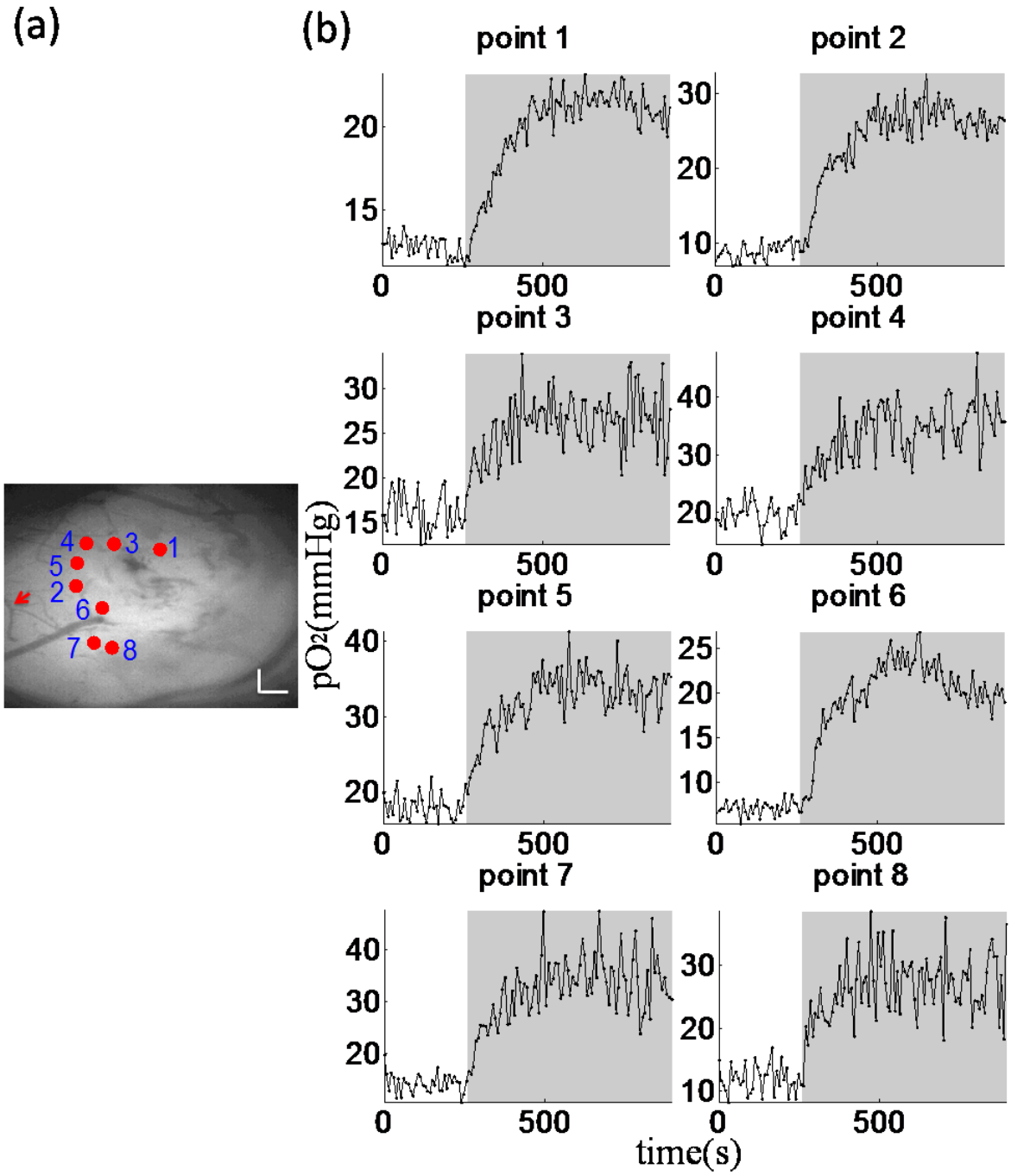

Figure 4-4: (a) Grayscale angiogram of cortical pial tissue with points of interest (red dots). Scale bar size: 0.2mm (b) Corresponding temporal profiles of PO_2 measured while altering FiO2. The gray segments denote the 10 minutes period during which FiO2 was increased up to 40%.

4.4.2 Tissue oxygenation at the focus and in the surrounding area during seizure-like activity

Seizure-like activity was elicited with injection of 4-AP and recorded by local field potentials with a tungsten electrode, and were characterized by fast rhythmic spiking activity of increasing amplitude and decreasing frequency, evolving into rhythmic spikes and slow wave activity prior to gradual offset (see e.g. Figure 4-5). One hundred and twenty-one (121) seizure-like events were recorded in 6 mice with mean (±SE) duration of 68.9±35.1s.

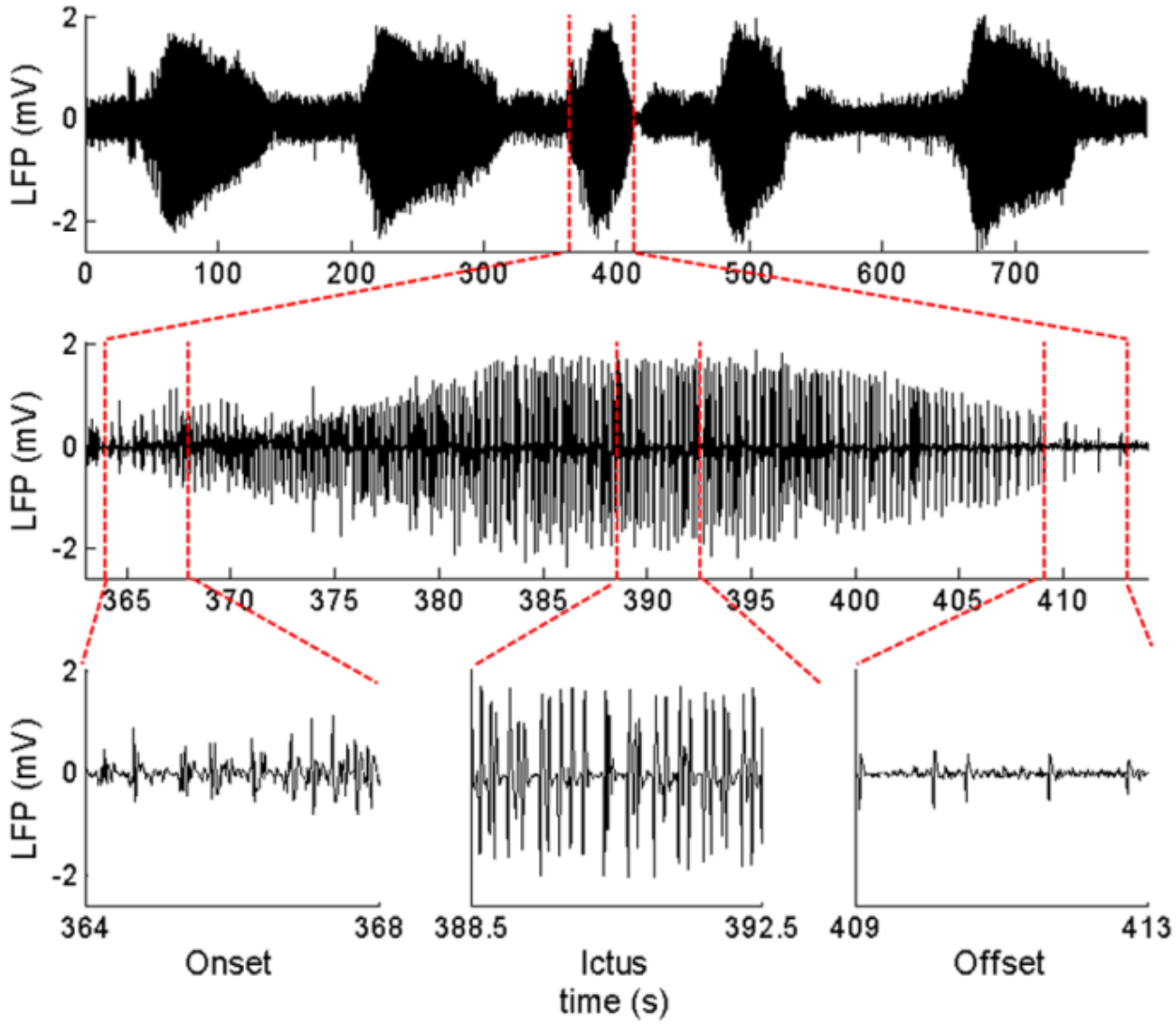

Figure 4-5: Electrophysiology of 4-AP induced epileptic activity. Top: example of ictal discharges after the 4-AP injection. Middle: zoom on an ictal discharge. Bottom: expanded view of showing the onset of the discharge, the intermediate phase and the offset.

To study simultaneously changes of tissue oxygenation at the focus and surrounding areas, points were selected both adjacent and distant from injection site in 3 mice (Figure 4-6a). An example of change in PO_2 in the focus and surrounding areas from a single animal is shown in Figure 4-6b. At the focus, the typical PO_2 profile was biphasic with an early dip after ictal onset (deoxygenation), followed by a longer duration increase in PO_2 (hyperoxygenation). The early dip in the focus was described in previous papers during seizures (Bahar et al., 2006) and was present in most seizures measured here. At a distance from the ictal focus, the PO_2 was monophasic and significantly increased, returning to the baseline at the offset of the seizure. These results were in agreement with tissue oxygen measured by oxygen microelectrodes (Zhao et al., 2009). To assess the spatial distribution of PO_2 around the focus, points were scanned near the focus in the form of a spiral during epileptic activity, where initial dips were measured. Figure 4-6c shows an example of measured percent of initial dip for different locations overlaid on a grayscale anatomical image. The higher values were obtained near the focus, and PO_2 decreased when points were farther away from the focus. These data indicated that the influx of blood into the focus was inadequate to perfuse the hypermetabolic neurons, after which there was a period of hyperperfusion and hyperoxygenation.

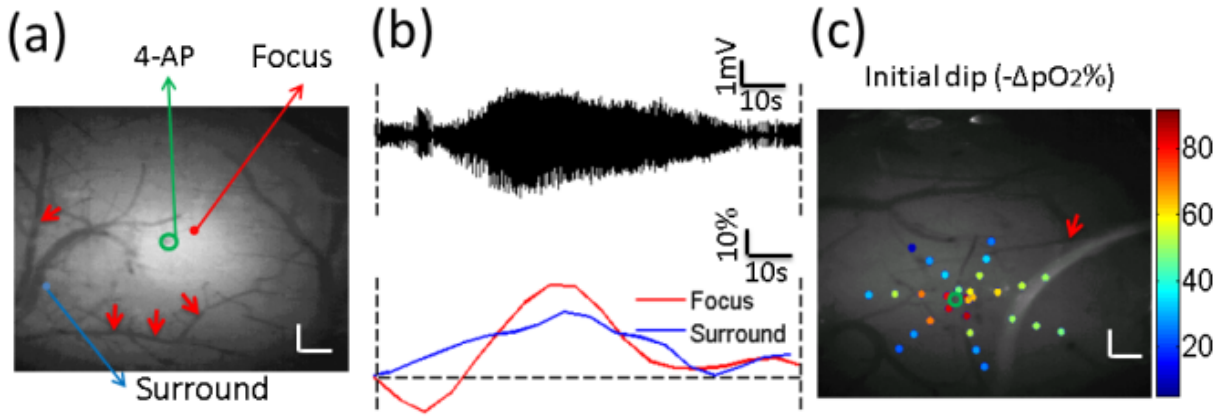

Figure 4-6: Obtained PO_2 values in tissue near the focus and surround. (a) Grayscale angiogram of cortical surface and locations for pO_2 measurement (red: focus; blue: surround). The artery was shown by the red arrows. Scale bar size: 0.2mm (b) Epileptic activity induced a transient dip

in tissue PO_2 followed by an increase in PO_2 in the focus. A sustained increase in PO_2 was seen in the surround. The dashed vertical lines show the ictal onset (left) and offset (right). (c) Distribution of percent of initial dip at multiple locations (color dotted) during epileptic activity. The 4-AP injection site is shown by green circle. The artery was shown by the red arrows. Scale bar size: 0.2mm

4.4.3 Correlation between the percent of initial dip and distance from the artery

To study oxidative metabolism near arteries during epileptic activity, 3 mice were recorded with measures at multiple locations near an artery that was close to the injection site. The percent PO_2 value changes adjacent to the artery were significantly lower than values located farther away (an example shown in Figure 4-7a) despite some points being closer to the focus. Figure 4-7b shows a linear relationship between arterial perpendicular distance and percent of initial dip which indicates a contribution of the vascular anatomy to define the focus-surround regions. Sites that were farther from an artery, located in the capillary bed, elicited a larger decrease in tissue PO_2 after onset. Extending data to the three mice, the slopes of these linear fit were combined over all seizures in Figure 4-7c, in all cases preserving the positive relationship. This data indicates that the vascular micro-environment contributes to oxygen consumption in the tissue during epileptic seizures.

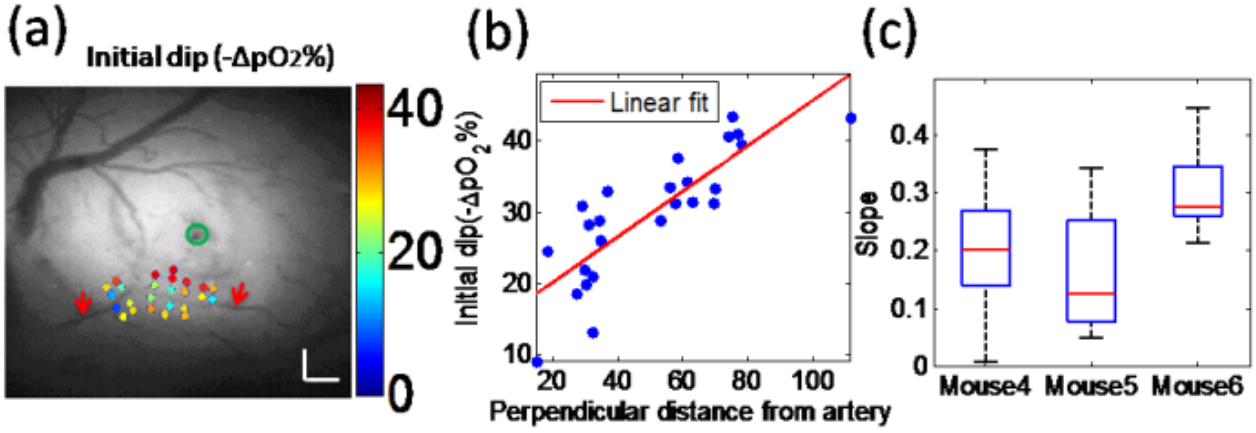

Figure 4-7: Correlation between percent change of the initial dip at multiple locations and distances from an artery (a) Measured PO_2 values of different points near an artery during the epileptic seizure (color dots), overlaid with a grayscale anatomy (with an artery shown by the red

arrows). Scale bar size: 0.2mm (b) Relationship between distance from an artery for multiple points and initial dip during one epileptic seizure. The line of linear fit is, $R^2 = 0.70$. (C) Boxplots of slopes of linear fits in 3 mice over 25 seizures.

4.4.4 Correlation between initial dip and seizure duration

Because seizures had different durations, it was of interest to see if correlations between oxygenation and electrographic seizure duration were present. Linear regressions between the initial dip expressed as a percent change and seizure duration indeed showed significant correlations (an example shown in Figure 4-8a). This data suggest that long epileptic seizures may be accompanied by early increased oxygen consumption in the tissue. The slopes of fit between epileptic seizure duration and initial dip, distributed over spatial location measurements (shown in Figure 4-8b) over all seizures. Data in all mice show similar results: a positive moderate correlation was found between early metabolism in the interstitial space near the focus and duration of epileptic activities though the relationship had significant variability across the population.

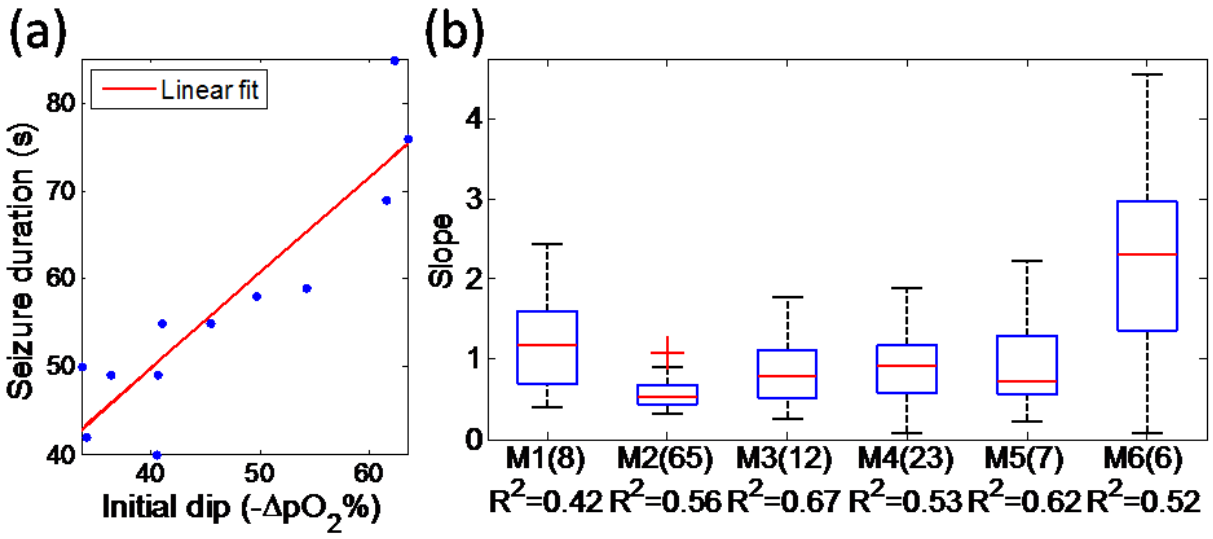

Figure 4-8: a) Correlation between initial dip (% change) and duration of epileptic activity. The line of linear fit was, R^2=0.81 (b) Statistical distribution of the slopes for all mice. M1 was the name of mouse and number in the bracket was the number of seizures that was calculated. The outliers were plotted with red plus sign. The average of goodness of fit (R^2) was listed for each mouse.

4.5 Discussion

The results of our investigation demonstrate that tissue oxygenation can be measured in the mouse cortex using a confocal phosphorescence lifetime measurements given appropriate excitation regime. With respect to brain studies, the key advantages of confocal lifetime system are its minimal disturbance of investigated tissue and the possibility to achieve high temporal and spatial resolution. The probe signal is independent of pH throughout the physiological range and is not affected by the presence of biological macromolecules (Esipova et al., 2011). However, each PO_2 measurements required collection of 100 decays at each point to yield a reliable PO_2 value, thus limiting the temporal resolution of the method. Moreover, light scattering by brain tissue limits our confocal PO_2 measurements to tissue located up to 100 μm deep near the cortical surface which may confound results investigating oxygen diffusion from arterioles. Combining lifetime-based PO_2 monitoring with multiphoton excitation may help overcome some of these issues in future cerebral oxygenation investigations.

We have successfully used confocal lifetime system to investigate tissue PO_2 in somatosensory cortex during normal state and epileptic activity induced by 4-AP. Our findings bring new evidence regarding tissue oxygen changes during epileptic activity, by characterizing the relationship between tissue oxygen changes and seizure duration.

4.5.1 Tissue PO_2 gradient near arteries in normoxia

Our work confirmed previous evidence that arteries are largely responsible for the heterogeneous oxygen distribution in the cortex. The observed variations in tissue PO_2 values near brain arteries showed a drop in the PO_2 values of points distant from an artery and located in the capillary bed during normoxia (Figure 4-3). Similar PO_2 gradients were also found by several investigators employing different methods (Sakadzić et al., 2010; Sharan et al., 2008). For instance, near the pial artery in the rat cortex, a similar tendency was reported by Sakadzic et al. (Sakadzić et al., 2010) with two-photon phosphorescence lifetime measurements. In addition, several theoretical models have predicted that steep PO_2 gradients arise in the vicinity of blood vessels (Ivanov et al., 1979; Secomb et al., 2000). Localized large tissue PO_2 values suggests that arteries provide a major source of O_2 to tissue (Sakadžić et al., 2014) while our PO_2 values of locations far away

from arteries (above ~60μm) most likely rely on capillaries which are invisible from the cortical surface (Kasischke et al., 2011).

4.5.2 Acute seizure activity leads to transient dip of PO_2 near epileptic focus

Some controversy remains in the literature as to whether local cerebral blood flow increases are adequate to meet supranormal oxygen demands throughout the ictus. Although the inadequacy of cerebral blood flow in addressing oxygen demands has been demonstrated by some investigators, there is also growing evidence of inadequate oxygenation at the onset or throughout shorter duration epileptic events (Nguyen et al., 2013; Schridde et al., 2008; Zhao et al., 2011). In this study, a clear transient decrease in tissue oxygenation at multiple locations near the injection site after onset was shown, indicating that the increased metabolism of oxygen overwhelms the ability of the brain to provide oxygenated blood by increasing cerebral blood flow during the seizure-like activity in and near the focus. This observation may be useful at predicting the location of seizures. A significant increase in tissue oxygen consumption at multiple locations close to the focus was observed in the somatosensory cortex when mice had seizure-like activity (Figure 4-6c). Moreover, farther away from the focus there was increase in tissue oxygen with respect to baseline.

Previous literature using oxygen microelectrodes documented a transient dip in two locations: near the focus and an increase in the surround in epileptic rats during seizures (Zhao et al., 2009). In our present work, which focused on tissue oxygen changes at multiple locations (>2) during acute epileptiform events, we show a significant initial dip at multiple locations in our mice. With the ability of our system to gather spatial measures, our results indicate that the distance between the surround and the injection site (around 1.5mm) was a little smaller than what was measured in previous work (around 2mm) (Zhao et al., 2009). Whether the observed difference is due to changes in animal species, high metabolic demand at seizure locations near vessels remains to be investigated.

4.5.3 The relationship between the initial dip and distance from arterioles

Exploiting the spatial measures, we investigated how tissue oxygen pressure changed at different points near a surface arteriole located in the focus region during epileptiform activity. Despite increased consumption in the focus, arteriolar O_2 diffusion remained partially unaffected: a

significant increase in the initial dip was observed with increased distance from the arteriole (see Figure 4-7) in three mice. These data are the first showing measurements of PO_2 gradients in brain arterioles during epileptic activity confirming that the arteriolar wall played a significant role in oxygen exchange between blood and tissue (Zhao et al., 2009). Our microscopic assessments thus paint a more complex spatial picture of oxygen consumption during epileptic seizures since arteries take part in diffusional exchange of respiratory gases (mainly oxygen) to tissue. This is in contrast to previous studies showing uniform cerebral blood volume (CBV) and cerebral blood flow (CBF) increase in the focus during epileptic events (Masamoto et al., 2003; Thompson et al., 2003) (Guevara et al., 2013; Zhao et al., 2009) to supply oxygen to meet demands of neuronal activity. The vascular architecture thus generates a microscopic structure to the epileptic focus, as our data showing increased initial dips far away from arteries, in capillary beds, suggest. Our results further suggest that the increased CBF and CBV will supply more oxygen to the tissue near an artery, but may not meet the demands of oxygen metabolism far away from an artery. Potential associated tissue and neuronal damage is thus more likely to occur, microscopically, in areas far from these feeding arteries.

4.5.4 The relationship between initial dip and seizure duration

Our data indicate that initial dips of greater amplitude are predictive of seizures of greater duration. Few studies have investigated such a link between oxygen metabolism and seizure duration. However, some researchers observed that a biphasic deoxyhemoglobin (HbR) response to ictal events with an initial decrease in HbR followed by a longer increase in HbR measured by NIRS may be related to longer seizure duration (Nguyen et al., 2013). These previous findings proposed that increased seizure duration could lead to increased oxidative metabolism. The etiology of tissue oxygen changes as the duration of seizures is increased remains unknown. The possibility is that longer seizures were induced by increased initial neuronal activities, which will lead to more decrease in tissue oxygenation (Masamoto et al., 2003; Thompson et al., 2003). Our study indicates that it might be possible to predict seizure duration from the initial dip amplitude.

4.5.5 Limitation

While we limited the number of pulses and counts during recordings to diminish photoconsumptive effects, survey scans could lead to the production of singlet oxygen as some

areas were subject to higher light intensity than required by our 3000 counts estimation during the calibration phase. To address this issue, our acquisitions were careful to limit light intensity during survey scans and a pause was done between survey scans and acquisitions presented here to insure tissue oxygen is replenished. Despite these steps, we cannot completely rule out the possibility of tissue damage during survey scans due to singlet oxygen generated by the probe. Furthermore, the elongated focus of the confocal setup failed to precisely assess distribution of oxygen in the depth axis, limiting conclusions on oxygen diffusion during seizure, this we hope to revisit using the recently developed two-photon technique. Finally, a potential bias in measured PO_2 values during epileptiform discharges may occur due to a small increase in temperature at the epileptic foci. Given the small change in decay parameters measured for G4 with fractional temperature change, this was neglected in estimations above.

4.6 Conclusion

We developed an imaging technique that provides absolute values of PO_2 in the brain cortex by means of confocal phosphorescence lifetime microscopy. The technique was applied to study partial oxygen pressure changes in tissue during epileptic activity in mice. To our knowledge, this is the first report of direct measurements of tissue oxygen at multiple locations (more than 2 locations) during epilepsy. In our work, following 4-AP injection in the somatosensory cortex of mice, we observed significant changes of PO_2 in tissue near the injection site, and investigated its changes along arteries and in the surround. This study supported the existence of an initial dip and characterized the spatial distribution of the initial dip around the focus and near pial arteries. In addition, we found a positive correlation between the early oxygen metabolism in tissue and the duration of seizures. With regards to clinical relevance, our observations may eventually help the cause of epileptic focus localization and elucidate the link relating seizure duration and initial dip amplitude.

4.7 Acknowledgments

We thank S. Vinogradov for discussions and generously sharing the G4 molecular probe and Marc-Antoine Gillis for his assistance in animal preparation.

4.8 References

Ances, B.M., Buerk, D.G., Greenberg, J.H., Detre, J.A., 2001. Temporal dynamics of the partial pressure of brain tissue oxygen during functional forepaw stimulation in rats. Neurosci. Lett. 306, 106–110.

Arthurs, O.J., Williams, E.J., Carpenter, T.A., Pickard, J.D., Boniface, S.J., 2000. Linear coupling between functional magnetic resonance imaging and evoked potential amplitude in human somatosensory cortex. Neuroscience 101, 803–806.

Bahar, S., Suh, M., Zhao, M., Schwartz, T.H., 2006. Intrinsic optical signal imaging of neocortical seizures: the "epileptic dip." Neuroreport 17, 499–503. doi:10.1097/01.wnr.0000209010.78599.f5

Cheng, M.Y., Wang, E.H., Woodson, W.J., Wang, S., Sun, G., Lee, A.G., Arac, A., Fenno, L.E., Deisseroth, K., Steinberg, G.K., 2014. Optogenetic neuronal stimulation promotes functional recovery after stroke. Proc. Natl. Acad. Sci. U. S. A. 111, 12913–12918. doi:10.1073/pnas.1404109111

Dunphy, I., Vinogradov, S.A., Wilson, D.F., 2002. Oxyphor R2 and G2: phosphors for measuring oxygen by oxygen-dependent quenching of phosphorescence. Anal. Biochem. 310, 191–198.

Esipova, T.V., Karagodov, A., Miller, J., Wilson, D.F., Busch, T.M., Vinogradov, S.A., 2011. Two new "protected" oxyphors for biological oximetry: properties and application in tumor imaging. Anal. Chem. 83, 8756–8765. doi:10.1021/ac2022234

Estrada, A.D., Ponticorvo, A., Ford, T.N., Dunn, A.K., 2008. Microvascular oxygen quantification using two-photon microscopy. Opt. Lett. 33, 1038–1040.

Ferris, C.F., Marella, M., Smerkers, B., Barchet, T.M., Gershman, B., Matsuno-Yagi, A., Yagi, T., 2013. A phenotypic model recapitulating the neuropathology of Parkinson's disease. Brain Behav. 3, 351–366. doi:10.1002/brb3.138

Finikova, O.S., Lebedev, A.Y., Aprelev, A., Troxler, T., Gao, F., Garnacho, C., Muro, S., Hochstrasser, R.M., Vinogradov, S.A., 2008. Oxygen microscopy by two-photon-excited phosphorescence. Chemphyschem Eur. J. Chem. Phys. Phys. Chem. 9, 1673–1679. doi:10.1002/cphc.200800296

Golub, A.S., Pittman, R.N., 2008. PO2 measurements in the microcirculation using phosphorescence quenching microscopy at high magnification. Am. J. Physiol. Heart Circ. Physiol. 294, H2905–2916. doi:10.1152/ajpheart.01347.2007

Guevara, E., Pouliot, P., Nguyen, D.K., Lesage, F., 2013. Optical imaging of acute epileptic networks in mice. J. Biomed. Opt. 18, 76021. doi:10.1117/1.JBO.18.7.076021

Hogan, M.C., 1999. Phosphorescence quenching method for measurement of intracellular in isolated skeletal muscle fibers. J. Appl. Physiol. 86, 720–724.

Hyder, F., Rothman, D.L., Shulman, R.G., 2002. Total neuroenergetics support localized brain activity: implications for the interpretation of fMRI. Proc. Natl. Acad. Sci. U. S. A. 99, 10771–10776. doi:10.1073/pnas.132272299

Ivanov, K.P., Kislayokov, Y.Y., Samoilov, M.O., 1979. Microcirculation and transport of oxygen to neurons of the brain. Microvasc. Res. 18, 434–441. doi:10.1016/0026-2862(79)90049-9

Kasischke, K.A., Lambert, E.M., Panepento, B., Sun, A., Gelbard, H.A., Burgess, R.W., Foster, T.H., Nedergaard, M., 2011. Two-photon NADH imaging exposes boundaries of oxygen diffusion in cortical vascular supply regions. J. Cereb. Blood Flow Metab. Off. J. Int. Soc. Cereb. Blood Flow Metab. 31, 68–81. doi:10.1038/jcbfm.2010.158

Lauritzen, M., 2001. Relationship of spikes, synaptic activity, and local changes of cerebral blood flow. J. Cereb. Blood Flow Metab. Off. J. Int. Soc. Cereb. Blood Flow Metab. 21, 1367–1383. doi:10.1097/00004647-200112000-00001

Lebedev, A.Y., Cheprakov, A.V., Sakadzić, S., Boas, D.A., Wilson, D.F., Vinogradov, S.A., 2009. Dendritic phosphorescent probes for oxygen imaging in biological systems. ACS Appl. Mater. Interfaces 1, 1292–1304. doi:10.1021/am9001698

Masamoto, K., Omura, T., Takizawa, N., Kobayashi, H., Katura, T., Maki, A., Kawaguchi, H., Tanishita, K., 2003. Biphasic changes in tissue partial pressure of oxygen closely related to localized neural activity in guinea pig auditory cortex. J. Cereb. Blood Flow Metab. Off. J. Int. Soc. Cereb. Blood Flow Metab. 23, 1075–1084. doi:10.1097/01.WCB.0000084248.20114.B3

Mintun, M.A., Lundstrom, B.N., Snyder, A.Z., Vlassenko, A.G., Shulman, G.L., Raichle, M.E., 2001. Blood flow and oxygen delivery to human brain during functional activity: theoretical

modeling and experimental data. Proc. Natl. Acad. Sci. U. S. A. 98, 6859–6864. doi:10.1073/pnas.111164398

Nagata, K., Sato, M., Satoh, Y., Watahiki, Y., Kondoh, Y., Sugawara, M., Box, G., Wright, D., Leung, S., Yuya, H., Shimosegawa, E., 2002. Hemodynamic aspects of Alzheimer's disease. Ann. N. Y. Acad. Sci. 977, 391–402.

Nguyen, D.K., Tremblay, J., Pouliot, P., Vannasing, P., Florea, O., Carmant, L., Lepore, F., Sawan, M., Lesage, F., Lassonde, M., 2013. Noninvasive continuous functional near-infrared spectroscopy combined with electroencephalography recording of frontal lobe seizures. Epilepsia 54, 331–340. doi:10.1111/epi.12011

Norup Nielsen, A., Lauritzen, M., 2001. Coupling and uncoupling of activity-dependent increases of neuronal activity and blood flow in rat somatosensory cortex. J. Physiol. 533, 773–785.

Osharina, V., Ponchel, E., Aarabi, A., Grebe, R., Wallois, F., 2010. Local haemodynamic changes preceding interictal spikes: a simultaneous electrocorticography (ECoG) and near-infrared spectroscopy (NIRS) analysis in rats. NeuroImage 50, 600–607. doi:10.1016/j.neuroimage.2010.01.009

Papkovsky, D.B., Dmitriev, R.I., 2013. Biological detection by optical oxygen sensing. Chem. Soc. Rev. 42, 8700–8732. doi:10.1039/c3cs60131e

Plant, R.L., Burns, D.H., 1993. Quantitative, Depth-Resolved Imaging of Oxygen Concentration by Phosphorescence Lifetime Measurement. Appl. Spectrosc. 47, 1594–1599.

Pouliot, P., Tremblay, J., Robert, M., Vannasing, P., Lepore, F., Lassonde, M., Sawan, M., Nguyen, D.K., Lesage, F., 2012. Nonlinear hemodynamic responses in human epilepsy: a multimodal analysis with fNIRS-EEG and fMRI-EEG. J. Neurosci. Methods 204, 326–340. doi:10.1016/j.jneumeth.2011.11.016

Quaranta, M., Borisov, S.M., Klimant, I., 2012. Indicators for optical oxygen sensors. Bioanal. Rev. 4, 115–157. doi:10.1007/s12566-012-0032-y

Rumsey, W.L., Vanderkooi, J.M., Wilson, D.F., 1988. Imaging of phosphorescence: a novel method for measuring oxygen distribution in perfused tissue. Science 241, 1649–1651.

Sakadžić, S., Mandeville, E.T., Gagnon, L., Musacchia, J.J., Yaseen, M.A., Yucel, M.A., Lefebvre, J., Lesage, F., Dale, A.M., Eikermann-Haerter, K., Ayata, C., Srinivasan, V.J., Lo, E.H., Devor, A., Boas, D.A., 2014. Large arteriolar component of oxygen delivery implies a safe margin of oxygen supply to cerebral tissue. Nat. Commun. 5, 5734. doi:10.1038/ncomms6734

Sakadzić, S., Roussakis, E., Yaseen, M.A., Mandeville, E.T., Srinivasan, V.J., Arai, K., Ruvinskaya, S., Devor, A., Lo, E.H., Vinogradov, S.A., Boas, D.A., 2010. Two-photon high-resolution measurement of partial pressure of oxygen in cerebral vasculature and tissue. Nat. Methods 7, 755–759. doi:10.1038/nmeth.1490

Secomb, T.W., Hsu, R., Beamer, N.B., Coull, B.M., 2000. Theoretical simulation of oxygen transport to brain by networks of microvessels: effects of oxygen supply and demand on tissue hypoxia. Microcirc. N. Y. N 1994 7, 237–247.

Sharan, M., Vovenko, E.P., Vadapalli, A., Popel, A.S., Pittman, R.N., 2008. Experimental and theoretical studies of oxygen gradients in rat pial microvessels. J. Cereb. Blood Flow Metab. Off. J. Int. Soc. Cereb. Blood Flow Metab. 28, 1597–1604. doi:10.1038/jcbfm.2008.51

Shonat, R.D., Kight, A.C., 2003. Oxygen tension imaging in the mouse retina. Ann. Biomed. Eng. 31, 1084–1096.

Shonat, R.D., Wachman, E.S., Niu, W., Koretsky, A.P., Farkas, D.L., 1997. Near-simultaneous hemoglobin saturation and oxygen tension maps in mouse brain using an AOTF microscope. Biophys. J. 73, 1223–1231.

Smith, L.M., Golub, A.S., Pittman, R.N., 2002. Interstitial PO(2) determination by phosphorescence quenching microscopy. Microcirc. N. Y. N 1994 9, 389–395. doi:10.1038/sj.mn.7800147

Thompson, J.K., Peterson, M.R., Freeman, R.D., 2003. Single-neuron activity and tissue oxygenation in the cerebral cortex. Science 299, 1070–1072. doi:10.1126/science.1079220

Torres Filho, I.P., Leunig, M., Yuan, F., Intaglietta, M., Jain, R.K., 1994. Noninvasive measurement of microvascular and interstitial oxygen profiles in a human tumor in SCID mice. Proc. Natl. Acad. Sci. U. S. A. 91, 2081–2085.

Vanderkooi, J.M., Maniara, G., Green, T.J., Wilson, D.F., 1987. An optical method for measurement of dioxygen concentration based upon quenching of phosphorescence. J. Biol. Chem. 262, 5476–5482.

Vinogradov, S.A., Wilson, D.F., 2011. Porphyrin dendrimers as biological oxygen sensors, in: Designing Dendrimers. John Wiley & Sons, pp. 463 – 503.

Wilson, D.F., Vinogradov, S.A., Grosul, P., Vaccarezza, M.N., Kuroki, A., Bennett, J., 2005. Oxygen distribution and vascular injury in the mouse eye measured by phosphorescence-lifetime imaging. Appl. Opt. 44, 5239–5248.

Zhao, M., Ma, H., Suh, M., Schwartz, T.H., 2009. Spatiotemporal dynamics of perfusion and oximetry during ictal discharges in the rat neocortex. J. Neurosci. Off. J. Soc. Neurosci. 29, 2814–2823. doi:10.1523/JNEUROSCI.4667-08.2009

Zhao, M., Nguyen, J., Ma, H., Nishimura, N., Schaffer, C.B., Schwartz, T.H., 2011. Preictal and ictal neurovascular and metabolic coupling surrounding a seizure focus. J. Neurosci. Off. J. Soc. Neurosci. 31, 13292–13300. doi:10.1523/JNEUROSCI.2597-11.2011

CHAPTER 5 ARTICLE 2: ASTROCYTIC ENDFOOT CA2+ MODULATES ARTERIOLAR RESPONSES DURING EPILEPSY: AN IN VIVO TWO-PHOTON LIFETIME MICROSCOPY STUDY

Cong Zhang[1], Maryam Tabatabaei[2], Samuel Bélanger[1], Hélène Girouard[3], and Frédéric Lesage[1,4]

1École Polytechnique de Montréal, Department of Electrical Engineering, C.P. 6079 succ.Centre-ville, Montreal, Quebec, Canada, H3C 3A7

2École Polytechnique de Montréal, Department of Computer Engineering, C.P. 6079 succ.Centre-ville, Montreal, Quebec, Canada, H3C 3A7

3University of Montreal, Department of Pharmacology, Montreal, Quebec, Canada, H3C 3J7

4Montreal Heart Institute, 5000 Bélanger street, Montreal, Quebec, Canada, H1T 1C8

Correspondance: Dr. Frédéric Lesage, École Polytechnique de Montréal, Department of Electrical Engineering, C.P. 6079 succ.Centre-ville, Montreal, Quebec, H3C 3A7; Tel: +1 514-340-4711x7542; Fax: +1 514-340-4611;

E-mail: frederic.lesage@polymtl.ca

This article aimed to address the second objective of this thesis. In this work, we applied the two-photon lifetime microscopy to simultaneously measure the calcium concentration in astrocytic endfeet and diameter of precapillary arterioles during epileptic seizures in mouse cortex. Our results confirm that the role of astrocytes in the control of local microcirculation and suggest a modulating role for baseline absolute Ca^{2+} concentration in astrocyte endfeet. This article was submitted to Journal of Cerebral Blood Flow & Metabolism and it is in revision.

5.1 Abstract

Neurovascular coupling (NVC) underlying the local increase in blood flow during neural activity forms the basis of functional brain imaging and is altered in epilepsy. Because astrocytic calcium (Ca^{2+}) signaling is involved in NVC, this study investigates the role of this pathway in epilepsy. Here we exploit 4-AP induced epileptic events to show that absolute Ca^{2+} concentration in cortical astrocyte endfeet in vivo modulates the diameter of precapillary arterioles during neural activity. We simultaneously monitored free Ca^{2+} concentration in astrocytic endfeet with the

Ca^{2+}-sensitive indicator OGB-1 and diameter of adjacent arterioles in the somatosensory cortex of adult mice by two-photon fluorescence lifetime measurements following 4-AP injection. Our results reveal that, regardless of the mechanism by which astrocytic endfoot Ca^{2+} was elevated during epileptic events, increases in Ca^{2+} induced vasodilation for each individual ictal event in the focus. In the remote area, increases in Ca^{2+} correlated with vasoconstriction at the onset of seizure and vasodilation during the later part of the seizure. Furthermore, a slow increase in absolute Ca^{2+} with time following multiple seizures was observed, which in turn, caused a trend of arteriolar constriction both at the epileptic focus and remote areas. These observations confirm the role of astrocytes in the control of local microcirculation and suggest a modulating role for baseline absolute Ca^{2+} concentration in astrocyte endfeet.

Keywords: Two-photon fluorescence lifetime imaging, Astrocyte, Intracellular calcium, Diameter, Epilepsy

5.2 Introduction

The brain has high-energy demand and requires a constant and continuous supply of oxygen and glucose for normal function. To ensure that blood supply matches metabolic needs, the brain possesses a major control mechanism, namely neurovascular coupling. Neurovascular coupling (Arthurs et al., 2000; Attwell et al., 2010; Otsu et al., 2015; Shih et al., 2012) or functional hyperemia is defined as a local increase in cerebral blood flow in response to neuronal activity. Part of this vascular regulation, via the synaptic activation of astrocytes, remains to be clearly defined. Astrocytes are a subtype of glial cells and a significant part of them are in close proximity of cerebral blood vessels with endfeet process almost completely enveloping cerebral blood vessels. The interplay between the astrocytic endfoot and the cerebral vasculature is an area of intense investigation. Recent evidence further suggests that neuronal activity is also encoded by astrocytes in the form of dynamic intracellular calcium (Ca^{2+}) signals, which travel to astrocytic endfoot encasing the arterioles in the brain. Astrocytic Ca^{2+} signaling has been implicated in the dilatory response of adjacent arterioles, linking neuronal activity to enhanced local blood flow (Filosa et al., 2006; Girouard et al., 2010; Gordon et al., 2008; Howarth, 2014; Straub et al., 2006; Takano et al., 2006).

Epilepsy is a common neurological disease characterized by recurrent unprovoked seizures, which result from abnormal and excessive neuronal activity in the brain. At a cellular level these events reflect intense and highly synchronous discharges that involve large numbers of cortical neurons (Truccolo et al., 2011). In both animal models and patients, the epileptic discharges can evoke drastic increases in cerebral blood flow (CBF) to meet the high metabolic demand caused by this intense neuronal activity (Nguyen et al., 2013; Zhao et al., 2011, 2009, 2007). However, observations of the hemodynamic response during seizures have also displayed non-linear phenomena, mostly less response than linear phenomena (Pouliot et al., 2012a). Mechanisms underlying these observations are to be identified. In brain slices, using uncaged Ca^{2+} in astrocytic endfeet, it was shown that a high increase in the absolute concentration of Ca^{2+} leads to vasoconstriction (Girouard et al., 2010). Whether this phenomenon contributes to the non-linear inhibitory effects observed in epilepsy is an open question. The relationship between absolute Ca^{2+} concentrations in astrocytic endfeet and the vascular response during ictal events is unknown, and it is unclear whether or not changes in endfeet Ca^{2+} can account for the full spectrum of vascular responses to neuronal activity in epilepsy.

In contrast to the common intensity-based measurements, fluorescence lifetime imaging (FLIM) techniques that use specific indicators to monitor nanometer-scale molecular interactions in live cells have been emerging (Pérez Koldenkova and Nagai, 2013; Zheng et al., 2015). It was also demonstrated that the fluorescence lifetime of some commonly used Ca^{2+} sensitive dyes, such as Oregon Green 488 BAPTA-1 (OGB-1), is sensitive to free Ca^{2+} in the physiological nanomolar range (Wilms et al., 2006; Wilms and Eilers, 2007). Compared to ratiometric methods to evaluate absolute concentration, the lifetime technique is immune to absorption and fluorescence bleaching effects making it more suitable for in vivo imaging. This property of OGB-1 has led to the successful evaluation of Ca^{2+} changes in astroglia of normal and Alzheimer's disease mice models (Kuchibhotla et al., 2009; Zheng et al., 2015). In this work we designed a two-photon FLIM system that enables imaging of deep brain tissue in live animals with single cell spatial resolution. We adapted the FLIM technique to investigate the role of astrocytes in the response of cerebral blood vessels to epileptiform discharges. By using a 4-aminopyridine (4-AP) model of focal seizures in vivo, we found that ictal, seizure-like discharges were rapidly followed by large Ca^{2+} increases in astrocyte endfeet.

5.3 Materials and Methods

5.3.1 Animal preparation

Animals were used according to the ARRIVE guidelines and the recommendations of the Canadian Council on Animal Care. The Animal Research Ethics Committee of the Montreal Heart Institute approved all procedures. Fourteen male C57/BL6 mice (Charles-River, postnatal 8 weeks old, 20-25g weight), of which three died before data acquisitions due to movement of the catheter in the femoral artery, were deeply anesthetized with 1-1.6g/kg urethane and body temperature was maintained at 37°C with a controlled physiological monitoring system that also monitored heart and respiration rates continuously (Labeotech Inc., CA). Mice breathed via a tracheal tube to reduce the risk of respiratory depression often seen with the use of this anesthetic. A moderate flow of ambient air lightly supplemented with oxygen was supplied next to the tracheotomy (10% oxygen, 90% air, 1 L/min). Animals were placed in a stereotaxic frame. A ~2×2 mm cranial window was opened over one hemisphere to expose the somatosensory cortex and surrounding brain (AP: -1.5 mm, DV: +1.5 mm). A small hole was drilled next to the cranial window for the injection of 4-AP (Figure 5-1C). After injection of the Ca^{2+} indicators, the cranial window was sealed with 1% agarose in artificial cerebrospinal fluid (aCSF, 125 mM NaCl, 10 mM HEPES, 10 mM glucose, 5 mM KCl, 1,5 mM CaCl2, 1 mM MgSO4) using a 150 µm-thick microscope coverslip. During the experiment, a catheter in the femoral artery was used to monitor the blood gases (PCO_2, 36-39 mmHg, and PO_2, 110-160 mmHg). The average blood pressure (80-110 mmHg) was obtained non-invasively by a tail-cuff blood pressure system (Kent Scientific). At the end of the surgery, 500 µL of saline was injected subcutaneously to avoid animal dehydration during imaging. Surgery was started in the morning and imaging sessions debuted around noon. Prior to procedures, mice were kept in a 12:12 hours light-dark cycle in ventilated cages.

5.3.2 Ca^{2+} indicator loading

Multi-cell bolus loading was performed to load neurons and glial cells with the Ca^{2+} sensitive fluorescence indicator OGB-1 and the astrocyte specific fluorescence marker, Sulforhodamine 101 (SR101). A patch pipette with a tip diameter of 30~60 µm was inserted into the cortex to a depth of ~300 µm from the surface. OGB-1 (50 µg, O-6807, Molecular probes-Invitrogen, CA,

USA) was dissolved in dimethyl sulfoxide (DMSO) containing 20% pluronic acid (F-127, Sigma-Aldrich) and mixed in 412 μM SR101 (Sigma-Aldrich) to a final concentration of 1 mM (Cirillo et al., 2012; Garaschuk et al., 2006). One uL OGB-1 and SR101 were injected with a micropipette using a microsyringe pump controller (UMP3, World Precision Instruments, Sarasota, FL) at a rate of 100 μL/min. After injection, we allowed one hour for loading. To label vasculature, Rhodamine B isothiocyanate-Dextran (200 μL of 100mg/mL solution, molecular weight ~ 70,000 Da, Sigma-Aldrich), which highlights blood plasma, was injected into the tail vein. Serial images from the pial surface to cortex layers 2/3 (~200 μm deep) revealed that OGB-1 signals strictly co-localized with SR101 staining in astrocytes (Figure 5-1B).

5.3.3 Epileptogenesis and electrophysiology

Ictal discharges were induced by injecting the potassium channel blocker 4-aminopyridine (4-AP; Sigma; 15mM, 0.5 μL) through a glass microelectrode using a syringe pump controller into a small hole next to the cranial window (Zhao et al., 2007) (Figure 5-1C), similar to the injection of mixed OGB-1 and SR101 described above. Extracellular local field potentials (LFP) were recorded with a tungsten electrode (impedance, 0.5-2 MΩ), and lowered to a depth of ~300 μm into the neocortex. The signal was filtered by a band-pass filter between 1 and 5000Hz, amplified 1000 times with a microelectrode AC amplifier (model 1800, A-M system, Sequim, WA), and digital filtered between 0.2 and 130 Hz (Zhang et al., 2015).

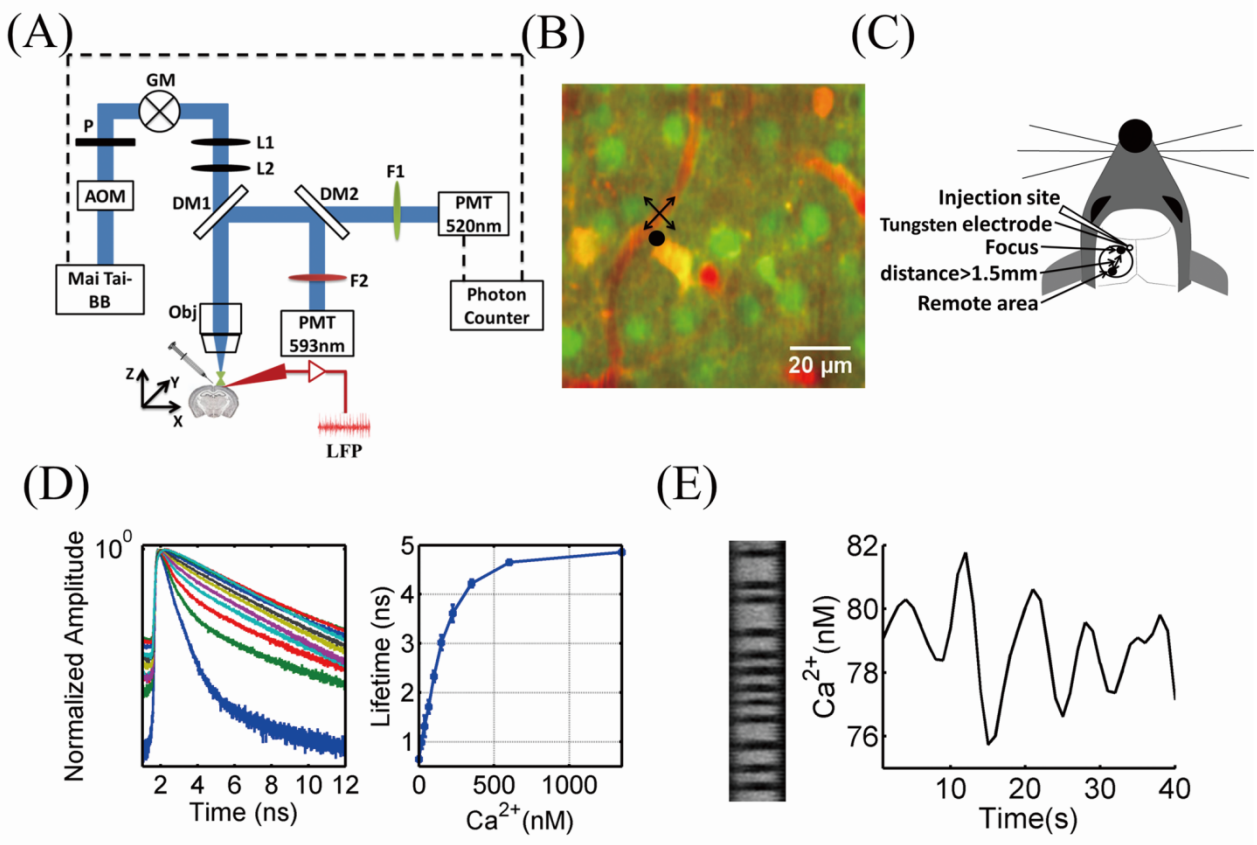

Figure 5-1: (A) Schematic of the two-photon lifetime microscopy system. Excitation light is provided by a MaiTai-BB laser oscillator (Mai Tai-BB) through an acousto-optic modulator (AOM) followed by a polarizer (P) to adjust the gain. A telescope (L_1 and L_2) expands the galvo-mirrors image onto the microscope objective pupil for illumination. Emitted fluorescence is separated using a first dichroic mirror (DM_1). The return beams are then split by a second dichroic mirror (DM2) sending the signal to detectors centered at wavelengths of 520nm (F_1) and 593nm (F_2). The Ca^{2+} concentration was monitored in the 520nm channel using a photon-counter for FLIM imaging. (B) In vivo fluorescence staining of neurons in green, astrocytes in yellow and vasculature in red. (C) Pictogram of measurement areas on the mouse brain. The craniotomy was done on the left side. The 4-AP injection location and electrode recordings were done at the same site. The remote area was defined to be that further than 1.5 mm from the focus. (D) Calibration of the fluorescence decay of OGB-1 at 10 different buffer Ca^{2+} concentrations. In this range, fit lifetime varied from ~4.86ns to ~0.65ns for high/low concentrations respectively. (E) Typical images at 593nm for longitudinal vessel scan, used to measure the diameter. The right figure shows measurements of absolute $[Ca^{2+}]_i$ in one astrocytic endfoot during resting state.

5.3.4 Two-Photon fluorescence lifetime setup

Measurements were collected using a custom-built 2-photon laser scanning fluorescence microscope (Figure 5-1(A)) with 80 MHz, 150 fs pulses from a MaiTai-BB laser oscillator (Newport corporation, USA) with a maximum output of ~2W through an acousto-optic modulator (ConOptics) to adjust the gain for depth-dependent two-photon excitation intensity. The laser pulses were scanned in a raster pattern by galvanometric mirrors. Reflected light was collected by a water-immersion objective (20×, 1.0 NA; Olympus), and then separated into 2 beams by dichroic mirrors. The beams were split and filtered around center wavelengths of 520 and 593nm, and measured on 2 distinct photomultiplier tubes (H10682-210 for photon counting at 520nm, R3896 for CW measures at 593nm, Hamamatsu photonics, Japan). To monitor Ca^{2+} changes, the excitation was set to 800 nm and the laser power reduced to limit the count rate to a maximum of 5% of the total number of laser pulses to remain in single-photon counting regime (< 70mW). Emission counts at 520nm were recorded using a photon counter (PicoHarp 300, PicoQuant). Scanning and data recordings were controlled by custom-designed software written in Matlab (MathWorks, USA).

Experiments were performed in two steps. Focus was first achieved on the cortex and then the objective was moved to a depth of ~200 μm. A point on the endfoot of interest and a perpendicular line on the encased vasculature by the endfoot were selected for measuring Ca^{2+} concentration ($[Ca^{2+}]_i$) and diameter. A custom scanning sequence, rapidly alternating between each type of measure was designed (gating the photon counter to only count while the beam was sitting on the endfoot) to have a simultaneous assessment of Ca^{2+} concentration and diameter (Figure 5-1E). Multiplexed Ca^{2+} measurements and line scan (200 lines) at a given location had a temporal resolution of 1s.

5.3.5 Fluorescence lifetime calibration

OGB-1 was used to monitor dynamic changes in intracellular Ca^{2+}, which can be measured through changes in lifetime. For calibration, we used the standard calibration method provided by the Invitrogen Ca^{2+} calibration buffer kit manual. Absolute $[Ca^{2+}]_i$ was determined independently of variations in dye concentration by measuring bound and unbound Ca^{2+} decay curves with fluorescence lifetime microscopy, which exhibit different lifetimes. The lifetime decay curves for

OGB-1 in each of 10 Ca^{2+} buffers were measured using samples of free dye in glass capillary tubes at varying Ca^{2+} concentrations (Lattarulo et al., 2011). In the absence of Ca^{2+}, OGB-1 had a single, fast decay leading to an effective lifetime of ~0.65 ns accounting for the PMT response function. At saturating levels of Ca^{2+} (1.35µM), OGB-1 had a single, slow decay leading to a lifetime of ~4.86 ns. While decays are bi-exponential within this range, we adopted an effective strategy of fitting a single decay curve on the first 80% of the decay, which was found to be robust at lower counts that in turn allowed faster in vivo recordings. Using this technique, effective calibration curves were generated for each buffer lifetime (Figure 5-1 D) that were found to be reproducible from calibration to calibration (see error bars) and also when decreasing the total number of counts.

5.3.6 Data analysis

All analyses were performed with Matlab using in-house code. The relationship between the fluorescence lifetime and $[Ca^{2+}]_i$ was obtained from the calibration (Figure 5-1 D, right). The resulting time decay curves obtained by the photon counter were fit with a single-exponential function from the maximum counts to 80% counts. The $[Ca^{2+}]_i$ was then calculated by fluorescence lifetime at each second using calibration results.

Due to the injected fluorescent dye (Rhodamine B), the plasma appears bright in the images while red blood cells appear as dark shadows (Figure 5-1 E left). Imaging plasma through successive line scans over the same region is the principle for measuring diameter (Desjardins et al., 2014b). The vessel diameter was defined by fitting to a Gaussian function whose full-width at half-maximum from the perpendicular scans was used as diameter (which may underestimate the real diameter) (Desjardins et al., 2014a). Small pre-capillary arterioles were chosen by size and identifying a surrounding endfoot process (to make sure it was not a capillary), a total of N=34 arterioles were studied with a mean diameter of D=6.68µm. The diameter data were converted to percent change by subtracting and then dividing the median value of the scan.

5.4 Results

Using two photon fluorescence lifetime measurements, $[Ca^{2+}]_i$ was measured in the somatosensory cortex astrocytes of anesthetized mice during normoxia. Resting Ca^{2+} concentration in glial cells was spatially heterogeneous; resting Ca^{2+} concentration in somatic

regions was significantly higher than in endfoot regions from 14 astrocytes in 7 mice (4-AP was injected after basal measurements) (Figure 5-2, paired t-test P<0.001) with mean values of 90.15 ± 1.62nM in the somata and 79.44 ± 1.63nM in endfeet which is in agreement with the sensitivity range of the dye and values previously obtained by in vivo two-photon florescence imaging (Kuchibhotla et al., 2009; Zheng et al., 2015) but slightly lower than ex vivo preparations (Girouard et al., 2010; Shain et al., 1989). We also quantified fluctuations of concentration over time and we observed no significant differences in fluctuations between somata and endfeet.

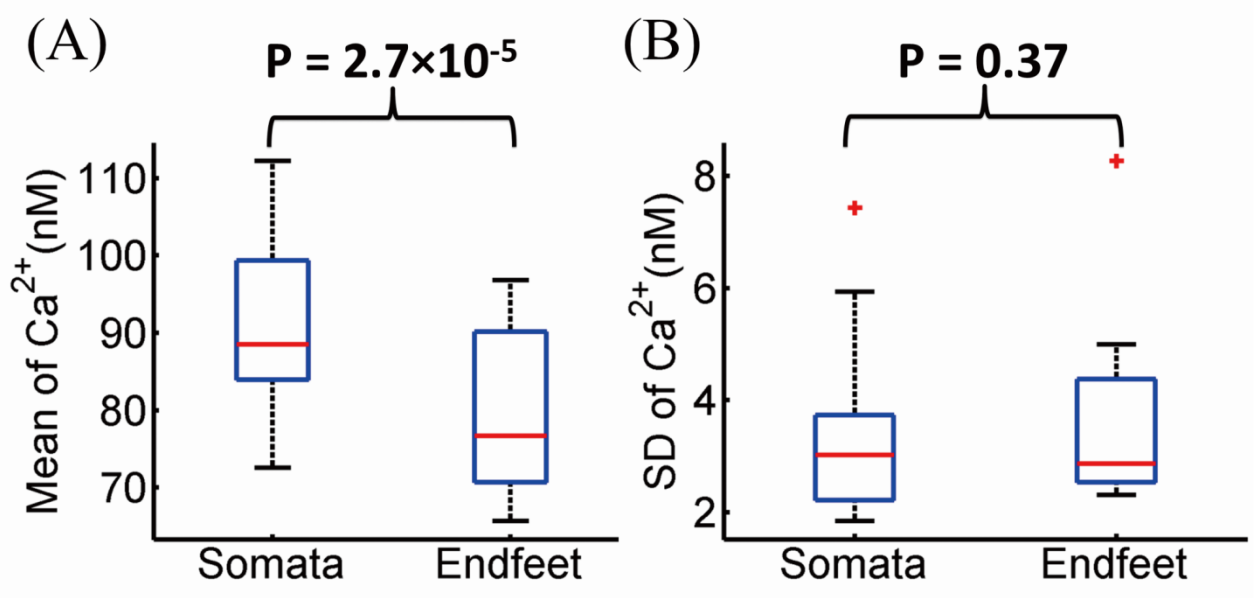

Figure 5-2: Paired t-test of $[Ca^{2+}]_i$ in astrocytic somata and endfeet during resting state. (A) Boxplot of the average of $[Ca^{2+}]_i$ in somata and endfeet in basal state. The [Ca2+]i in somata was significantly larger than endfeet ($p<0.001$). (B) Boxplot of the standard deviation (SD) of $[Ca^{2+}]_i$ in somata and endfeet during baseline over time. There was no difference in SD of $[Ca^{2+}]_i$ between the somata and endfeet.

5.4.1 Diameter changes in the epileptic focus and remote areas during the seizure-like activity

Seizure-like activity was elicited with injection of 4-AP and recorded by local field potentials with a tungsten electrode. They were characterized by first rhythmic spiking of increasing amplitude and decreasing frequency, evolving into rhythmic spikes and slow wave activity prior to gradual offset (see e.g. Figure 5-3A top and Figure 5-3B top).

We simultaneously measured $[Ca^{2+}]_i$ in astrocytic endfeet and diameter of adjacent arterioles in the somatosensory cortex of mice during epileptic events (Figure 5-3) to study how absolute $[Ca^{2+}]_i$ in astrocytic endfeet modulate the diameter of adjacent arterioles in local (<1.5mm) and remote areas from 4-AP injection site (>1.5mm) (Zhang et al., 2015) (Figure 5-1C). A typical time-course of changes in astrocytic endfoot Ca^{2+} and diameter at the epileptic focus (Figure 5-3A) and remote areas (Figure 5-3B) is shown in Figure 5-3. During epileptic events, Ca^{2+} significantly increased, returning to the baseline after seizure both at the epileptic focus and remote areas. At distances over 1.5mm from the site of injection, we observed early arteriolar constriction followed by delayed dilation (Figure 5-3B) during seizure. These results were in agreement with previous works where similar vascular responses were observed with a two-photon microscope (Zhao et al., 2011, 2009).

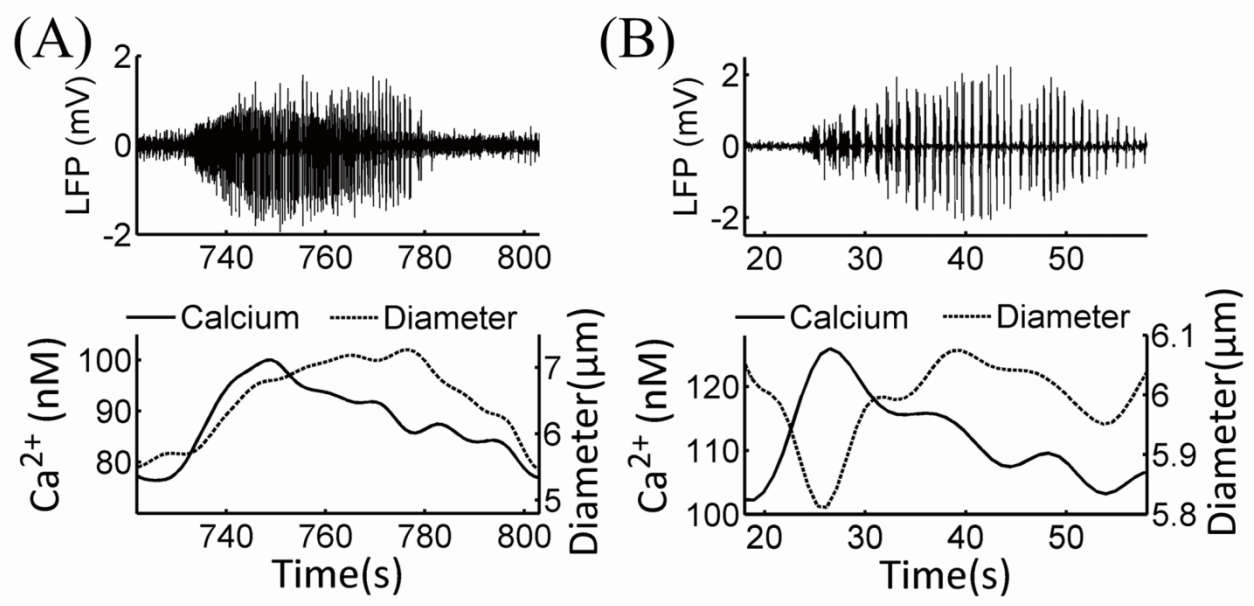

Figure 5-3: Simultaneous measurements of absolute Ca^{2+} in astrocytic endfoot and diameter of adjacent arterioles during epileptic events in local (A) and remote (B) areas. The time course of LFP indicates seizure initiation (top of (A) and (B) panels). (A) Nearby the injection site, simultaneous measures of Ca^{2+} and diameter show that Ca^{2+} and diameter display a monophasic increase with ictal discharge. (B) In remote areas, arteriole constricted at the onset of ictal event, then dilated while Ca^{2+} remains elevated throughout seizures.

5.4.2 Astrocytic endfoot baseline Ca^{2+} determines the level of arterial response during seizures

To investigate the relationship between astrocytic endfoot Ca^{2+} and arteriolar diameter changes at different distances from the epileptic focus, 7 mice were recorded with measurements close to the injection site and 4 mice were measured far away from the injection site (>1.5mm) (Figure 5-1C). Seizure-like activities evoked an increase in neuronal activity and a widespread increase in astrocytic Ca^{2+}, and were also associated with vasodilation. Figure 5-4A shows representative data from one mouse comparing the relative changes across observed seizures and indeed shows a linear relationship between relative increase in diameter and relative increase in (rCa^{2+}) for each seizure. We then analyzed the data by calculating the relative diameter and rCa^{2+} changes as a function of absolute baseline concentration $[Ca^{2+}]_i$ (estimated between seizures) over 7 mice (90 seizures, Figure 5-4B and Figure 5-4C). With increasing baseline $[Ca^{2+}]_i$, the relative diameter and rCa^{2+} changes decreased in amplitude either suggesting a constrictive modulation associated with increasing baseline $[Ca^{2+}]_i$ or the fact that with increasing baseline $[Ca^{2+}]_i$, the vessels partially dilate decreasing remaining reserve to dilate further.

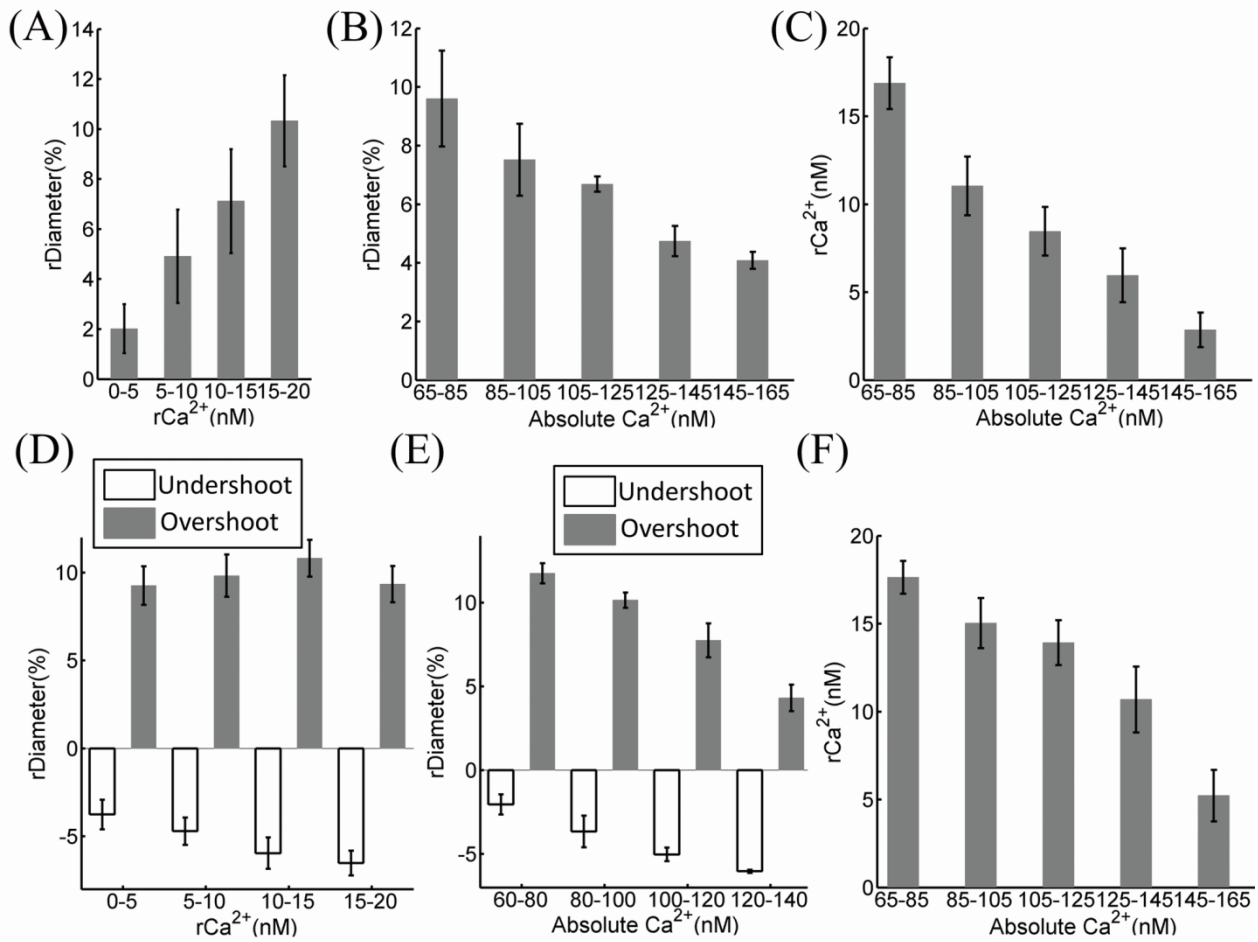

Figure 5-4: The relationship between $[Ca^{2+}]_i$ in astrocytic endfoot and the arteriolar changes in diameter during epileptic events in the focus ((A), (B) and (C)) and remote areas ((D), (E) and (F)). (A) Relationship between the relative $[Ca^{2+}]_i$ (rCa^{2+}) and relative changes in diameter (rDiameter) during epileptic events at the focus over 8 seizures from one animal. Note that during ictal events, $[Ca^{2+}]_i$ increases in the encasing astrocytic endfoot are accompanied by arteriolar dilations. (B) Correlation between the absolute baseline $[Ca^{2+}]_i$ and relative changes in diameter in the focus (from 7 mice, 90 seizures). (C) Relationship between the relative $[Ca^{2+}]_i$ and absolute $[Ca^{2+}]_i$ at the focus (from 7 mice, 90 seizures). (D) Relationship between the relative [Ca2+]i and relative changes in diameter during epileptic seizures in a remote area over two recording sessions (8 seizures) from one mouse. For each seizure, $[Ca^{2+}]_i$ increased in the endfoot with arterioles constricting at the beginning of seizures followed by dilation. (E) Correlation between the absolute $[Ca^{2+}]_i$ and relative diameter changes in remote areas (from 4 mice 58 seizures). (F) Relationship between the relative $[Ca^{2+}]_i$ during seizures and absolute $[Ca^{2+}]_i$ in remote areas (from 4 mice, 58 seizures).

To validate whether this observation reflected a difference in the resting state tone due to elevated Ca^{2+}, which would lead to a reduced reserve for dilation, we analyzed the absolute diameter during seizures across the recording session for the same animal. By plotting diameter during seizures against the absolute $[Ca^{2+}]_i$ (Figure 5-5A, two sessions, diameter normalized to its median), we observed a negative trend between single arteriole diameter and $[Ca^{2+}]_i$: at higher Ca^{2+} concentrations during seizures, the corresponding diameter decreased contradicting the reserve hypothesis. We also performed a correlation between the absolute Ca^{2+} concentration in all astrocytic endfeet and the median diameter over the time course of the experiments and observed no correlation (Figure 5-5C Correlation coefficient: R=0.09). Furthermore, we observed that in remote areas, the relative constriction with respect to baseline diameter also increased with increasing $[Ca^{2+}]_i$ (despite a decrease in absolute diameter).

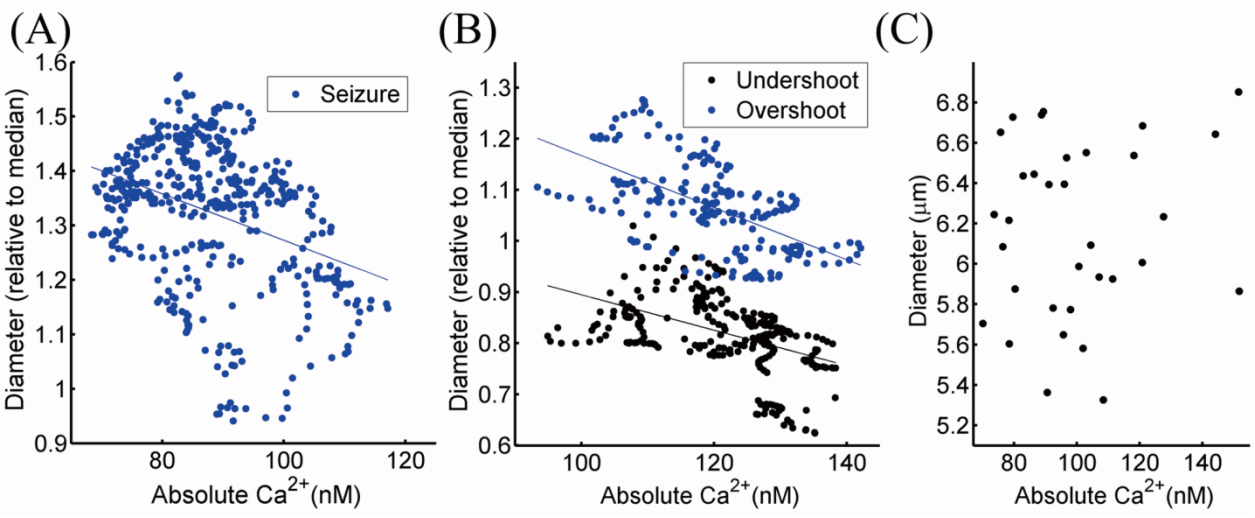

Figure 5-5 Scatter plot illustrating the relationship between absolute $[Ca^{2+}]_i$ in one astrocytic endfoot and the arteriolar diameter. (A) Correlation between the absolute $[Ca^{2+}]_i$ and diameter during epileptic events in local area (over two recording sessions, 8 seizures from one animal). The linear fit is: $y = -0.004x + 1.70$, $R^2 = 0.13$. (B) Correlation between the absolute $[Ca^{2+}]_i$ and relative diameter change during epileptic seizures in remote areas (over two sessions (8 seizures) from one animal). The linear fit for undershoot is: $y = -0.004x + 1.241$, $R^2 = 0.22$ while for the overshoot: $y = -0.005x + 1.676$, $R^2 = 0.35$. (C) The relationship between the absolute $[Ca^{2+}]_i$ and median of diameter over all measurements. The Spearman correlation coefficient is R=0.09.

Consolidating data from all mice with measures at the focus (7 mice, 21 astrocytes, 90 seizures), the average of $[Ca^{2+}]_i$ in astrocytic endfeet during seizures was significantly larger than baseline

level (Figure 5-6A, $p<0.005$). As expected, the increase in arterioles diameter was also significant during ictal discharges (Figure 5-6B $p<0.001$). However, when measuring diameter versus absolute $[Ca^{2+}]_i$ over the time course of the session, we observed a significant negative association between $[Ca^{2+}]_i$ and the diameter as quantified by their slope (Figure 5-6C, one sample t-test of slope against zero), in all cases preserving the negative relationship seen in Figure 5-5A and Figure 5-5B.

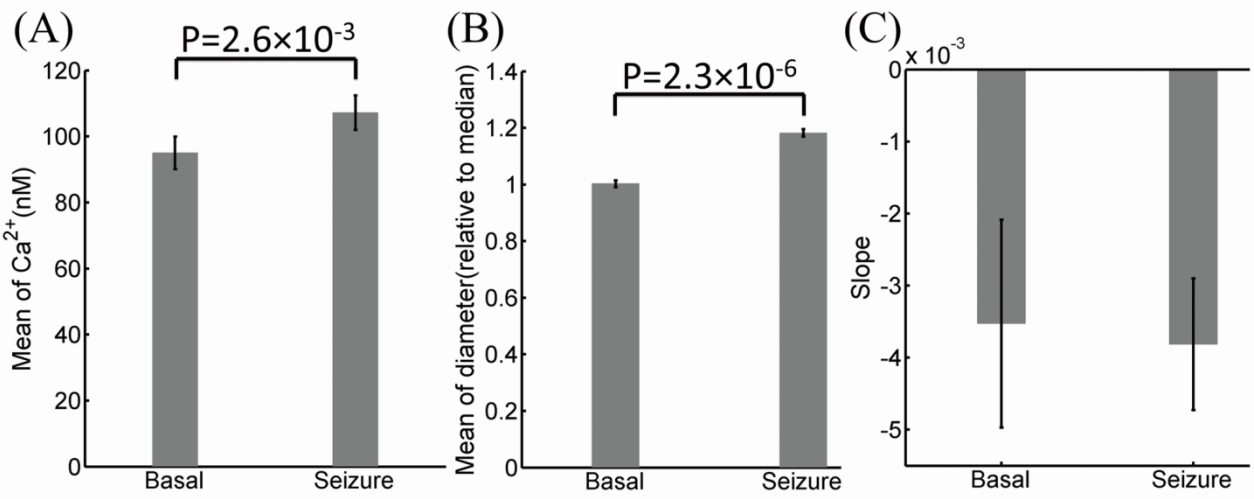

Figure 5-6: Relationship between absolute $[Ca^{2+}]_i$ in the astrocytic endfeet and arteriole diameter over all mice (7 mice). (A) Paired t- test of the average and SD of $[Ca^{2+}]_i$ values during baseline and epileptic seizures for all mice. The average $[Ca^{2+}]_i$ during ictal discharges was higher than baseline ($p<0.001$). The SD of $[Ca^{2+}]_i$ did not significantly vary between the seizure and basal level. (B) Paired t-test of the average and SD of diameter in all mice. The mean diameter had a significant increase with ictal events ($p<0.001$) and there were no significant differences in the SD of diameter between seizures and baseline. (C) Bar plots of the slopes of linear fits (as shown in Figure 5-4A and Figure 5-4B) in 21 astrocytes of 7 mice over 90 seizures. Slopes were significantly negative (both for basal ($p=0.05$) and for seizures ($p=0.006$), one sample t-test).

5.4.3 Astrocytic endfoot baseline Ca^{2+} determines the level of arteriole constriction first then of dilation with seizures in remote areas

To study the relationship between astrocytic endfoot $[Ca^{2+}]_i$ and arteriolar diameter changes during epileptic events in remote areas, measurements at a distance over 1.5mm from the injection site were done in 4 mice. Seizure-like activities evoked an increase in astrocytic Ca^{2+}

that was associated with a constriction at the beginning of the seizure followed by dilation (representative data from one mouse shown in Figure 5-3(B)). We analyzed the data in a similar way than at the epileptic focus: first by calculating the changes of relative diameter and the relative $[Ca^{2+}]_i$ (Figure 5-4D). Figure 5-4D shows that relative changes during seizures indeed show a biphasic vascular response (constriction followed by a vasodilation) while $[Ca^{2+}]_i$ remain elevated at each seizure. However, when the full data (Figure 5-4E) is analyzed using absolute Ca^{2+} concentration, we observed a positive trend between relative arteriole constriction and Ca^{2+} increase, and a negative trend between relative arteriole dilation and Ca^{2+} increase. These results indicate that the higher the absolute $[Ca^{2+}]_i$, the weaker is the dilation or the stronger is the constriction for a given seizure. We also calculated the relationship between the relative $[Ca^{2+}]_i$ and absolute $[Ca^{2+}]_i$ over 4 mice (58 seizures). Figure 5-4(F) shows that the relative $[Ca^{2+}]_i$ decreases as the absolute $[Ca^{2+}]_i$ increases similarly to the focus.

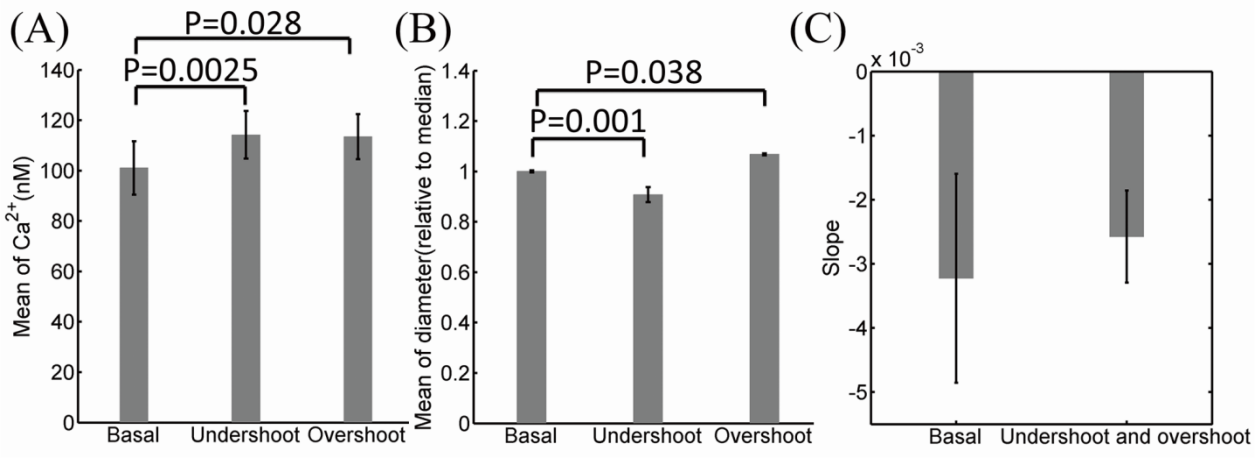

Figure 5-7: Relationship between absolute $[Ca^{2+}]_i$ in the astrocytic endfoot and diameter in arteriole over all mice (4 mice) in the remote area. (A) Paired t- test of the average and SD of absolute $[Ca^{2+}]_i$ values during undershoot or overshoot and baseline for all mice. The average of $[Ca^{2+}]_i$ during the beginning of seizure and the duration of seizure was higher than baseline (p=0.025 and p=0.028). The SD of $[Ca^{2+}]_i$ did not significantly vary between the undershoot or overshoot and basal level. (B) Paired t-test of the average and SD of the percent change of diameter in all mice. The mean diameter had a significant decrease during the beginning of seizure (p=0.001) and the average of diameter during the duration of seizure was higher than the baseline (p =0.038). There were no significant differences in the SD of diameter between undershoot or overshoot and baseline. (C) Bar plots of slopes of linear fits between relative

diameter changes and absolute $[Ca^{2+}]_i$ (as shown in Figure 5-5D) in 13 astrocytes of 4 mice over 58 seizures. Slopes were negative (For basal, p=0.014, for seizure, p=0.009, one sample t-test).

Using data from all mice with measures in remote areas (4 mice, 13 astrocytes, 58 seizures), we observed that the average of $[Ca^{2+}]_i$ in astrocytic endfeet during the undershoot and the overshoot, was significantly larger than at baseline level (Figure 5-7A, p=0.025 and p=0.028). The undershoot and overshoot periods were associated with a decrease and an increase in vascular diameter, respectively. The average decrease in arteriolar diameter was significant during the beginning of seizures (Figure 5-7B, p=0.001) as well as their ensuing increase (Figure 5-7B, p=0.038). When measuring the diameter versus absolute $[Ca^{2+}]_i$, we observed a significant constrictive trend quantified by their slope (Figure 5-7C), in all cases preserving the negative relationship seen in Figure 5-5B. This data indicates that seizure-like activities increase absolute $[Ca^{2+}]_i$ which in turn, leads to an increased constriction during the undershoot, and a decreased dilation during the overshoot. This suggests that the baseline $[Ca^{2+}]_i$ determines the fractional change of arteriole diameter during seizures in the remote area.

5.5 Discussion

In this work, we showed that absolute $[Ca^{2+}]_i$ of astrocyte endfeet and diameter of adjacent arterioles can be simultaneously measured in the mouse cortex in vivo using two-photon fluorescence lifetime measurements with an appropriate excitation regime. In similar brain studies, the key advantages of two-photon fluorescence lifetime measures of Ca^{2+} are their relative immunity to changes in fluorophore concentration, light attenuation and bleaching thus opening the door to investigating quantitatively changes in Ca^{2+} at different depths in the cortex with good spatial resolution. Here we used this technique to investigate absolute $[Ca^{2+}]_i$ changes in astrocytic endfeet and diameter of arterioles they were encasing during epileptic event induced by 4-AP. Our findings provide new correlative evidence regarding potential Ca^{2+} mediated diameter changes during epileptic activity, by characterizing the relationship between $[Ca^{2+}]_i$ and diameter.

The key findings of this study were the following: (1) the free $[Ca^{2+}]_i$ in astrocytes was measured and a spatially heterogeneous distribution of Ca^{2+} was observed in astrocytic soma and endfoot. (2) seizure activity induced a Ca^{2+} elevation in endfeet with simultaneous arteriolar dilation at the

epileptic focus. In remote areas, the Ca2+ increase was associated with arteriolar constriction at the onset of seizure and dilation later during the seizure. (3) a negative relationship between basal Ca^{2+} in astrocytic endfeet and diameter changes in arterioles was found. These novel observations have implications for understanding the relationship between astrocytic endfeet $[Ca^{2+}]_i$ and adjacent arteriolar diameter.

5.5.1 Center-surround phenomena during acute seizure activity

Using epileptic seizures induced by 4-AP in vivo, we investigated in this study the $[Ca^{2+}]_i$ in astrocytic endfoot and diameter of adjacent arterioles simultaneously. Our data showed that, in the epileptic focus, the elevation of Ca^{2+} was accompanied by arteriolar dilation (Figure 5-3A). In the remote area, a clear transient decrease in the diameter of arterioles despite a sustained increase of Ca^{2+} in astrocytic endfoot was shown (Figure 5-3B). Similar diameter changes during ictal discharges were investigated by several investigators with various methods (Zhao et al., 2011, 2009). The simplest explanation for this inhomogeneous response is a passive model whereby vasodilation response propagates upstream in a stepwise manner. Early in the seizure, vasodilation in the focus shunts blood from the surround to the focus. As vasodilation propagates further upstream, vessels dilate in the surround as well. This observation however seems to be in contradiction with our observed decrease of dilation at the focus and increase of constriction in the surround with increasing absolute $[Ca^{2+}]_i$. In the passive model, one would expect constriction to be reduced in the surround when dilation is reduced in the focus, which is not the case here. Alternatively, our observations could be due to neurotransmitters released by interneurons, e.g. neuropeptide Y (NPY), as 4-AP is known to induce the release of NPY which is a strong constrictor in remote areas.

5.5.2 The relationship between calcium and diameter

The elevation of $[Ca^{2+}]_i$ in astrocytic endfoot dilated the arteriole with epileptic events at the epileptic foci. Our data is similar to results from sensory stimulation (Wang et al., 2006). Meanwhile, the slow increase of basal $[Ca^{2+}]_i$ was also accompanied by a decrease of relative arteriolar dilation during seizures over the whole time course of the experiment.

The link between astrocytic $[Ca^{2+}]_i$ levels and arteriole dilation has been the subject of much debate (Bazargani and Attwell, 2016) an whether astrocytes regulate vasodilation remains

controversial: initial studies indicated that increase in levels of $[Ca^{2+}]_i$ in astrocytes led to a release of arachidonic acid– derived messengers, prostaglandins, epoxyeicosatrienoic acids (EETs) and 20-hydroxyeicosatetraenoic acid (20-HETE), each known to have a modulating role on vascular smooth muscles (Gordon et al., 2008; Mulligan and MacVicar, 2004; Zonta et al., 2003). However this initial interpretation was mitigated by evidence showing that $[Ca^{2+}]_i$ signals in astrocytes were slow when compared to blood flow elevation caused by neuronal activity (Nizar et al., 2013; Schulz et al., 2012; Schummers et al., 2008). In more recent work, this was again questioned with the observation that astrocyte processes had distinct $[Ca^{2+}]_i$ transients that are more frequent than that found in the somata (Grosche et al., 1999). For these reasons we focused our measures on these processes. As our sampling rate (1 second) for the dual ($[Ca^{2+}]_i$ and diameter) measures was slow, our work does not contribute new data related to the neurovascular response associated with astrocytes, rather we focus on slow fluctuations of basal $[Ca^{2+}]_i$ and observed a negative correlation between response and absolute calcium values. One hypothesis is that this negative correlation corresponds to the relationship between vascular tone and extravascular potassium concentrations released by large-conductance calcium sensitive potassium channel, as was demonstrated in slices at higher endfeet $[Ca^{2+}]_i$ (Girouard et al., 2010). This would suggest that the transition between vasodilation and vasoconstriction described in (Girouard et al., 2010) is gradual and proportional to $[Ca^{2+}]_i$.

5.5.3 Non-linear hemodynamic responses to seizures

Among original motivations for this work was the observation of inhibitory non-linear hemodynamic phenomena(Pouliot et al., 2012a) in epilepsy. Our data correlating the increase of basal $[Ca^{2+}]_i$ to an inhibitory dilation of adjacent arterioles suggests that $[Ca^{2+}]_i$ may indeed contribute to these observations. In the context of epilepsy, this decrease response may contribute to local hypoxia during seizures. More work is required however, using different epileptogenic agents and models as well as in vivo uncaging of calcium and chelators to further understand the relative importance of $[Ca^{2+}]_i$ in this inhibitory phenomenon.

5.6 Conclusion

We developed a technique that simultaneously provided absolute values of $[Ca^{2+}]_i$ in astrocytic endfoot and diameter in adjacent arteriole in the brain cortex by means of two-photon

fluorescence lifetime microscopy. The technique was applied to study how the astrocytic endfoot controls encased arterioles during epileptic activity in mice. To our knowledge, this is the first report of simultaneously measurements of absolute $[Ca^{2+}]_i$ values and diameter changes during epilepsy. In our work, following 4-AP injection in the somatosensory cortex of mice, we observed significant changes of $[Ca^{2+}]_i$ in endfoot and diameter in arteriole at focus and in the remote areas. This study support the existence of the elevation of $[Ca^{2+}]_i$ causing arteriolar dilation at focus during stimulation. In addition, we found a negative correlation between basal $[Ca^{2+}]_i$ in endfoot and the amplitude of dilation for all measurements, while, in the remote areas, there was a positive correlation between $[Ca^{2+}]_i$ in endfoot during the onset of seizures and the level of vasoconstriction. This study provides information that could help to understand the association between astrocytic Ca^{2+} levels and the vascular tone.

5.7 Acknowledgements

We thank Marc-Antoine Gillis and Natacha Duquette for their assistance in animal preparation. This study was funded by a Natural Sciences and Engineering Research Council of Canada (NSERC, 239876-2011) discovery grant and Canadian Institutes of Health Research (MOP-299166) to F. Lesage.

5.8 Declaration of conflicting interests

F. Lesage and S. Bélanger are minority owners of Labeo Technologies Inc. Other authors have no conflict of interest.

Authors' contributions:

C.Z. and F.L. designed the experiment. C.Z., S.B., H.G. and F.L. analyzed results. M.T. built the microscope. C.Z., H.G. and F.L. wrote the paper.

5.9 Reference

Arthurs, O.J., Williams, E.J., Carpenter, T.A., Pickard, J.D., Boniface, S.J., 2000. Linear coupling between functional magnetic resonance imaging and evoked potential amplitude in human somatosensory cortex. Neuroscience 101, 803–806. doi:10.1016/S0306-4522(00)00511-X

Attwell, D., Buchan, A.M., Charpak, S., Lauritzen, M., MacVicar, B.A., Newman, E.A., 2010. Glial and neuronal control of brain blood flow. Nature 468, 232–243. doi:10.1038/nature09613

Bazargani, N., Attwell, D., 2016. Astrocyte calcium signaling: the third wave. Nat. Neurosci. 19, 182–189. doi:10.1038/nn.4201

Cirillo, G., De Luca, D., Papa, M., 2012. Calcium Imaging of Living Astrocytes in the Mouse Spinal Cord following Sensory Stimulation. Neural Plast. 2012, e425818. doi:10.1155/2012/425818

Desjardins, M., Berti, R., Lefebvre, J., Dubeau, S., Lesage, F., 2014a. Aging-related differences in cerebral capillary blood flow in anesthetized rats. Neurobiol. Aging 35, 1947–1955. doi:10.1016/j.neurobiolaging.2014.01.136

Desjardins, M., Berti, R., Pouliot, P., Dubeau, S., Lesage, F., 2014b. Multimodal study of the hemodynamic response to hypercapnia in anesthetized aged rats. Neurosci. Lett. 563, 33–37. doi:10.1016/j.neulet.2014.01.027

Filosa, J.A., Bonev, A.D., Straub, S.V., Meredith, A.L., Wilkerson, M.K., Aldrich, R.W., Nelson, M.T., 2006. Local potassium signaling couples neuronal activity to vasodilation in the brain. Nat. Neurosci. 9, 1397–1403. doi:10.1038/nn1779

Garaschuk, O., Milos, R.-I., Konnerth, A., 2006. Targeted bulk-loading of fluorescent indicators for two-photon brain imaging in vivo. Nat. Protoc. 1, 380–386. doi:10.1038/nprot.2006.58

Girouard, H., Bonev, A.D., Hannah, R.M., Meredith, A., Aldrich, R.W., Nelson, M.T., 2010. Astrocytic endfoot Ca2+ and BK channels determine both arteriolar dilation and constriction. Proc. Natl. Acad. Sci. U. S. A. 107, 3811–3816. doi:10.1073/pnas.0914722107

Gordon, G.R.J., Choi, H.B., Rungta, R.L., Ellis-Davies, G.C.R., MacVicar, B.A., 2008. Brain metabolism dictates the polarity of astrocyte control over arterioles. Nature 456, 745–749. doi:10.1038/nature07525

Grosche, J., Matyash, V., Möller, T., Verkhratsky, A., Reichenbach, A., Kettenmann, H., 1999. Microdomains for neuron-glia interaction: parallel fiber signaling to Bergmann glial cells. Nat. Neurosci. 2, 139–143. doi:10.1038/5692

Howarth, C., 2014. The contribution of astrocytes to the regulation of cerebral blood flow. Front. Neurosci. 8. doi:10.3389/fnins.2014.00103

Kuchibhotla, K.V., Lattarulo, C.R., Hyman, B.T., Bacskai, B.J., 2009. Synchronous Hyperactivity and Intercellular Calcium Waves in Astrocytes in Alzheimer Mice. Science 323, 1211–1215. doi:10.1126/science.1169096

Lattarulo, C., Thyssen, D., Kuchibholta, K.V., Hyman, B.T., Bacskaiq, B.J., 2011. Microscopic imaging of intracellular calcium in live cells using lifetime-based ratiometric measurements of Oregon Green BAPTA-1. Methods Mol. Biol. Clifton NJ 793, 377–389. doi:10.1007/978-1-61779-328-8_25

Mulligan, S.J., MacVicar, B.A., 2004. Calcium transients in astrocyte endfeet cause cerebrovascular constrictions. Nature 431, 195–199. doi:10.1038/nature02827

Nguyen, D.K., Tremblay, J., Pouliot, P., Vannasing, P., Florea, O., Carmant, L., Lepore, F., Sawan, M., Lesage, F., Lassonde, M., 2013. Noninvasive continuous functional near-infrared spectroscopy combined with electroencephalography recording of frontal lobe seizures. Epilepsia 54, 331–340. doi:10.1111/epi.12011

Nizar, K., Uhlirova, H., Tian, P., Saisan, P.A., Cheng, Q., Reznichenko, L., Weldy, K.L., Steed, T.C., Sridhar, V.B., MacDonald, C.L., Cui, J., Gratiy, S.L., Sakadzić, S., Boas, D.A., Beka, T.I., Einevoll, G.T., Chen, J., Masliah, E., Dale, A.M., Silva, G.A., Devor, A., 2013. In vivo stimulus-induced vasodilation occurs without IP3 receptor activation and may precede astrocytic calcium increase. J. Neurosci. Off. J. Soc. Neurosci. 33, 8411–8422. doi:10.1523/JNEUROSCI.3285-12.2013

Otsu, Y., Couchman, K., Lyons, D.G., Collot, M., Agarwal, A., Mallet, J.-M., Pfrieger, F.W., Bergles, D.E., Charpak, S., 2015. Calcium dynamics in astrocyte processes during neurovascular coupling. Nat. Neurosci. 18, 210–218. doi:10.1038/nn.3906

Pérez Koldenkova, V., Nagai, T., 2013. Genetically encoded Ca2 + indicators: Properties and evaluation. Biochim. Biophys. Acta BBA - Mol. Cell Res., 12th European Symposium on Calcium 1833, 1787–1797. doi:10.1016/j.bbamcr.2013.01.011

Pouliot, P., Tremblay, J., Robert, M., Vannasing, P., Lepore, F., Lassonde, M., Sawan, M., Nguyen, D.K., Lesage, F., 2012. Nonlinear hemodynamic responses in human epilepsy: a

multimodal analysis with fNIRS-EEG and fMRI-EEG. J. Neurosci. Methods 204, 326–340. doi:10.1016/j.jneumeth.2011.11.016

Schulz, K., Sydekum, E., Krueppel, R., Engelbrecht, C.J., Schlegel, F., Schröter, A., Rudin, M., Helmchen, F., 2012. Simultaneous BOLD fMRI and fiber-optic calcium recording in rat neocortex. Nat. Methods 9, 597–602. doi:10.1038/nmeth.2013

Schummers, J., Yu, H., Sur, M., 2008. Tuned Responses of Astrocytes and Their Influence on Hemodynamic Signals in the Visual Cortex. Science 320, 1638–1643. doi:10.1126/science.1156120

Shain, W., Connor, J.A., Madelian, V., Martin, D.L., 1989. Spontaneous and beta-adrenergic receptor-mediated taurine release from astroglial cells are independent of manipulations of intracellular calcium. J. Neurosci. Off. J. Soc. Neurosci. 9, 2306–2312.

Shih, A.Y., Driscoll, J.D., Drew, P.J., Nishimura, N., Schaffer, C.B., Kleinfeld, D., 2012. Two-photon microscopy as a tool to study blood flow and neurovascular coupling in the rodent brain. J. Cereb. Blood Flow Metab. 32, 1277–1309. doi:10.1038/jcbfm.2011.196

Straub, S.V., Bonev, A.D., Wilkerson, M.K., Nelson, M.T., 2006. Dynamic inositol trisphosphate-mediated calcium signals within astrocytic endfeet underlie vasodilation of cerebral arterioles. J. Gen. Physiol. 128, 659–669. doi:10.1085/jgp.200609650

Takano, T., Tian, G.-F., Peng, W., Lou, N., Libionka, W., Han, X., Nedergaard, M., 2006. Astrocyte-mediated control of cerebral blood flow. Nat. Neurosci. 9, 260–267. doi:10.1038/nn1623

Truccolo, W., Donoghue, J.A., Hochberg, L.R., Eskandar, E.N., Madsen, J.R., Anderson, W.S., Brown, E.N., Halgren, E., Cash, S.S., 2011. Single-neuron dynamics in human focal epilepsy. Nat. Neurosci. 14, 635–641. doi:10.1038/nn.2782

Wang, X., Lou, N., Xu, Q., Tian, G.-F., Peng, W.G., Han, X., Kang, J., Takano, T., Nedergaard, M., 2006. Astrocytic Ca2+ signaling evoked by sensory stimulation in vivo. Nat. Neurosci. 9, 816–823. doi:10.1038/nn1703

Wilms, C.D., Eilers, J., 2007. Photo-physical properties of Ca2+-indicator dyes suitable for two-photon fluorescence-lifetime recordings. J. Microsc. 225, 209–213. doi:10.1111/j.1365-2818.2007.01746.x

Wilms, C.D., Schmidt, H., Eilers, J., 2006. Quantitative two-photon Ca2+ imaging via fluorescence lifetime analysis. Cell Calcium 40, 73–79. doi:10.1016/j.ceca.2006.03.006

Zhang, C., Bélanger, S., Pouliot, P., Lesage, F., 2015. Measurement of Local Partial Pressure of Oxygen in the Brain Tissue under Normoxia and Epilepsy with Phosphorescence Lifetime Microscopy. PLoS ONE 10. doi:10.1371/journal.pone.0135536

Zhao, M., Ma, H., Suh, M., Schwartz, T.H., 2009. Spatiotemporal dynamics of perfusion and oximetry during ictal discharges in the rat neocortex. J. Neurosci. Off. J. Soc. Neurosci. 29, 2814–2823. doi:10.1523/JNEUROSCI.4667-08.2009

Zhao, M., Nguyen, J., Ma, H., Nishimura, N., Schaffer, C.B., Schwartz, T.H., 2011. Preictal and ictal neurovascular and metabolic coupling surrounding a seizure focus. J. Neurosci. Off. J. Soc. Neurosci. 31, 13292–13300. doi:10.1523/JNEUROSCI.2597-11.2011

Zhao, M., Suh, M., Ma, H., Perry, C., Geneslaw, A., Schwartz, T.H., 2007. Focal increases in perfusion and decreases in hemoglobin oxygenation precede seizure onset in spontaneous human epilepsy. Epilepsia 48, 2059–2067. doi:10.1111/j.1528-1167.2007.01229.x

Zheng, K., Bard, L., Reynolds, J.P., King, C., Jensen, T.P., Gourine, A.V., Rusakov, D.A., 2015. Time-Resolved Imaging Reveals Heterogeneous Landscapes of Nanomolar Ca2+ in Neurons and Astroglia. Neuron 88, 277–288. doi:10.1016/j.neuron.2015.09.043

Zonta, M., Angulo, M.C., Gobbo, S., Rosengarten, B., Hossmann, K.-A., Pozzan, T., Carmignoto, G., 2003. Neuron-to-astrocyte signaling is central to the dynamic control of brain microcirculation. Nat. Neurosci. 6, 43–50. doi:10.1038/nn980

CHAPTER 6 ARTICLE 3: SPATIAL LANDSCAPE OF OXYGEN IN AND AROUND MICROVASCULATURE DURING EPILEPTIC EVENTS

Cong Zhang,[a] Mohammad Moeini,[a,b] and Frédéric Lesage [a,b,*]

[a]École Polytechnique de Montréal, Department of Electrical Engineering, C.P. 6079 succ.Centre-ville, Montreal, Quebec, Canada, H3C 3A7

[b]Montreal Heart Institute, 5000 Bélanger street, Montreal, Quebec, Canada, H1T 1C8

This article aimed to address the third objective of this thesis. The main purpose of the article was to investigate the oxygen partial pressure in microvascular and tissue of anesthetized mice during epileptiform activity. The neurotoxin 4-Aminopyridine (4-AP) was used in live mice to model epileptiform activity. We characterized the distribution of the "initial dip" in oxygen partial pressure in arterioles, veins and tissue near the 4-AP injection site. These results reveal a correlation between the oxygen partial pressure signal during the "initial dip" and the diameter of arteries and veins. This article has been published to Neurophotonics.

6.1 Abstract

Measuring changes in cerebral oxygen in tissue microdomains during epilepsy is important to identify hypoxic potential and susceptibility for neural damage. Here, using a custom-built two-photon microscopy system, we present microscopic measurements of oxygen partial pressure (PO_2) in cortical microvessels and tissue of anesthetized mice during 4-AP induced epileptic seizures. Investigating epileptic events, we characterized the distribution of the "initial dip" in PO_2 in arterioles, veins and tissue near the 4-AP injection site. Our results reveal a correlation between the percent change in PO2 during the "initial dip" and the diameter of nearest arteries and veins.

Keywords: Two-photon phosphorescence lifetime microscopy, oxygen partial pressure, epilepsy.

6.2 Introduction

The global architecture of blood supply to the brain consists of a planar mesh of pial arteries and veins branching and diving into the cortex, to supply and drain the blood (Dalkara and Alarcon-Martinez, 2015; Duvernoy et al., 1981; Lauwers et al., 2008) in support of metabolic needs. A thorough understanding of the dynamics of oxygen supply and consumption in the cerebral cortex is important not only because neuronal activity relies on oxygen availability, but also because a large number of functional imaging techniques (e.g. functional magnetic resonance (Hu and Yacoub, 2012) and optical imaging of intrinsic signal (Bahar et al., 2006; Pouliot et al., 2012b)) rely on the changes in blood oxygenation to image brain function. Oxygen is transported to the brain by blood and delivered to tissue at the arteriole and capillary level by diffusion. With increases in neural activity and metabolic consumption the delivery of oxygen to tissue increases through changes in cerebral blood flow (CBF) (Buxton and Frank, 1997; Zheng et al., 2002). Under normal conditions, blood flow increases slightly overshoot the need required to satisfy tissue oxygen consumption, an overshoot sometimes argued to be neuroprotective. However, during excessive neuronal activity, as seen in epilepsy, supply might be insufficient (Schridde et al., 2008).

Epilepsy is a common neurological disease characterized by recurrent unprovoked seizures, which result from abnormal and excessive neuronal activity in the brain. In both animal models and patients, the epileptic events can evoke drastic increases in CBF to meet the high metabolic demand caused by this intense neuronal activity (Geneslaw et al., 2011; Zhao et al., 2011, 2007). Measures of oxygen partial pressure (PO_2) in tissue during seizures have displayed an initial dip with various methods (Zhang et al., 2015; Zhao et al., 2009) but the spatial landscape of this phenomenon has not been thoroughly documented. In normal conditions, it was shown that most capillaries released little oxygen at baseline acting as an oxygen reserve that was recruited during increased neuronal activity (Sakadžić et al., 2014). Whether this redistribution of the delivery of PO_2 around and in capillaries during itcal events remains valid is unknown, and it is unclear how larger vessels modulate the spatial landscape of the PO_2 distribution. In this study, we used two-photon microscopy (TPM) and the O_2-sensitive phosphorescent dye PtP-C343 (Finikova et al., 2008) to measure PO_2 in arterioles, venules and tissue during epileptic events to characterize oxygen delivery during these periods of high demand.

6.3 Materials and Methods

6.3.1 Animal preparation

A total of N=11 male C57/BL6 mice (postnatal 8 weeks old, 20-25g weight) were used for this study, of which three died before data acquisitions. Four mice were used for vascular PO_2 measurements and four mice were used for tissue PO_2 recording. The Animal Research Ethics Committee of the Montreal Heart Institute approved all surgical procedures, which were performed according to the recommendations of the Canadian Council on Animal Care. All procedures were done according to the ARRIVE guidelines.

Animals were anesthetized with urethane (1-1.6g/kg, intraperitoneal injection (IP)), tracheotomized and maintained at constant body temperature (37 °C) with a controlled physiological monitoring system (Labeotech, CA). A moderate flow of ambient air lightly supplemented with oxygen was supplied next to the tracheotomy (10% oxygen, 90% air, 1L/min). The mice were then head-fixed with a stereotaxic device. After the injection of a local anesthetic (Xylocaine, subcutaneous (SC), 0.2%) under the scalp, a ~2×2 mm cranial window was opened over the right hemisphere to expose the somatosensory cortex and surrounding brain (AP: -1.5 mm, DV: +1.5mm). A small hole was drilled next to the cranial window for the injection of 4-AP. For tissue PO_2 measurements, ~1 µL of the oxygen-sensitive dye (PtP-C343, 200 µM, synthetized based on published procedures (Lecoq et al., 2011)) was injected into the tissue and the cranial window was sealed with 1% agarose in artificial cerebrospinal fluid (aCSF, 125 mM NaCl, 10 mM HEPES, 10 mM glucose, 5 mM KCl, 1,5 mM $CaCl_2$, 1 mM $MgSO_4$) using a 150 µm-thick microscope coverslip. For vascular measurements, the same dye was injected through the tail vein at 10-15 µM initial concentration. A catheter in the femoral artery was used to monitor blood gases (PCO_2, 36-39mmHg and PO_2, 110-160 mmHg). The average blood pressure (80-110 mmHg) was measured using volume-pressure recordings (VPR) performed immediately prior to imaging. For each experiment, we labelled the blood plasma with fluorescein isothiocyanate (FITC) conjugated with dextran (Sigma; 128mM, 200µL) and used TPM to obtain a high-resolution structural image of the microvasculature. A larger image of the surface

microvasculature (~2×2 mm) was also obtained, which was later used for easier tracing of the pial arterioles and venules.

6.3.2 Epileptogenesis and electriohysiology

Epilepsy was induced by injection the potassium channel blocker 4-aminopyridine (4-AP; Sigma; 15 mM, 0.5 μL) (Zhao et al., 2007) through a glass microelectrode using a syringe pump controller (UMP3, WPI) into a small hole with a depth of ~300μm next to the cranial window at a rate of 100 μL/min. Extracellular local field potentials (LFPs) were recorded with a tungsten electrode (impedance, ~1-2 MΩ) lowered to a depth ~300μm into the neocortex. The signal from the electrode was filtered by a band-pass filter (1~5000Hz), amplified with a microelectrode AC amplifier (model 1800, A-M system, Sequim, WA), and digital filtered between 0.2 and 130 Hz (Zhang et al., 2015).)

6.3.3 Two-photon microscopy setup, acquisition and processing

Measurements were collected on a custom-built two-photon phosphorescence lifetime microscopy with 80 MHz, 150 fs pulses from a MaiTai-BB laser oscillator (Newport corporation, USA) with output going through an acousto-optic modulator (ConOptics) to adjust the gain for depth-dependent two-photon excitation intensity. Reflected light was collected by a water-immersion objective (20×, 1.0 NA; Olympus), and then separated into 2 beams (phosphorescent photons and fluorescent photons) by dichroic mirrors. Phosphorescent light was passed through a filter centered at 680 nm and detected by a first photomultiplier tube (H7422, Hamamatsu, Photonics, Japan) and fluorescent light was filtered around center wavelength of 520 nm and detected by the second photomultiplier tube (R3896, Hamamatsu Photonics, Japan). Scanning and data recordings were controlled by custom-designed software written in Matlab (MathWorks, USA). Phosphorescence lifetime was fitted with a single-exponential function using a least-squares method. The lifetime was converted to PO_2 using a calibration plot obtained in independent oxygen titration experiments of the same dye batch (Finikova et al., 2008).

For each animal, a picture of the craniotomy along with the real-time display of the surface vessels scanned was used to localize arterioles and venules. Then an angiogram was acquired as a 3D scan over 600 μm × 600 μm × 400μm regions using depth steps of Δz = 5 μm. These were used to guide manual positioning of PO_2 recordings on and along targeted vessels. The tissue PO_2

measurements were at a depth ~200µm - 300µm and were chosen close to arterioles. The vascular PO_2 measurements were recorded from the surface until a depth ~250µm.

6.3.4 Simulation of oxygen diffusion in tissue using a Krogh-Erlang Model

The Krogh model was used to simulate oxygen diffusion in the tissue and compare with experimental data using (Krogh, 1919)

$$PO_2(x) = PO_2^{VES} - \frac{Q}{K}\left(\frac{1}{2}R^2 \cdot \ln\left(\frac{x}{r}\right) - \frac{x^2 - r^2}{4}\right) \quad (6\text{-}1)$$

Here, PO_2^{VES} is the vessel oxygen tension (atm) and $PO_2(x)$ is the tissue oxygen tension at radial distance x (cm) from the vessel center. The rate of oxygen consumption Q is equivalent to the product of the cerebral metabolic rate of oxygen ($CMRO_2$) and the density ρ of brain tissue. The Krogh diffusion constant K is the product of the oxygen diffusion coefficient D (1.5×10^3 µm^2/s) and the oxygen solubility α (1.3×10^{-3}cm^3/(cm$^3\times$760mmHg)). The Krogh model postulates that a central vessel with radius r and infinite length supplies a concentric tissue cylinder with radius R with radially diffusing oxygen. The diffusion equation and Krogh model were applied to simulate the diffusion time used in tissue during epilepsy. For the mouse brain the $CMRO_2$ was 2.6 µmol/g/min at baseline (Cui et al., 2013) and increased ~12% during epileptic seizures (Zhao et al., 2011).

6.4 Results

6.4.1 PO_2 changes in tissue at the epileptic focus during seizure-like activity

Seizure-like activity was characterized by first rhythmic spiking of increasing amplitude and decreasing frequency, evolving into rhythmic spikes and slow wave activity prior to gradual offset (see e.g. Figure 6-1A middle and Figure 6-1B middle).

Using two-photon phosphorescence lifetime microscopy, PO_2 was measured in tissue close to arterioles. A typical change in tissue PO_2 is shown in Figure 6-1A. The typical PO_2 time-profile was biphasic with an early dip after ictal onset, followed by a longer duration increase in PO_2. These results were in agreement with previous works where similar responses were observed using confocal microscopy or oxygen electrodes (Bahar et al., 2006; Zhang et al., 2015a).

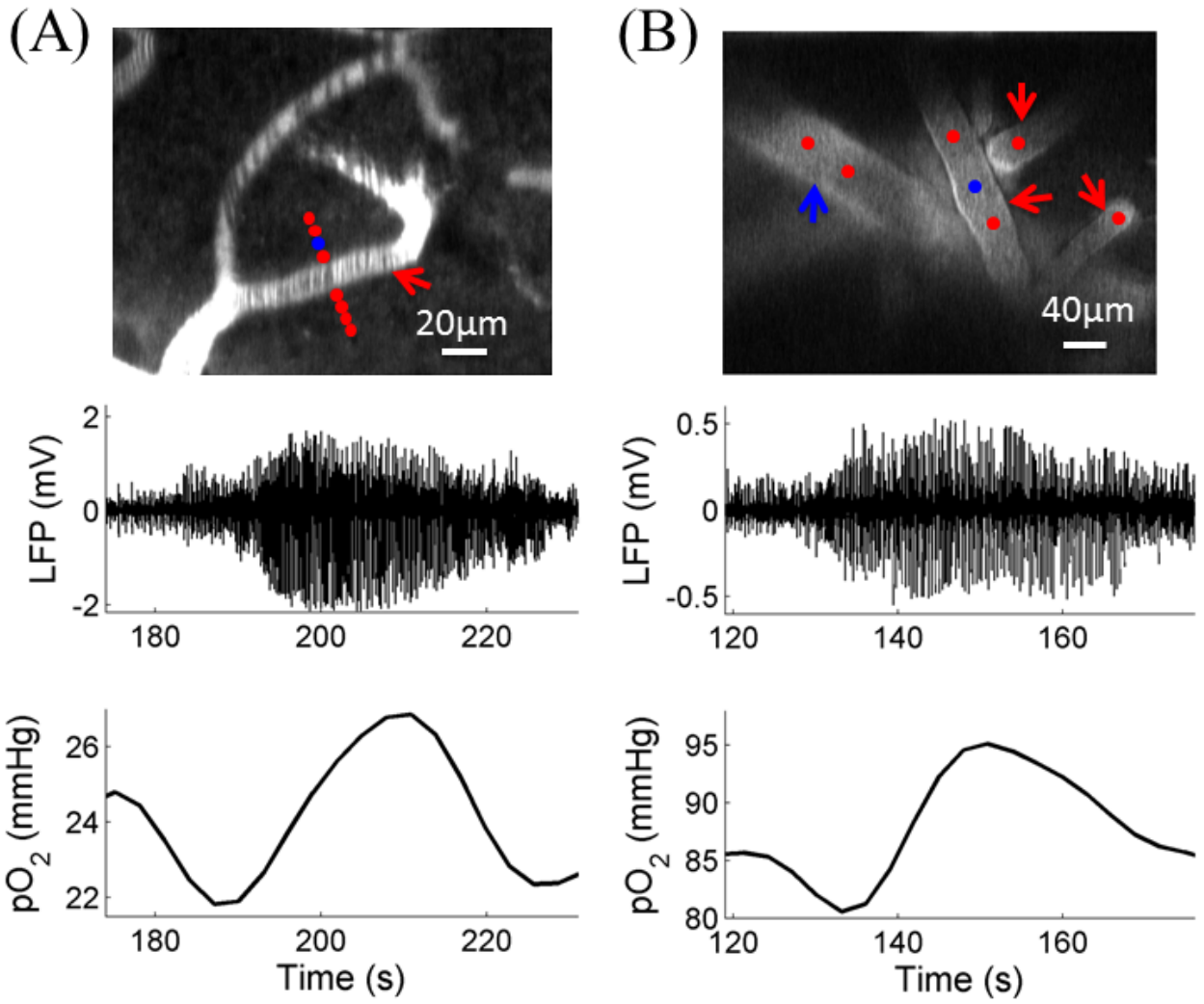

Figure 6-1: Representative changes in oxygen partial pressure (PO_2) in tissue (A) and artery (B), in response to epileptic events in a local area. Grayscale angiogram of cortical pial tissue with points of interest (with arteries shown by the red arrows, a vein shown by the blue arrow and a typical PO_2 time course shown for the blue points, top of (A) and (B) panels). The time course of LFPs indicates seizure initiation. (A) Epileptic activity induced a transient dip in tissue PO_2 followed by an increase in PO_2 at the focus. (B) In the artery, the PO_2 profile was also biphasic with an early dip followed by an increase.

We then investigated the spatial distribution of this dip along small arterioles. Four mice were used to measure the PO_2 in tissue at multiple locations near an arteriole that was located in the epileptic focus, i.e. <1.5mm from the 4-AP injection site. Figure 6-2A shows that the percent PO_2 changes during the dip were significantly lower in tissue closer to arterioles than that located

father away. This change was vessel size-dependent as seen by separating data according to diameter in two groups, 12.60 ± 0.83 μm (n=38) and 14.65 ± 1.05 μm (n=25) with significantly larger changes in tissue surrounding smaller arterioles (*t*-test, p<0.001).

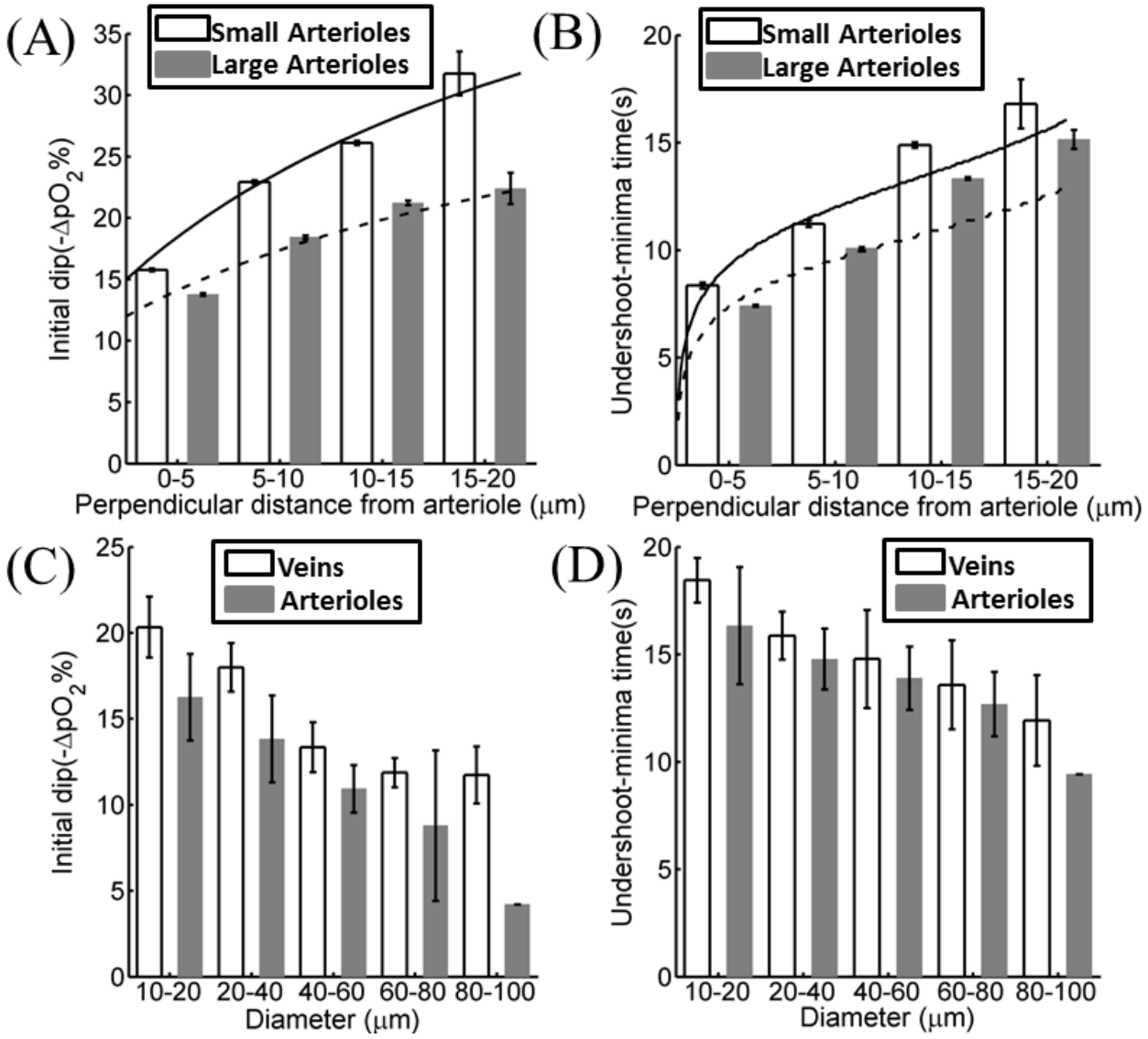

Figure 6-2 : (A) Changes in the amplitude of the percent initial dip around small and large arterioles, as a function of the perpendicular distance. The solid line and dashed line show simulated results with small and large arterioles separately. Error bars represent standard error of the mean (SEM). (B) Timing of the dip extrema as a function of arteriolar size and perpendicular distance with simulated results. (C) Percent change of the initial dip in arteries and veins in response to seizure-like activity, grouped by vessel diameter, with corresponding standard error

reported. (D) The undershoot-minima time in arteries and veins, grouped by vessel diameter, with corresponding SEM.

The undershoot-minima time (Figure 6-2B) was also seen to be lower when the point was located closer to the arteriole or next to a larger vessel (*t*-test, p=0.005). Both trends of initial-dip and undershoot-minima time could be predicted from simulations with the Krogh-Erlang model (lines in Figure 6- 2A and Figure 6-2B).

6.4.2 Epileptic seizures induced PO_2 response in vasculature at the epileptic focus

Since smaller arterioles are likely to be located further downstream than larger ones, we investigated PO_2 changes in upstream and downstream vascular segments during similar ictal events. Four mice were used to gather recordings at multiple locations in arteries and veins at the epileptic focus (<1.5mm from the injection site). Figure 6-2C and Figure 6-2D show the percent changes associated with the initial dip and undershoot-minima time in arterioles and veins categorized by diameter. Figure 6-2C shows a size dependent initial dip with smaller vessels seeing larger changes. Moreover, the observed variations in PO_2 were larger in venules than arterioles (*t*-test with p=0.03). Figure 6-2D further indicates that the undershoot-minima time of large arterioles and veins occurred earlier than small arterioles and veins. There was also a significant difference between the undershoot-minima time values of the arterioles and veins (*t*-test with p=0.01).

6.5 Discussion

Epilepsy-evoked changes in cerebral tissue oxygenation have been observed previously by Clark microelectrodes (Zhao et al., 2007) and confocal phosphorescence lifetime microscopy (Zhang et al., 2015). Polarographic electrode oxygen measurements have limited spatial accuracy, and are limited in the number of point measurements achievable. In our previous work, confocal phosphorescence lifetime microscopy was also limited due to its inability to reach deeper tissue making investigations of the impact of microvascular morphology on delivery difficult. To our knowledge, the current study is the first to perform absolute measurements of PO_2 in multiple individual microvascular compartments and tissue locations with high spatial and temporal resolution during epileptic seizures.

6.5.1 The relationship between the initial dip and distance from arterioles

Exploiting spatial measures around small arterioles, we investigated how tissue oxygen pressure changed near arterioles located in the epileptic focus region during epileptiform activity. Our data indicate an increase in PO_2 percent changes surrounding small arteries during early phases of epileptic activity (initial dip) which can be attributed to increased tissue metabolic consumption using a Krogh-Erlang model. While a proportional shift of delivery may move towards capillaries, in these events they do not fully compensate for consumption needs with small and large arterioles remaining largely responsible for oxygen distribution in the cortex (Sharan et al., 2008). This is consistent with previous findings of oxygen exchange between large arteries and tissue (Zhang et al., 2015). Our results further suggest that it is tissue areas located far from larger arterioles, in the capillary bed, that are more susceptible to hypoxia rather than tissue next to arteries. Temporally, our data show that points far away from the arteriolar wall take more time to recover basal PO_2 than locations near small arterioles with a size-dependent arteriolar influence. The delay times observed are larger than typical blood transit time (~2 sec) in the neurovascular unit. Overall these results suggest that the increased CBF and CBV in the focus during epileptic events will supply more oxygen to the tissue near arterioles, but may not meet the demands of oxygen metabolism in capillary areas.

6.5.2 The relationship between the initial dip and diameter of arteries and veins

It is interesting that the largest fractional decreases in vascular PO_2 were measured in small veins and small arteries. In addition, the largest decrease in PO_2 was calculated to take place in veins. The explanation of these results may be that the upstream vessels deliver more oxygen during intense neural activity. Temporally, the undershoot-minima time in vascular PO_2 was first observed in the large arteries and veins followed by the small arteries and veins. The largest decrease in PO_2 was observed in small veins. Our results suggest that the blood flow-driven increases in PO_2 start from arterioles and propagate to veins.

6.6 Conclusion

In conclusion, this study provided absolute PO_2 measurements in tissue, arteries and veins with two-photon microscopy during 4-AP evoked epileptic events. In this work, we observed significant changes of PO_2 delivery as a function of the vascular architecture.

6.7 Acknowledgments

We thank Marc-Antoine Gillis and Natacha Duquette for their assistance in animal preparation. We also thank Sergei Vinogradov for calibrating the PtP-C343 dye for us.

6.8 References

Bahar, S., Suh, M., Zhao, M., Schwartz, T.H., 2006. Intrinsic optical signal imaging of neocortical seizures: the "epileptic dip." Neuroreport 17, 499–503. doi:10.1097/01.wnr.0000209010.78599.f5

Berwick, J., Johnston, D., Jones, M., Martindale, J., Redgrave, P., McLoughlin, N., Schiessl, I., Mayhew, J.E.W., 2005. Neurovascular coupling investigated with two-dimensional optical imaging spectroscopy in rat whisker barrel cortex. Eur. J. Neurosci. 22, 1655–1666. doi:10.1111/j.1460-9568.2005.04347.x

Burton, A.C., 1954. Relation of structure to function of the tissues of the wall of blood vessels. Physiol. Rev. 34, 619–642.

Buxton, R.B., Frank, L.R., 1997. A model for the coupling between cerebral blood flow and oxygen metabolism during neural stimulation. J. Cereb. Blood Flow Metab. Off. J. Int. Soc. Cereb. Blood Flow Metab. 17, 64–72. doi:10.1097/00004647-199701000-00009

Dalkara, T., Alarcon-Martinez, L., 2015. Cerebral microvascular pericytes and neurogliovascular signaling in health and disease. Brain Res. 1623, 3–17. doi:10.1016/j.brainres.2015.03.047

Duvernoy, H.M., Delon, S., Vannson, J.L., 1981. Cortical blood vessels of the human brain. Brain Res. Bull. 7, 519–579.

Finikova, O.S., Lebedev, A.Y., Aprelev, A., Troxler, T., Gao, F., Garnacho, C., Muro, S., Hochstrasser, R.M., Vinogradov, S.A., 2008. Oxygen Microscopy by Two-Photon-Excited

Phosphorescence. Chemphyschem Eur. J. Chem. Phys. Phys. Chem. 9, 1673–1679. doi:10.1002/cphc.200800296

Hillman, E.M.C., Devor, A., Bouchard, M.B., Dunn, A.K., Krauss, G.W., Skoch, J., Bacskai, B.J., Dale, A.M., Boas, D.A., 2007. Depth-resolved optical imaging and microscopy of vascular compartment dynamics during somatosensory stimulation. NeuroImage 35, 89–104. doi:10.1016/j.neuroimage.2006.11.032

Hu, X., Yacoub, E., 2012. The story of the initial dip in fMRI. NeuroImage 62, 1103–1108. doi:10.1016/j.neuroimage.2012.03.005

Kim, T., Hendrich, K.S., Masamoto, K., Kim, S.-G., 2007. Arterial versus total blood volume changes during neural activity-induced cerebral blood flow change: implication for BOLD fMRI. J. Cereb. Blood Flow Metab. Off. J. Int. Soc. Cereb. Blood Flow Metab. 27, 1235–1247. doi:10.1038/sj.jcbfm.9600429

Lauwers, F., Cassot, F., Lauwers-Cances, V., Puwanarajah, P., Duvernoy, H., 2008. Morphometry of the human cerebral cortex microcirculation: general characteristics and space-related profiles. NeuroImage 39, 936–948. doi:10.1016/j.neuroimage.2007.09.024

Pouliot, P., Truong, V.T., Zhang, C., Dubeau, S., Lesage, F., 2012. Tight neurovascular coupling in a rat model of quasi-periodic interictal spiking using multispectral optical imaging. pp. 841203–841203–6. doi:10.1117/12.2000717

Sakadžić, S., Mandeville, E.T., Gagnon, L., Musacchia, J.J., Yaseen, M.A., Yucel, M.A., Lefebvre, J., Lesage, F., Dale, A.M., Eikermann-Haerter, K., Ayata, C., Srinivasan, V.J., Lo, E.H., Devor, A., Boas, D.A., 2014. Large arteriolar component of oxygen delivery implies a safe margin of oxygen supply to cerebral tissue. Nat. Commun. 5, 5734. doi:10.1038/ncomms6734

Sharan, M., Vovenko, E.P., Vadapalli, A., Popel, A.S., Pittman, R.N., 2008. Experimental and theoretical studies of oxygen gradients in rat pial microvessels. J. Cereb. Blood Flow Metab. Off. J. Int. Soc. Cereb. Blood Flow Metab. 28, 1597–1604. doi:10.1038/jcbfm.2008.51

Zhang, C., Bélanger, S., Pouliot, P., Lesage, F., 2015. Measurement of Local Partial Pressure of Oxygen in the Brain Tissue under Normoxia and Epilepsy with Phosphorescence Lifetime Microscopy. PLoS ONE 10, e0135536. doi:10.1371/journal.pone.0135536

Zhao, M., Ma, H., Suh, M., Schwartz, T.H., 2009. Spatiotemporal dynamics of perfusion and oximetry during ictal discharges in the rat neocortex. J. Neurosci. Off. J. Soc. Neurosci. 29, 2814–2823. doi:10.1523/JNEUROSCI.4667-08.2009

Zhao, M., Nguyen, J., Ma, H., Nishimura, N., Schaffer, C.B., Schwartz, T.H., 2011. Preictal and ictal neurovascular and metabolic coupling surrounding a seizure focus. J. Neurosci. Off. J. Soc. Neurosci. 31, 13292–13300. doi:10.1523/JNEUROSCI.2597-11.2011

Zhao, M., Suh, M., Ma, H., Perry, C., Geneslaw, A., Schwartz, T.H., 2007. Focal increases in perfusion and decreases in hemoglobin oxygenation precede seizure onset in spontaneous human epilepsy. Epilepsia 48, 2059–2067. doi:10.1111/j.1528-1167.2007.01229.x

Zheng, Y., Martindale, J., Johnston, D., Jones, M., Berwick, J., Mayhew, J., 2002. A model of the hemodynamic response and oxygen delivery to brain. NeuroImage 16, 617–637.

CHAPTER 7 GENERAL DISCUSSION

This thesis reports recent results and progresses in using optical imaging techniques to study the neurovascular coupling in focal epilepsy. Three scientific papers were presented in chapter 4, 5 and 6, focusing on the study of neurovascular coupling during focal epilepsy in the mouse cortex. This chapter reviews the objectives that are initially proposed in chapter 1, validates the corresponding hypotheses, and discusses the limitations of each article.

7.1 Objective 1

The first objective of this thesis was to develop the confocal phosphorescence lifetime microscopy system and use it to study the tissue PO_2 changes during 4-AP evoked focal epilepsy in the mouse cortex. This article presented in chapter 4 addresses this objective, with developing a confocal phosphorescence lifetime microscopy system. The system was used to measure tissue PO_2 during normoxia and epilepsy with a dendritic phosphorescent probe, Oxyphor G4. The system enabled minimally invasive measurements of PO_2 in cerebral tissue with high spatial and temporal resolution during 4-AP induced epileptic seizures.

On one hand, this study supports the idea that the tissue PO_2 change associated with epileptic seizures can be observed by confocal phosphorescence lifetime microscopy. In this work, following 4-AP injection in the somatosensory cortex of mice, significant changes of PO_2 in tissue near the injection site were observed, and its changes along arteries and in the surrounding area were investigated. This study supports the existence of an initial dip and characterizes the spatial distribution of the initial dip around the focus and near pial arteries. A positive correlation between the early oxygen metabolism in tissue and the duration of seizures was found, which may eventually help localize the epileptic focus and predict the length of seizure.

However, the system had limitations: the confocal phosphorescence lifetime microscopy system may suffer from the photoconsumptive effects. To diminish the photonconsumption, survey scans were done before the recording, which could lead to the production of singlet oxygen as some areas were subject to higher light intensity than required by our 3000 counts estimation during the calibration phase. Our measurements were careful to limit the intensity during survey scans and a pause was done between survey scans and acquisitions to ensure tissue oxygen was replenished. Despite these steps, we cannot completely rule out the possibility of tissue damage

during survey scans. Furthermore, the elongated focus of the confocal microscope in diffusive conditions failed to precisely assess distribution of oxygen in the depth axis and around small vessels, which limit conclusions on oxygen diffusion during seizures. Finally, a potential bias in measured PO_2 values during epileptiform discharges may occur due to a small increase in temperature at the epileptic foci. Tokiwa et al found that the elevation of the focal brain temperature increased around 0.65 ± 0.24°C during epileptiform discharges in the rat brain (Tokiwa et al., 2013). There is a small change in decay parameters measured for Oxyphor G4 with fractional temperature change, but this was not considered in this paper.

7.2 Objective 2

The second objective of this thesis was to simultaneously monitor the changes of calcium concentration in astrocytic endfeet and diameter of encased arterioles. The article presented in chapter 5 addresses this objective. In this objective, we developed two-photon microscopy and applied it to simultaneously measure the calcium concentration in astrocytic endfeet and diameter of adjacent arterioles with calcium-sensitive indicator OGB-1 under normoxia and epilepsy. This system enabled simultaneous measurement of calcium concentration and diameter with high spatial (~0.3μm) and temporal resolution (~ 0.9s).

In this article, we exploited 4-AP induced epileptic events to show that absolute calcium concentration in cortical astrocytic endfeet *in vivo* correlates with the diameter of precapillary arterioles during neural activity. Two-photon fluorescence lifetime microscopy was applied to simultaneously monitor free calcium concentration in astrocytic endfeet with OGB-1 and the diameter of adjacent arterioles in the somatosensory cortex of adult mice following 4-AP injections. The results reveal that astrocytic endfoot calcium concentration was elevated during epileptic events and increases in calcium concentration induced vasodilation for each individual ictal event at the focus. In the remote area, increases in calcium concentration correlated with vasoconstriction at the onset of seizure and vasodilation during the later part of the seizure, which supports the existence of the elevation of calcium concentration causing arteriolar dilation at the focus during stimulation. Moreover, following multiple seizures a slow increase in absolute calcium concentration was observed, which caused a trend of arteriolar constriction at the epileptic focus and remote areas. This study confirms the role of astrocytes in control of local

microcirculation and provides information that could help to understand the association between astrocytic calcium concentration levels and the vascular tone.

The first weakness of this study was that our data correlating the increase of basal calcium concentration to an inhibitory dilation of adjacent arterioles suggested that calcium concentration may indeed contribute to the observation of inhibitory non-linear hemodynamic phenomena in epilepsy. More work is required, using different epileptogenic agents and models as well as *in vivo* uncaging of calcium and chelators to further understand the relative importance of calcium concentration in this inhibitory phenomenon. In addition, the cerebral blood flow in arterioles was not measured simultaneously with calcium concentration in this study. According to Grubb et al. (Grubb et al., 1974), CBF and CBV can be related by a simple power law equation, which the coefficient was called the Grubb exponent. However, the Grubb exponent is known to change under neuropathologies in the brain. Hence, measuring CBF simultaneously with absolute calcium concentration would contribute additional useful information. Lastly, the length and frequency of the seizure were not considered in calcium concentration changes in astrocytic endfeet and diameter changes of arterioles. Our study has found the length of seizure was correlated with the PO_2 changes in tissue and PO_2 changes adjust the release of calcium concentration in astrocytic endfeet.

7.3 Objective 3

The last objective of this thesis was to measure the PO_2 changes in tissue near arterioles and in cerebral vasculature during epileptic events induced by 4-AP in mouse brain with two-photon phosphorescence microscopy. The article presented in chapter 6 addresses this objective. In this study, we applied two-photon phosphorescence microscopy technique to measure the PO_2 changes in tissue near arterioles and in microvessels in mouse somatosensory cortex during 4-AP induced epileptic events. This system enables minimally invasive measurements of PO_2 deeply in mouse cortex with high spatial (~0.3μm) and temporal resolution (~0.3s) following 4-AP evoked epileptic seizures.

In this study, a custom-built two-photon microscopy system was used to measure the PO_2 in tissue near various sizes of arterioles and in microvessels of different size with oxygen-sensitive dye (PtP-C343) during epileptic seizures. In this study significant PO_2 changes were observed in

tissue near arterioles and in vessels following epileptic events in mouse somatosensory cortex and these changes were correlated with the size of the microvessels. The distribution of the initial dip in arterioles, veins and tissue were characterized near the 4-AP injection site. The results reveal that the arterioles contribute to oxygen consumption in the tissue and the percent change in PO_2 signal during the initial dip is correlated with the diameter of arteries and veins during epileptic events.

The first limitation of this study is the difficulty to measure the PO_2 in small capillaries with two-photon microscopy. During the experiment, we found the two-photon microscopy was sensitive to the position of the capillary because of the high spatial resolution. Thus PO_2 in capillaries was not measured in this study, which may supply more information in the deep brain during epilepsy. In addition, CBF was not recorded in this study during epilepsy. When brain has epileptic events, the cerebral blood flow will increase and bring more glucose and oxygen to meet the demand of neural activity. In this work, an initial dip was found in tissue and vessel during epilepsy, which means that blood flow did not meet the demand of neuronal activity, which was not confirmed with direct measurements of CBF.

Overall, 4-AP acts as a K^+ channel blocker and a potent convulsant that was applied to induce the epileptic events in neocortex. Focal 4-AP injection in the neocortex generates focal epileptic seizures *in vivo*. 4-AP can also be applied to produce seizures with a generalized way in the whole slice *in vitro* (Yang et al., 2010). Besides, the epileptic events are generated in multiple layers and multiple locations and in an uncontrolled way *in vitro*. Some studies have showed that the γ-aminobutyric acid played an important role in the 4-AP induced epilepsy animal model (Avoli et al., 2002; Gonzalez-Sulser et al., 2011). Since 4-AP induced seizures are sensitive to anticonvulsants, combing with the γ-aminobutyric acid antagonist bicuculline was applied to induce pharmacoresistant activities (Brückner et al., 1999).

CHAPTER 8 CONCLUSION

In this thesis, confocal microscopy was employed to study the neurovascular coupling changes in mouse somatosensory cortex during 4-AP evoked epileptic seizures. We first developed the confocal phosphorescence lifetime microscopy system that provided absolute values of PO_2 in the brain cortex. We applied this technique to study PO_2 changes in tissue during epileptic activity in mice. Following 4-AP injection in the somatosensory cortex of mice, the significant changes of PO_2 in tissue near the injection site and in the surrounding were observed. This study supported the existence of an initial dip and investigated the spatial distribution of the initial dip around the focus and near pial arteries. The positive correlation between the early oxygen metabolism in tissue and the duration of seizures was found, which may eventually help localize the epileptic focus and predict the length of seizure.

Following the first work, two-photon fluorescence microscopy was applied to simultaneously provide absolute values of calcium concentration in astrocytic endfoot and diameter in adjacent arteriole in the brain cortex. This technique was developed to study how astrocytic endfoot controls encased arterioles during epileptic activity in the mouse cortex. In this work, following 4-AP injection in the somatosensory cortex of mice, we observed significant changes of calcium concentration in endfeet and diameter in arterioles at focus and in the remote areas. In addition, we found a negative correlation between basal calcium concentration in endfoot and the amplitude of dilation for all measurements at focus, while, in the remote areas, there was a positive correlation between calcium concentration in endfeet during the onset of seizures and the level of vasoconstriction. This study could help to understand the association between astrocytic calcium concentration levels and vascular tone.

However, the PO_2 changes in the deep tissue near arterioles and in microvessels during epilepsy are also important to the calcium release from the astrocytic endfoot. To address that, we proposed to use two-photon phosphorescence microscopy with high spatial and temporal resolution to measure the PO_2 changes in tissue and microvessels during epilepsy. The significant PO_2 changes in tissue and microvessels were found in mouse somatosensory cortex during 4-AP induced epileptic seizures. In tissue, the positive correlation was revealed between the distance from arterioles and percent changes of initial dip or the undershoot-minima time, which correlated with the diameter of arterioles. In vessels, a negative correlation was shown between

the diameter of vessels and initial dip changes or the undershoot-minima time. This study could help to evaluate microvascular oxygen delivery capacity to support cerebral tissue in epilepsy.

BIBLIOGRAPHY

Adelson, P.D., Nemoto, E., Scheuer, M., Painter, M., Morgan, J., Yonas, H., 1999. Noninvasive continuous monitoring of cerebral oxygenation periictally using near-infrared spectroscopy: a preliminary report. Epilepsia 40, 1484–1489.

Ances, B.M., Buerk, D.G., Greenberg, J.H., Detre, J.A., 2001. Temporal dynamics of the partial pressure of brain tissue oxygen during functional forepaw stimulation in rats. Neurosci. Lett. 306, 106–110.

An, D., Fahoum, F., Hall, J., Olivier, A., Gotman, J., Dubeau, F., 2013. Electroencephalography/functional magnetic resonance imaging responses help predict surgical outcome in focal epilepsy. Epilepsia 54, 2184–2194. doi:10.1111/epi.12434

Arca Diaz, G., Cesaron, E., Alfonso, I., Dunoyer, C., Yaylali, I., 2006. Near infrared spectroscopy in the management of status epilepticus in a young infant. Eur. J. Paediatr. Neurol. EJPN Off. J. Eur. Paediatr. Neurol. Soc. 10, 19–21. doi:10.1016/j.ejpn.2005.11.001

Arthurs, O.J., Williams, E.J., Carpenter, T.A., Pickard, J.D., Boniface, S.J., 2000. Linear coupling between functional magnetic resonance imaging and evoked potential amplitude in human somatosensory cortex. Neuroscience 101, 803–806.

Attwell, D., Buchan, A.M., Charpak, S., Lauritzen, M., MacVicar, B.A., Newman, E.A., 2010. Glial and neuronal control of brain blood flow. Nature 468, 232–243. doi:10.1038/nature09613

Attwell, D., Laughlin, S.B., 2001. An energy budget for signaling in the grey matter of the brain. J. Cereb. Blood Flow Metab. Off. J. Int. Soc. Cereb. Blood Flow Metab. 21, 1133–1145. doi:10.1097/00004647-200110000-00001

Avoli, M., D'Antuono, M., Louvel, J., Köhling, R., Biagini, G., Pumain, R., D'Arcangelo, G., Tancredi, V., 2002. Network and pharmacological mechanisms leading to epileptiform synchronization in the limbic system in vitro. Prog. Neurobiol. 68, 167–207. doi:10.1016/S0301-0082(02)00077-1

Bahar, S., Suh, M., Mehta, A., Schwartz, T.H., 2005. In Vivo Intrinsic Optical Signal Imaging of Neocortical Epilepsy, in: Broderick, P.A., Rahni, D.N., MD, E.H.K. (Eds.), Bioimaging in Neurodegeneration, Contemporary Neuroscience. Humana Press, pp. 149–175.

Bahar, S., Suh, M., Zhao, M., Schwartz, T.H., 2006. Intrinsic optical signal imaging of neocortical seizures: the "epileptic dip." Neuroreport 17, 499–503. doi:10.1097/01.wnr.0000209010.78599.f5

Bai, X., Guo, J., Killory, B., Vestal, M., Berman, R., Negishi, M., Danielson, N., Novotny, E.J., Constable, R.T., Blumenfeld, H., 2011. Resting functional connectivity between the hemispheres in childhood absence epilepsy. Neurology 76, 1960–1967. doi:10.1212/WNL.0b013e31821e54de

Bazargani, N., Attwell, D., 2016. Astrocyte calcium signaling: the third wave. Nat. Neurosci. 19, 182–189. doi:10.1038/nn.4201

Bénar, C.G., Gross, D.W., Wang, Y., Petre, V., Pike, B., Dubeau, F., Gotman, J., 2002. The BOLD response to interictal epileptiform discharges. NeuroImage 17, 1182–1192.

Bénar, C.-G., Grova, C., Kobayashi, E., Bagshaw, A.P., Aghakhani, Y., Dubeau, F., Gotman, J., 2006. EEG-fMRI of epileptic spikes: concordance with EEG source localization and intracranial EEG. NeuroImage 30, 1161–1170. doi:10.1016/j.neuroimage.2005.11.008

Berg, A.T., Vickrey, B.G., Langfitt, J.T., Sperling, M.R., Walczak, T.S., Shinnar, S., Bazil, C.W., Pacia, S.V., Spencer, S.S., Multicenter Study of Epilepsy Surgery, 2003. The multicenter study of epilepsy surgery: recruitment and selection for surgery. Epilepsia 44, 1425–1433.

Berger, M.S., Ghatan, S., Haglund, M.M., Dobbins, J., Ojemann, G.A., 1993. Low-grade gliomas associated with intractable epilepsy: seizure outcome utilizing electrocorticography during tumor resection. J. Neurosurg. 79, 62–69. doi:10.3171/jns.1993.79.1.0062

Bernasconi, A., Bernasconi, N., Bernhardt, B.C., Schrader, D., 2011. Advances in MRI for "cryptogenic" epilepsies. Nat. Rev. Neurol. 7, 99–108. doi:10.1038/nrneurol.2010.199

Berwick, J., Johnston, D., Jones, M., Martindale, J., Redgrave, P., McLoughlin, N., Schiessl, I., Mayhew, J.E.W., 2005. Neurovascular coupling investigated with two-dimensional optical imaging spectroscopy in rat whisker barrel cortex. Eur. J. Neurosci. 22, 1655–1666. doi:10.1111/j.1460-9568.2005.04347.x

Boorman, L., Kennerley, A.J., Johnston, D., Jones, M., Zheng, Y., Redgrave, P., Berwick, J., 2010. Negative Blood Oxygen Level Dependence in the Rat:A Model for Investigating the Role of Suppression in Neurovascular Coupling. J. Neurosci. 30, 4285–4294. doi:10.1523/JNEUROSCI.6063-09.2010

Borbély, S., Körössy, C., Somogyvári, Z., Világi, I., 2014. In vitro intrinsic optical imaging can be used for source determination in cortical slices. Eur. J. Neurosci. 39, 72–82. doi:10.1111/ejn.12384

Bouilleret, V., Valenti, M.P., Hirsch, E., Semah, F., Namer, I.J., 2002. Correlation Between PET and SISCOM in Temporal Lobe Epilepsy. J. Nucl. Med. 43, 991–998.

Brieu, N., Beaumont, E., Dubeau, S., Cohen-Adad, J., Lesage, F., 2010. Characterization of the hemodynamic response in the rat lumbar spinal cord using intrinsic optical imaging and laser speckle. J. Neurosci. Methods 191, 151–157. doi:10.1016/j.jneumeth.2010.06.012

Brodbeck, V., Spinelli, L., Lascano, A.M., Wissmeier, M., Vargas, M.-I., Vulliemoz, S., Pollo, C., Schaller, K., Michel, C.M., Seeck, M., 2011. Electroencephalographic source imaging: a prospective study of 152 operated epileptic patients. Brain 134, 2887–2897. doi:10.1093/brain/awr243

Brückner, K., Pablo Labrador, J., Scheiffele, P., Herb, A., Seeburg, P.H., Klein, R., 1999. EphrinB ligands recruit GRIP family PDZ adaptor proteins into raft membrane microdomains. Neuron 22, 511–524.

Buchheim, K., Obrig, H., v Pannwitz, W., Müller, A., Heekeren, H., Villringer, A., Meierkord, H., 2004. Decrease in haemoglobin oxygenation during absence seizures in adult humans. Neurosci. Lett. 354, 119–122.

Buehler, C., Kim, K.H., Dong, C.Y., Masters, B.R., So, P.T.C., 1999. Innovations in two-photon deep tissue microscopy. IEEE Eng. Med. Biol. Mag. 18, 23–30. doi:10.1109/51.790988

Buxton, R.B., 2013. The physics of functional magnetic resonance imaging (fMRI). Rep. Prog. Phys. Phys. Soc. G. B. 76, 096601. doi:10.1088/0034-4885/76/9/096601

Buxton, R.B., Frank, L.R., 1997. A model for the coupling between cerebral blood flow and oxygen metabolism during neural stimulation. J. Cereb. Blood Flow Metab. Off. J. Int. Soc. Cereb. Blood Flow Metab. 17, 64–72. doi:10.1097/00004647-199701000-00009

Callaghan, B.C., Anand, K., Hesdorffer, D., Hauser, W.A., French, J.A., 2007. Likelihood of seizure remission in an adult population with refractory epilepsy. Ann. Neurol. 62, 382–389. doi:10.1002/ana.21166

Cascino, G.D., Buchhalter, J.R., Mullan, B.P., So, E.L., 2004. Ictal SPECT in nonlesional extratemporal epilepsy. Epilepsia 45 Suppl 4, 32–34. doi:10.1111/j.0013-9580.2004.04007.x

Cascino, G.D., Buchhalter, J.R., Sirven, J.I., So, E.L., Drazkowski, J.F., Zimmerman, R.S., Raffel, C., 2004. Peri-ictal SPECT and surgical treatment for intractable epilepsy related to schizencephaly. Neurology 63, 2426–2428.

Cascino, G.D., Sharbrough, F.W., Trenerry, M.R., Marsh, W.R., Kelly, P.J., So, E., 1994. Extratemporal cortical resections and lesionectomies for partial epilepsy: complications of surgical treatment. Epilepsia 35, 1085–1090.

Centonze, V.E., White, J.G., 1998. Multiphoton excitation provides optical sections from deeper within scattering specimens than confocal imaging. Biophys. J. 75, 2015–2024.

Chassoux, F., Devaux, B., Landré, E., Turak, B., Nataf, F., Varlet, P., Chodkiewicz, J.P., Daumas-Duport, C., 2000. Stereoelectroencephalography in focal cortical dysplasia: a 3D approach to delineating the dysplastic cortex. Brain J. Neurol. 123 (Pt 8), 1733–1751.

Cheng, M.Y., Wang, E.H., Woodson, W.J., Wang, S., Sun, G., Lee, A.G., Arac, A., Fenno, L.E., Deisseroth, K., Steinberg, G.K., 2014. Optogenetic neuronal stimulation promotes functional recovery after stroke. Proc. Natl. Acad. Sci. U. S. A. 111, 12913–12918. doi:10.1073/pnas.1404109111

Chen, J.W., O'Farrell, A.M., Toga, A.W., 2000. Optical intrinsic signal imaging in a rodent seizure model. Neurology 55, 312–315.

Cirillo, G., De Luca, D., Papa, M., 2012. Calcium imaging of living astrocytes in the mouse spinal cord following sensory stimulation. Neural Plast. 2012, 425818. doi:10.1155/2012/425818

Cooper, R.J., Hebden, J.C., O'Reilly, H., Mitra, S., Michell, A.W., Everdell, N.L., Gibson, A.P., Austin, T., 2011. Transient haemodynamic events in neurologically compromised infants: a

simultaneous EEG and diffuse optical imaging study. NeuroImage 55, 1610–1616. doi:10.1016/j.neuroimage.2011.01.022

Cui, W., Zhu, X.-H., Vollmers, M.L., Colonna, E.T., Adriany, G., Tramm, B., Dubinsky, J.M., Öz, G., 2013. Non-invasive measurement of cerebral oxygen metabolism in the mouse brain by ultra-high field (17)O MR spectroscopy. J. Cereb. Blood Flow Metab. Off. J. Int. Soc. Cereb. Blood Flow Metab. 33, 1846–1849. doi:10.1038/jcbfm.2013.172

Dalkara, T., Alarcon-Martinez, L., 2015. Cerebral microvascular pericytes and neurogliovascular signaling in health and disease. Brain Res. 1623, 3–17. doi:10.1016/j.brainres.2015.03.047

d'Asseler, Y.M., Koole, M., Lemahieu, I., Achten, E., Boon, P., De Deyn, P.P., Dierckx, R.A., 1997. Recent and future evolutions in NeuroSPECT with particular emphasis on the synergistic use and fusion of imaging modalities. Acta Neurol. Belg. 97, 154–162.

Dean, P.N., 2001. Confocal microscopy: principles and practices. Curr. Protoc. Cytom. Editor. Board J Paul Robinson Manag. Ed. Al Chapter 2, Unit 2.8. doi:10.1002/0471142956.cy0208s05

Dean, P.N., 2001. Confocal Microscopy: Principles and Practices, in: Current Protocols in Cytometry. John Wiley & Sons, Inc.

de Curtis, M., Avanzini, G., 2001. Interictal spikes in focal epileptogenesis. Prog. Neurobiol. 63, 541–567.

Delpy, D.T., Cope, M., 1997. Quantification in tissue near-infrared spectroscopy. Philos. Trans. R. Soc. B Biol. Sci. 352, 649–659. doi:10.1098/rstb.1997.0046

Denk, W., Delaney, K.R., Gelperin, A., Kleinfeld, D., Strowbridge, B.W., Tank, D.W., Yuste, R., 1994. Anatomical and functional imaging of neurons using 2-photon laser scanning microscopy. J. Neurosci. Methods, Imaging Techniques in Neurobiology 54, 151–162. doi:10.1016/0165-0270(94)90189-9

Denk, W., Detwiler, P.B., 1999. Optical recording of light-evoked calcium signals in the functionally intact retina. Proc. Natl. Acad. Sci. U. S. A. 96, 7035–7040.

Denk, W., Strickler, J.H., Webb, W.W., 1990. Two-photon laser scanning fluorescence microscopy. Science 248, 73–76. doi:10.1126/science.2321027

Desai, A., Bekelis, K., Thadani, V.M., Roberts, D.W., Jobst, B.C., Duhaime, A.-C., Gilbert, K., Darcey, T.M., Studholme, C., Siegel, A., 2013. Interictal PET and ictal subtraction SPECT: sensitivity in the detection of seizure foci in patients with medically intractable epilepsy. Epilepsia 54, 341–350. doi:10.1111/j.1528-1167.2012.03686.x

Desjardins, M., Berti, R., Lefebvre, J., Dubeau, S., Lesage, F., 2014a. Aging-related differences in cerebral capillary blood flow in anesthetized rats. Neurobiol. Aging 35, 1947–1955. doi:10.1016/j.neurobiolaging.2014.01.136

Desjardins, M., Berti, R., Pouliot, P., Dubeau, S., Lesage, F., 2014b. Multimodal study of the hemodynamic response to hypercapnia in anesthetized aged rats. Neurosci. Lett. 563, 33–37. doi:10.1016/j.neulet.2014.01.027

Diaspro, A., 2001. Building a Two-Photon Microscope Using a Laser Scanning Confocal Architecture, in: Periasamy, A. (Ed.), Methods in Cellular Imaging, Methods in Physiology. Springer New York, pp. 162–179.

Driscoll, J.D., Shih, A.Y., Drew, P.J., Cauwenberghs, G., Kleinfeld, D., 2013. Two-photon imaging of blood flow in the rat cortex. Cold Spring Harb. Protoc. 2013, 759–767. doi:10.1101/pdb.prot076513

Drzezga, A., Arnold, S., Minoshima, S., Noachtar, S., Szecsi, J., Winkler, P., Römer, W., Tatsch, K., Weber, W., Bartenstein, P., 1999. 18F-FDG PET studies in patients with extratemporal and temporal epilepsy: evaluation of an observer-independent analysis. J. Nucl. Med. Off. Publ. Soc. Nucl. Med. 40, 737–746.

Dunphy, I., Vinogradov, S.A., Wilson, D.F., 2002. Oxyphor R2 and G2: phosphors for measuring oxygen by oxygen-dependent quenching of phosphorescence. Anal. Biochem. 310, 191–198.

Duvernoy, H.M., Delon, S., Vannson, J.L., 1981. Cortical blood vessels of the human brain. Brain Res. Bull. 7, 519–579. doi:10.1016/0361-9230(81)90007-1

Ekstrom, A., 2010. How and when the fMRI BOLD signal relates to underlying neural activity: the danger in dissociation. Brain Res. Rev. 62, 233–244. doi:10.1016/j.brainresrev.2009.12.004

Eliashiv, D.S., Elsas, S.M., Squires, K., Fried, I., Engel, J., 2002. Ictal magnetic source imaging as a localizing tool in partial epilepsy. Neurology 59, 1600–1610.

Engel, J., 2003. A Greater Role for Surgical Treatment of Epilepsy: Why and When? Epilepsy Curr. 3, 37–40. doi:10.1046/j.1535-7597.2003.03201.x

Engel, J., 1993. Update on surgical treatment of the epilepsies Summary of The Second International Palm Desert Conference on the Surgical Treatment of the Epilepsies (1992). Neurology 43, 1612–1612. doi:10.1212/WNL.43.8.1612

Esipova, T.V., Karagodov, A., Miller, J., Wilson, D.F., Busch, T.M., Vinogradov, S.A., 2011. Two new "protected" oxyphors for biological oximetry: properties and application in tumor imaging. Anal. Chem. 83, 8756–8765. doi:10.1021/ac2022234

Estrada, A.D., Ponticorvo, A., Ford, T.N., Dunn, A.K., 2008. Microvascular oxygen quantification using two-photon microscopy. Opt. Lett. 33, 1038–1040.

Feng, G., Laskowski, M.B., Feldheim, D.A., Wang, H., Lewis, R., Frisen, J., Flanagan, J.G., Sanes, J.R., 2000. Roles for Ephrins in Positionally Selective Synaptogenesis between Motor Neurons and Muscle Fibers. Neuron 25, 295–306. doi:10.1016/S0896-6273(00)80895-8

Ferris, C.F., Marella, M., Smerkers, B., Barchet, T.M., Gershman, B., Matsuno-Yagi, A., Yagi, T., 2013. A phenotypic model recapitulating the neuropathology of Parkinson's disease. Brain Behav. 3, 351–366. doi:10.1002/brb3.138

Filosa, J.A., Bonev, A.D., Straub, S.V., Meredith, A.L., Wilkerson, M.K., Aldrich, R.W., Nelson, M.T., 2006. Local potassium signaling couples neuronal activity to vasodilation in the brain. Nat. Neurosci. 9, 1397–1403. doi:10.1038/nn1779

Finikova, O.S., Lebedev, A.Y., Aprelev, A., Troxler, T., Gao, F., Garnacho, C., Muro, S., Hochstrasser, R.M., Vinogradov, S.A., 2008. Oxygen Microscopy by Two-Photon-Excited Phosphorescence. Chemphyschem Eur. J. Chem. Phys. Phys. Chem. 9, 1673–1679. doi:10.1002/cphc.200800296

Folbergrová, J., Ingvar, M., Siesjö, B.K., 1981. Metabolic changes in cerebral cortex, hippocampus, and cerebellum during sustained bicuculline-induced seizures. J. Neurochem. 37, 1228–1238.

Foster, T.H., Murant, R.S., Bryant, R.G., Knox, R.S., Gibson, S.L., Hilf, R., 1991. Oxygen Consumption and Diffusion Effects in Photodynamic Therapy. Radiat. Res. 126, 296–303. doi:10.2307/3577919

Friedrich, R.W., Korsching, S.I., 1998. Chemotopic, Combinatorial, and Noncombinatorial Odorant Representations in the Olfactory Bulb Revealed Using a Voltage-Sensitive Axon Tracer. J. Neurosci. 18, 9977–9988.

Friedrich, R.W., Korsching, S.I., 1997. Combinatorial and Chemotopic Odorant Coding in the Zebrafish Olfactory Bulb Visualized by Optical Imaging. Neuron 18, 737–752. doi:10.1016/S0896-6273(00)80314-1

Frostig, R.D., Lieke, E.E., Ts'o, D.Y., Grinvald, A., 1990. Cortical functional architecture and local coupling between neuronal activity and the microcirculation revealed by in vivo high-resolution optical imaging of intrinsic signals. Proc. Natl. Acad. Sci. U. S. A. 87, 6082–6086.

Fukuda, O., Endo, S., Kuwayama, N., Harada, J., Takaku, A., 1995. The characteristics of laser-Doppler flowmetry for the measurement of regional cerebral blood flow. Neurosurgery 36, 358–364.

Gadhoumi, K., Gotman, J., Lina, J.M., 2015. Scale Invariance Properties of Intracerebral EEG Improve Seizure Prediction in Mesial Temporal Lobe Epilepsy. PLOS ONE 10, e0121182. doi:10.1371/journal.pone.0121182

Gaillard, W.D., Bhatia, S., Bookheimer, S.Y., Fazilat, S., Sato, S., Theodore, W.H., 1995a. FDG-PET and volumetric MRI in the evaluation of patients with partial epilepsy. Neurology 45, 123–126.

Gaillard, W.D., Fazilat, S., White, S., Malow, B., Sato, S., Reeves, P., Herscovitch, P., Theodore, W.H., 1995b. Interictal metabolism and blood flow are uncoupled in temporal lobe cortex of patients with complex partial epilepsy. Neurology 45, 1841–1847.

Gambardella, A., Palmini, A., Andermann, F., Dubeau, F., Da Costa, J.C., Quesney, L.F., Andermann, E., Olivier, A., 1996. Usefulness of focal rhythmic discharges on scalp EEG of patients with focal cortical dysplasia and intractable epilepsy. Electroencephalogr. Clin. Neurophysiol. 98, 243–249.

Garaschuk, O., Milos, R.-I., Konnerth, A., 2006. Targeted bulk-loading of fluorescent indicators for two-photon brain imaging in vivo. Nat. Protoc. 1, 380–386. doi:10.1038/nprot.2006.58

Geneslaw, A.S., Zhao, M., Ma, H., Schwartz, T.H., 2011. Tissue hypoxia correlates with intensity of interictal spikes. J. Cereb. Blood Flow Metab. Off. J. Int. Soc. Cereb. Blood Flow Metab. 31, 1394–1402. doi:10.1038/jcbfm.2011.16

Girouard, H., Bonev, A.D., Hannah, R.M., Meredith, A., Aldrich, R.W., Nelson, M.T., 2010. Astrocytic endfoot Ca2+ and BK channels determine both arteriolar dilation and constriction. Proc. Natl. Acad. Sci. U. S. A. 107, 3811–3816. doi:10.1073/pnas.0914722107

Golshani, P., Portera-Cailliau, C., 2008. In Vivo 2-Photon Calcium Imaging in Layer 2/3 of Mice. J. Vis. Exp. JoVE. doi:10.3791/681

Golub, A.S., Pittman, R.N., 2008. Po2 measurements in the microcirculation using phosphorescence quenching microscopy at high magnification. Am. J. Physiol. - Heart Circ. Physiol. 294, H2905–H2916. doi:10.1152/ajpheart.01347.2007

Gonzalez-Sulser, A., Wang, J., Motamedi, G.K., Avoli, M., Vicini, S., Dzakpasu, R., 2011. THE 4-AMINOPYRIDINE IN VITRO EPILEPSY MODEL ANALYZED WITH A PERFORATED MULTI-ELECTRODE ARRAY. Neuropharmacology 60, 1142–1153. doi:10.1016/j.neuropharm.2010.10.007

Gordon, G.R.J., Choi, H.B., Rungta, R.L., Ellis-Davies, G.C.R., MacVicar, B.A., 2008. Brain metabolism dictates the polarity of astrocyte control over arterioles. Nature 456, 745–749. doi:10.1038/nature07525

Gourdie, R.G., 1994. Cell biological applications of confocal microscopy (methods in cell biology, vol. 38). Trends Neurosci. 17, 354–355. doi:10.1016/0166-2236(94)90181-3

Graham, D., Faulds, K., Dougan, J.A., 2013. Surface-Enhanced Raman Spectroscopy for Bioanalytics, in: Roberts, G.C.K. (Ed.), Encyclopedia of Biophysics. Springer Berlin Heidelberg, pp. 2537–2547.

Grinberg, O., Novozhilov, B., Grinberg, S., Friedman, B., Swartz, H.M., 2005. Axial Oxygen Diffusion in the Krogh Model, in: Oxygen Transport to Tissue XXVI. Springer, Boston, MA, pp. 127–134.

Grosche, J., Matyash, V., Möller, T., Verkhratsky, A., Reichenbach, A., Kettenmann, H., 1999. Microdomains for neuron-glia interaction: parallel fiber signaling to Bergmann glial cells. Nat. Neurosci. 2, 139–143. doi:10.1038/5692

Grova, C., Daunizeau, J., Lina, J.-M., Bénar, C.G., Benali, H., Gotman, J., 2006. Evaluation of EEG localization methods using realistic simulations of interictal spikes. NeuroImage 29, 734–753. doi:10.1016/j.neuroimage.2005.08.053

Grubb, R.L., Raichle, M.E., Eichling, J.O., Ter-Pogossian, M.M., 1974. The Effects of Changes in PaCO2 Cerebral Blood Volume, Blood Flow, and Vascular Mean Transit Time. Stroke 5, 630–639. doi:10.1161/01.STR.5.5.630

Guevara, E., Pouliot, P., Nguyen, D.K., Lesage, F., 2013. Optical imaging of acute epileptic networks in mice. J. Biomed. Opt. 18, 76021. doi:10.1117/1.JBO.18.7.076021

Haglund, M.M., Ojemann, G.A., Hochman, D.W., 1992. Optical imaging of epileptiform and functional activity in human cerebral cortex. Nature 358, 668–671. doi:10.1038/358668a0

Hamel, E., 2006. Perivascular nerves and the regulation of cerebrovascular tone. J. Appl. Physiol. Bethesda Md 1985 100, 1059–1064. doi:10.1152/japplphysiol.00954.2005

Hauser, W.A., Annegers, J.F., Kurland, L.T., 1991. Prevalence of epilepsy in Rochester, Minnesota: 1940-1980. Epilepsia 32, 429–445.

Heers, M., Hedrich, T., An, D., Dubeau, F., Gotman, J., Grova, C., Kobayashi, E., 2014. Spatial correlation of hemodynamic changes related to interictal epileptic discharges with electric and magnetic source imaging. Hum. Brain Mapp. 35, 4396–4414. doi:10.1002/hbm.22482

Heintzmann, R., Sarafis, V., Munroe, P., Nailon, J., Hanley, Q.S., Jovin, T.M., 2003. Resolution enhancement by subtraction of confocal signals taken at different pinhole sizes. Micron, Super-Resolution 34, 293–300. doi:10.1016/S0968-4328(03)00054-4

Hell, S.W., 2007. Far-Field Optical Nanoscopy. Science 316, 1153–1158. doi:10.1126/science.1137395

Helmchen, F., 2009. Two-Photon Functional Imaging of Neuronal Activity, in: Frostig, R.D. (Ed.), In Vivo Optical Imaging of Brain Function, Frontiers in Neuroscience. CRC Press/Taylor & Francis, Boca Raton (FL).

Hikima, A., Mochizuki, H., Oriuchi, N., Endo, K., Morikawa, A., 2004. Semiquantitative analysis of interictal glucose metabolism between generalized epilepsy and localization related epilepsy. Ann. Nucl. Med. 18, 579–584.

Hill, D.K., Keynes, R.D., 1949. Opacity changes in stimulated nerve. J. Physiol. 108, 278–281.

Hillman, E.M.C., 2014. Coupling Mechanism and Significance of the BOLD Signal: A Status Report. Annu. Rev. Neurosci. 37, 161–181. doi:10.1146/annurev-neuro-071013-014111

Hogan, M.C., 1999. Phosphorescence quenching method for measurement of intracellular PO2 in isolated skeletal muscle fibers. J. Appl. Physiol. Bethesda Md 1985 86, 720–724.

Horsley, V., 1892. An Address on the Origin and Seat of Epileptic Disturbance: Delivered before the Cardiff Medical Society. Br. Med. J. 1, 693–696.

Ho, S.S., Berkovic, S.F., Berlangieri, S.U., Newton, M.R., Egan, G.F., Tochon-Danguy, H.J., McKay, W.J., 1995. Comparison of ictal SPECT and interictal PET in the presurgical evaluation of temporal lobe epilepsy. Ann. Neurol. 37, 738–745. doi:10.1002/ana.410370607

Howarth, C., 2014. The contribution of astrocytes to the regulation of cerebral blood flow. Front. Neurosci. 8. doi:10.3389/fnins.2014.00103

Huneau, C., Benali, H., Chabriat, H., 2015. Investigating Human Neurovascular Coupling Using Functional Neuroimaging: A Critical Review of Dynamic Models. Neuroenergetics Nutr. Brain Health 467. doi:10.3389/fnins.2015.00467

Hu, X., Yacoub, E., 2012. The story of the initial dip in fMRI. NeuroImage 62, 1103–1108. doi:10.1016/j.neuroimage.2012.03.005

Hwang, S.I., Kim, J.H., Park, S.W., Han, M.H., Yu, I.K., Lee, S.H., Lee, D.S., Lee, S.K., Chung, C.K., Chang, K.H., 2001. Comparative analysis of MR imaging, positron emission tomography, and ictal single-photon emission CT in patients with neocortical epilepsy. AJNR Am. J. Neuroradiol. 22, 937–946.

Hyder, F., Rothman, D.L., Shulman, R.G., 2002. Total neuroenergetics support localized brain activity: Implications for the interpretation of fMRI. Proc. Natl. Acad. Sci. 99, 10771–10776. doi:10.1073/pnas.132272299

Iadecola, C., Nedergaard, M., 2007. Glial regulation of the cerebral microvasculature. Nat. Neurosci. 10, 1369–1376. doi:10.1038/nn2003

Ingvar, M., 1986. Cerebral blood flow and metabolic rate during seizures. Relationship to epileptic brain damage. Ann. N. Y. Acad. Sci. 462, 194–206.

Irani, F., Platek, S.M., Bunce, S., Ruocco, A.C., Chute, D., 2007. Functional near infrared spectroscopy (fNIRS): an emerging neuroimaging technology with important applications for the study of brain disorders. Clin. Neuropsychol. 21, 9–37. doi:10.1080/13854040600910018

Ivanov, K.P., Kislayokov, Y.Y., Samoilov, M.O., 1979. Microcirculation and transport of oxygen to neurons of the brain. Microvasc. Res. 18, 434–441. doi:10.1016/0026-2862(79)90049-9

Ives, J.R., Warach, S., Schmitt, F., Edelman, R.R., Schomer, D.L., 1993. Monitoring the patient's EEG during echo planar MRI. Electroencephalogr. Clin. Neurophysiol. 87, 417–420. doi:10.1016/0013-4694(93)90156-P

Jacobs, J., Levan, P., Moeller, F., Boor, R., Stephani, U., Gotman, J., Siniatchkin, M., 2009. Hemodynamic changes preceding the interictal EEG spike in patients with focal epilepsy investigated using simultaneous EEG-fMRI. NeuroImage 45, 1220–1231. doi:10.1016/j.neuroimage.2009.01.014

Jöbsis, F.F., 1977. Noninvasive, infrared monitoring of cerebral and myocardial oxygen sufficiency and circulatory parameters. Science 198, 1264–1267.

Jöbsis, F.F., O'Connor, M., Vitale, A., Vreman, H., 1971. Intracellular redox changes in functioning cerebral cortex. I. Metabolic effects of epileptiform activity. J. Neurophysiol. 34, 735–749.

Juhász, C., Chugani, D.C., Muzik, O., Chugani, H.T., 2005. Positron-Emission Tomography in Epilepsy, in: Jackson, G.D. (Ed.), Magnetic Resonance in Epilepsy (Second Edition). Academic Press, Burlington, pp. 395–411.

Jung, J., Bouet, R., Delpuech, C., Ryvlin, P., Isnard, J., Guenot, M., Bertrand, O., Hammers, A., Mauguière, F., 2013. The value of magnetoencephalography for seizure-onset zone localization in magnetic resonance imaging-negative partial epilepsy. Brain J. Neurol. 136, 3176–3186. doi:10.1093/brain/awt213

Kasischke, K.A., Lambert, E.M., Panepento, B., Sun, A., Gelbard, H.A., Burgess, R.W., Foster, T.H., Nedergaard, M., 2011. Two-photon NADH imaging exposes boundaries of oxygen diffusion in cortical vascular supply regions. J. Cereb. Blood Flow Metab. Off. J. Int. Soc. Cereb. Blood Flow Metab. 31, 68–81. doi:10.1038/jcbfm.2010.158

Kerr, J.N.D., Kock, C.P.J. de, Greenberg, D.S., Bruno, R.M., Sakmann, B., Helmchen, F., 2007. Spatial Organization of Neuronal Population Responses in Layer 2/3 of Rat Barrel Cortex. J. Neurosci. 27, 13316–13328. doi:10.1523/JNEUROSCI.2210-07.2007

Khan, B., Chand, P., Alexandrakis, G., 2011. Spatiotemporal relations of primary sensorimotor and secondary motor activation patterns mapped by NIR imaging. Biomed. Opt. Express 2, 3367–3386. doi:10.1364/BOE.2.003367

Killory, B.D., Bai, X., Negishi, M., Vega, C., Spann, M.N., Vestal, M., Guo, J., Berman, R., Danielson, N., Trejo, J., Shisler, D., Novotny, E.J., Constable, R.T., Blumenfeld, H., 2011. Impaired attention and network connectivity in childhood absence epilepsy. NeuroImage 56, 2209–2217. doi:10.1016/j.neuroimage.2011.03.036

Kim, K.H., Buehler, C., Bahlmann, K., Ragan, T., Lee, W.-C.A., Nedivi, E., Heffer, E.L., Fantini, S., So, P.T.C., 2007. Multifocal multiphoton microscopy based on multianode photomultiplier tubes. Opt. Express 15, 11658–11678.

Kim, S., Mountz, J.M., 2011. SPECT Imaging of Epilepsy: An Overview and Comparison with F-18 FDG PET. Int. J. Mol. Imaging 2011, e813028. doi:10.1155/2011/813028

Kim, Y.K., Lee, D.S., Lee, S.K., Chung, C.K., Chung, J.-K., Lee, M.C., 2002. (18)F-FDG PET in localization of frontal lobe epilepsy: comparison of visual and SPM analysis. J. Nucl. Med. Off. Publ. Soc. Nucl. Med. 43, 1167–1174.

Knowlton, R.C., Elgavish, R.A., Limdi, N., Bartolucci, A., Ojha, B., Blount, J., Burneo, J.G., Ver Hoef, L., Paige, L., Faught, E., Kankirawatana, P., Riley, K., Kuzniecky, R., 2008. Functional imaging: I. Relative predictive value of intracranial electroencephalography. Ann. Neurol. 64, 25–34. doi:10.1002/ana.21389

Knowlton, R.C., Elgavish, R., Howell, J., Blount, J., Burneo, J.G., Faught, E., Kankirawatana, P., Riley, K., Morawetz, R., Worthington, J., Kuzniecky, R.I., 2006. Magnetic source imaging

versus intracranial electroencephalogram in epilepsy surgery: a prospective study. Ann. Neurol. 59, 835–842. doi:10.1002/ana.20857

Knowlton, R.C., Laxer, K.D., Ende, G., Hawkins, R.A., Wong, S.T., Matson, G.B., Rowley, H.A., Fein, G., Weiner, M.W., 1997. Presurgical multimodality neuroimaging in electroencephalographic lateralized temporal lobe epilepsy. Ann. Neurol. 42, 829–837. doi:10.1002/ana.410420603

Kobat, D., Durst, M.E., Nishimura, N., Wong, A.W., Schaffer, C.B., Xu, C., 2009. Deep tissue multiphoton microscopy using longer wavelength excitation. Opt. Express 17, 13354–13364.

Kobayashi, E., Bagshaw, A.P., Bénar, C.-G., Aghakhani, Y., Andermann, F., Dubeau, F., Gotman, J., 2006a. Temporal and extratemporal BOLD responses to temporal lobe interictal spikes. Epilepsia 47, 343–354. doi:10.1111/j.1528-1167.2006.00427.x

Kobayashi, E., Bagshaw, A.P., Grova, C., Dubeau, F., Gotman, J., 2006b. Negative BOLD responses to epileptic spikes. Hum. Brain Mapp. 27, 488–497. doi:10.1002/hbm.20193

Koessler, L., Benar, C., Maillard, L., Badier, J.-M., Vignal, J.P., Bartolomei, F., Chauvel, P., Gavaret, M., 2010. Source localization of ictal epileptic activity investigated by high resolution EEG and validated by SEEG. NeuroImage 51, 642–653. doi:10.1016/j.neuroimage.2010.02.067

Kosslyn, S.M., 1999. If neuroimaging is the answer, what is the question? Philos. Trans. R. Soc. B Biol. Sci. 354, 1283–1294.

Kreisman, N.R., Magee, J.C., Brizzee, B.L., 1991. Relative hypoperfusion in rat cerebral cortex during recurrent seizures. J. Cereb. Blood Flow Metab. Off. J. Int. Soc. Cereb. Blood Flow Metab. 11, 77–87. doi:10.1038/jcbfm.1991.9

Kreisman, N.R., Rosenthal, M., LaManna, J.C., Sick, T.J., 1983. Cerebral oxygenation during recurrent seizures. Adv. Neurol. 34, 231–239.

Kreisman, N.R., Sick, T.J., Rosenthal, M., 1984. Concepts of brain oxygen sufficiency during seizures. Adv. Exp. Med. Biol. 180, 381–392.

Kretschmer, S., Pieper, M., Hüttmann, G., Bölke, T., Wollenberg, B., Marsh, L.M., Garn, H., König, P., 2016. Autofluorescence multiphoton microscopy for visualization of tissue

morphology and cellular dynamics in murine and human airways. Lab. Investig. J. Tech. Methods Pathol. 96, 918–931. doi:10.1038/labinvest.2016.69

Krogh, A., 1919. The number and distribution of capillaries in muscles with calculations of the oxygen pressure head necessary for supplying the tissue. J. Physiol. 52, 409–415.

Kuchibhotla, K.V., Lattarulo, C.R., Hyman, B.T., Bacskai, B.J., 2009. Synchronous Hyperactivity and Intercellular Calcium Waves in Astrocytes in Alzheimer Mice. Science 323, 1211–1215. doi:10.1126/science.1169096

Kwong, K.K., Belliveau, J.W., Chesler, D.A., Goldberg, I.E., Weisskoff, R.M., Poncelet, B.P., Kennedy, D.N., Hoppel, B.E., Cohen, M.S., Turner, R., 1992. Dynamic magnetic resonance imaging of human brain activity during primary sensory stimulation. Proc. Natl. Acad. Sci. 89, 5675–5679. doi:10.1073/pnas.89.12.5675

Lattarulo, C., Thyssen, D., Kuchibholta, K.V., Hyman, B.T., Bacskaiq, B.J., 2011. Microscopic imaging of intracellular calcium in live cells using lifetime-based ratiometric measurements of Oregon Green BAPTA-1. Methods Mol. Biol. Clifton NJ 793, 377–389. doi:10.1007/978-1-61779-328-8_25

Lauritzen, M., 2001. Relationship of spikes, synaptic activity, and local changes of cerebral blood flow. J. Cereb. Blood Flow Metab. Off. J. Int. Soc. Cereb. Blood Flow Metab. 21, 1367–1383. doi:10.1097/00004647-200112000-00001

Lauwers, F., Cassot, F., Lauwers-Cances, V., Puwanarajah, P., Duvernoy, H., 2008. Morphometry of the human cerebral cortex microcirculation: general characteristics and space-related profiles. NeuroImage 39, 936–948. doi:10.1016/j.neuroimage.2007.09.024

Lavy, S., Melamed, E., Portnoy, Z., Carmon, A., 1976. Interictal regional cerebral blood flow in patients with partial seizures. Neurology 26, 418–422.

Lebedev, A.Y., Cheprakov, A.V., Sakadzić, S., Boas, D.A., Wilson, D.F., Vinogradov, S.A., 2009. Dendritic phosphorescent probes for oxygen imaging in biological systems. ACS Appl. Mater. Interfaces 1, 1292–1304. doi:10.1021/am9001698

Lecoq, J., Parpaleix, A., Roussakis, E., Ducros, M., Houssen, Y.G., Vinogradov, S.A., Charpak, S., 2011. Simultaneous two-photon imaging of oxygen and blood flow in deep cerebral vessels. Nat. Med. 17, 893–898. doi:10.1038/nm.2394

Lecrux, C., Hamel, E., 2011. The neurovascular unit in brain function and disease. Acta Physiol. 203, 47–59. doi:10.1111/j.1748-1716.2011.02256.x

Lee, H.W., Hong, S.B., Tae, W.S., 2000. Opposite ictal perfusion patterns of subtracted SPECT. Hyperperfusion and hypoperfusion. Brain J. Neurol. 123 (Pt 10), 2150–2159.

Lee, S.K., Lee, S.-Y., Yun, C.-H., Lee, H.-Y., Lee, J.-S., Lee, D.-S., 2006. Ictal SPECT in neocortical epilepsies: clinical usefulness and factors affecting the pattern of hyperperfusion. Neuroradiology 48, 678–684. doi:10.1007/s00234-006-0106-z

Lemieux, L., Krakow, K., Fish, D.R., 2001. Comparison of spike-triggered functional MRI BOLD activation and EEG dipole model localization. NeuroImage 14, 1097–1104. doi:10.1006/nimg.2001.0896

Li, J., Mack, J.A., Souren, M., Yaksi, E., Higashijima, S., Mione, M., Fetcho, J.R., Friedrich, R.W., 2005. Early development of functional spatial maps in the zebrafish olfactory bulb. J. Neurosci. Off. J. Soc. Neurosci. 25, 5784–5795. doi:10.1523/JNEUROSCI.0922-05.2005

Lindvere, L., Dorr, A., Stefanovic, B., 2010. Two-photon fluorescence microscopy of cerebral hemodynamics. Cold Spring Harb. Protoc. 2010, pdb.prot5494.

Liu, H.L., Kochunov, P., Hou, J., Pu, Y., Mahankali, S., Feng, C.M., Yee, S.H., Wan, Y.L., Fox, P.T., Gao, J.H., 2001. Perfusion-weighted imaging of interictal hypoperfusion in temporal lobe epilepsy using FAIR-HASTE: comparison with H(2)(15)O PET measurements. Magn. Reson. Med. 45, 431–435.

Logothetis, N.K., Pauls, J., Augath, M., Trinath, T., Oeltermann, A., 2001. Neurophysiological investigation of the basis of the fMRI signal. Nature 412, 150–157. doi:10.1038/35084005

Logothetis, N.K., Wandell, B.A., 2004. Interpreting the BOLD signal. Annu. Rev. Physiol. 66, 735–769. doi:10.1146/annurev.physiol.66.082602.092845

Luo, C., Li, Q., Xia, Y., Lei, X., Xue, K., Yao, Z., Lai, Y., Martínez-Montes, E., Liao, W., Zhou, D., Valdes-Sosa, P.A., Gong, Q., Yao, D., 2012. Resting state basal ganglia network in idiopathic generalized epilepsy. Hum. Brain Mapp. 33, 1279–1294. doi:10.1002/hbm.21286

Malonek, D., Grinvald, A., 1996. Interactions between electrical activity and cortical microcirculation revealed by imaging spectroscopy: implications for functional brain mapping. Science 272, 551–554.

Mané, M., Müller, M., 2012. Temporo-Spectral Imaging of Intrinsic Optical Signals during Hypoxia-Induced Spreading Depression-Like Depolarization. PLOS ONE 7, e43981. doi:10.1371/journal.pone.0043981

Masamoto, K., Omura, T., Takizawa, N., Kobayashi, H., Katura, T., Maki, A., Kawaguchi, H., Tanishita, K., 2003. Biphasic changes in tissue partial pressure of oxygen closely related to localized neural activity in guinea pig auditory cortex. J. Cereb. Blood Flow Metab. Off. J. Int. Soc. Cereb. Blood Flow Metab. 23, 1075–1084. doi:10.1097/01.WCB.0000084248.20114.B3

Masters, B.R., So, P.T., Gratton, E., 1997. Multiphoton excitation fluorescence microscopy and spectroscopy of in vivo human skin. Biophys. J. 72, 2405–2412. doi:10.1016/S0006-3495(97)78886-6

Masterton, R.A., Carney, P.W., Jackson, G.D., 2012. Cortical and thalamic resting-state functional connectivity is altered in childhood absence epilepsy. Epilepsy Res. 99, 327–334. doi:10.1016/j.eplepsyres.2011.12.014

Mathiesen, C., Caesar, K., Lauritzen, M., 2000. Temporal coupling between neuronal activity and blood flow in rat cerebellar cortex as indicated by field potential analysis. J. Physiol. 523, 235–246. doi:10.1111/j.1469-7793.2000.t01-1-00235.x

Mayevsky, A., Chance, B., 1975. Metabolic responses of the awake cerebral cortex to anoxia hypoxia spreading depression and epileptiform activity. Brain Res. 98, 149–165.

Mayhew, J., Johnston, D., Berwick, J., Jones, M., Coffey, P., Zheng, Y., 2000. Spectroscopic analysis of neural activity in brain: increased oxygen consumption following activation of barrel cortex. NeuroImage 12, 664–675. doi:10.1006/nimg.2000.0656

McGonigal, A., Bartolomei, F., Régis, J., Guye, M., Gavaret, M., Trébuchon-Da Fonseca, A., Dufour, H., Figarella-Branger, D., Girard, N., Péragut, J.-C., Chauvel, P., 2007. Stereoelectroencephalography in presurgical assessment of MRI-negative epilepsy. Brain J. Neurol. 130, 3169–3183. doi:10.1093/brain/awm218

Meldrum, B.S., 2002. Concept of activity-induced cell death in epilepsy: historical and contemporary perspectives. Prog. Brain Res. 135, 3–11. doi:10.1016/S0079-6123(02)35003-9

Mesquita, R.C., Franceschini, M.A., Boas, D.A., 2010. Resting state functional connectivity of the whole head with near-infrared spectroscopy. Biomed. Opt. Express 1, 324–336. doi:10.1364/BOE.1.000324

Minsky, M., 1988. Memoir on inventing the confocal scanning microscope. Scanning 10, 128–138. doi:10.1002/sca.4950100403

Minsky, M., 1961. Microscopy apparatus. US3013467 A.

Mintun, M.A., Lundstrom, B.N., Snyder, A.Z., Vlassenko, A.G., Shulman, G.L., Raichle, M.E., 2001. Blood Flow and Oxygen Delivery to Human Brain during Functional Activity: Theoretical Modeling and Experimental Data. Proc. Natl. Acad. Sci. U. S. A. 98, 6859–6864.

Moeller, F., Tyvaert, L., Nguyen, D.K., LeVan, P., Bouthillier, A., Kobayashi, E., Tampieri, D., Dubeau, F., Gotman, J., 2009. EEG-fMRI: adding to standard evaluations of patients with nonlesional frontal lobe epilepsy. Neurology 73, 2023–2030. doi:10.1212/WNL.0b013e3181c55d17

Mrsic-Flogel, T.D., Hofer, S.B., Ohki, K., Reid, R.C., Bonhoeffer, T., Hübener, M., 2007. Homeostatic regulation of eye-specific responses in visual cortex during ocular dominance plasticity. Neuron 54, 961–972. doi:10.1016/j.neuron.2007.05.028

Mulligan, S.J., MacVicar, B.A., 2004. Calcium transients in astrocyte endfeet cause cerebrovascular constrictions. Nature 431, 195–199. doi:10.1038/nature02827

Nagata, K., Sato, M., Satoh, Y., Watahiki, Y., Kondoh, Y., Sugawara, M., Box, G., Wright, D., Leung, S., Yuya, H., Shimosegawa, E., 2002. Hemodynamic aspects of Alzheimer's disease. Ann. N. Y. Acad. Sci. 977, 391–402.

Nemoto, M., Sheth, S., Guiou, M., Pouratian, N., Chen, J.W.Y., Toga, A.W., 2004. Functional signal- and paradigm-dependent linear relationships between synaptic activity and hemodynamic responses in rat somatosensory cortex. J. Neurosci. Off. J. Soc. Neurosci. 24, 3850–3861. doi:10.1523/JNEUROSCI.4870-03.2004

Nemoto, T., Kawakami, R., Hibi, T., Iijima, K., Otomo, K., 2015. Two-photon excitation fluorescence microscopy and its application in functional connectomics. Microsc. Oxf. Engl. 64, 9–15. doi:10.1093/jmicro/dfu110

Nersesyan, H., Hyder, F., Rothman, D.L., Blumenfeld, H., 2004. Dynamic fMRI and EEG recordings during spike-wave seizures and generalized tonic-clonic seizures in WAG/Rij rats. J. Cereb. Blood Flow Metab. Off. J. Int. Soc. Cereb. Blood Flow Metab. 24, 589–599. doi:10.1097/01.WCB.0000117688.98763.23

Nguyen, D.K., Tremblay, J., Pouliot, P., Vannasing, P., Florea, O., Carmant, L., Lepore, F., Sawan, M., Lesage, F., Lassonde, M., 2013. Noninvasive continuous functional near-infrared spectroscopy combined with electroencephalography recording of frontal lobe seizures. Epilepsia 54, 331–340. doi:10.1111/epi.12011

Niell, C.M., Smith, S.J., 2005. Functional Imaging Reveals Rapid Development of Visual Response Properties in the Zebrafish Tectum. Neuron 45, 941–951. doi:10.1016/j.neuron.2005.01.047

Niels A. Lassen, R.G.B., 1989. Technetium-99m—d,l-HM-PAO, The Development of a New Class of 99mTc-Labeled Tracers: An Overview. J. Cereb. Blood Flow Metab. Off. J. Int. Soc. Cereb. Blood Flow Metab. 8, S1–3. doi:10.1038/jcbfm.1988.26

Nizar, K., Uhlirova, H., Tian, P., Saisan, P.A., Cheng, Q., Reznichenko, L., Weldy, K.L., Steed, T.C., Sridhar, V.B., MacDonald, C.L., Cui, J., Gratiy, S.L., Sakadzić, S., Boas, D.A., Beka, T.I., Einevoll, G.T., Chen, J., Masliah, E., Dale, A.M., Silva, G.A., Devor, A., 2013. In vivo stimulus-induced vasodilation occurs without IP3 receptor activation and may precede astrocytic calcium increase. J. Neurosci. Off. J. Soc. Neurosci. 33, 8411–8422. doi:10.1523/JNEUROSCI.3285-12.2013

Norup Nielsen, A., Lauritzen, M., 2001. Coupling and uncoupling of activity-dependent increases of neuronal activity and blood flow in rat somatosensory cortex. J. Physiol. 533, 773–785.

O'Brien, T.J., So, E.L., Cascino, G.D., Hauser, M.F., Marsh, W.R., Meyer, F.B., Sharbrough, F.W., Mullan, B.P., 2004. Subtraction SPECT coregistered to MRI in focal malformations of cortical development: localization of the epileptogenic zone in epilepsy surgery candidates. Epilepsia 45, 367–376. doi:10.1111/j.0013-9580.2004.54703.x

O'Brien, T.J., So, E.L., Mullan, B.P., Hauser, M.F., Brinkmann, B.H., Bohnen, N.I., Hanson, D., Cascino, G.D., Jack, C.R., Sharbrough, F.W., 1998. Subtraction ictal SPECT co-registered to MRI improves clinical usefulness of SPECT in localizing the surgical seizure focus. Neurology 50, 445–454.

Ogawa, S., Lee, T.M., Kay, A.R., Tank, D.W., 1990a. Brain magnetic resonance imaging with contrast dependent on blood oxygenation. Proc. Natl. Acad. Sci. 87, 9868–9872.

Ogawa, S., Lee, T.M., Nayak, A.S., Glynn, P., 1990b. Oxygenation-sensitive contrast in magnetic resonance image of rodent brain at high magnetic fields. Magn. Reson. Med. 14, 68–78.

Ohki, K., Chung, S., Ch'ng, Y.H., Kara, P., Reid, R.C., 2005. Functional imaging with cellular resolution reveals precise micro-architecture in visual cortex. Nature 433, 597–603. doi:10.1038/nature03274

Ohki, K., Chung, S., Kara, P., Hübener, M., Bonhoeffer, T., Reid, R.C., 2006. Highly ordered arrangement of single neurons in orientation pinwheels. Nature 442, 925–928. doi:10.1038/nature05019

Okunieff, P., Williams, J.P., Chen, Y., 2006. Oxygen Transport to Tissue XXVI. Springer Science & Business Media.

Oron, D., Tal, E., Silberberg, Y., 2005. Scanningless depth-resolved microscopy. Opt. Express 13, 1468–1476.

Osharina, V., Ponchel, E., Aarabi, A., Grebe, R., Wallois, F., 2010. Local haemodynamic changes preceding interictal spikes: a simultaneous electrocorticography (ECoG) and near-infrared spectroscopy (NIRS) analysis in rats. NeuroImage 50, 600–607. doi:10.1016/j.neuroimage.2010.01.009

Otsu, Y., Couchman, K., Lyons, D.G., Collot, M., Agarwal, A., Mallet, J.-M., Pfrieger, F.W., Bergles, D.E., Charpak, S., 2015. Calcium dynamics in astrocyte processes during neurovascular coupling. Nat. Neurosci. 18, 210–218. doi:10.1038/nn.3906

Paddock, S.W., 2000. Principles and practices of laser scanning confocal microscopy. Mol. Biotechnol. 16, 127–149. doi:10.1385/MB:16:2:127

Palikaras, K., Tavernarakis, N., 2001. Multiphoton Fluorescence Light Microscopy, in: eLS. John Wiley & Sons, Ltd.

Palmer, G.M., Fontanella, A.N., Zhang, G., Hanna, G., Fraser, C.L., Dewhirst, M.W., 2010. Optical imaging of tumor hypoxia dynamics. J. Biomed. Opt. 15, 066021. doi:10.1117/1.3523363

Papkovsky, D.B., Dmitriev, R.I., 2013. Biological detection by optical oxygen sensing. Chem. Soc. Rev. 42, 8700–8732. doi:10.1039/c3cs60131e

Papkovsky, D.B., O'Riordan, T.C., 2005. Emerging Applications of Phosphorescent Metalloporphyrins. J. Fluoresc. 15, 569–584. doi:10.1007/s10895-005-2830-x

Patil, S., Biassoni, L., Borgwardt, L., 2007. Nuclear medicine in pediatric neurology and neurosurgery: epilepsy and brain tumors. Semin. Nucl. Med. 37, 357–381. doi:10.1053/j.semnuclmed.2007.04.002

Pellegrino, G., Hedrich, T., Chowdhury, R., Hall, J.A., Lina, J.-M., Dubeau, F., Kobayashi, E., Grova, C., 2016. Source localization of the seizure onset zone from ictal EEG/MEG data. Hum. Brain Mapp. 37, 2528–2546. doi:10.1002/hbm.23191

Pérez Koldenkova, V., Nagai, T., 2013. Genetically encoded Ca(2+) indicators: properties and evaluation. Biochim. Biophys. Acta 1833, 1787–1797. doi:10.1016/j.bbamcr.2013.01.011

Perissinotti, A., Setoain, X., Aparicio, J., Rubí, S., Fuster, B.M., Donaire, A., Carreño, M., Bargalló, N., Rumiá, J., Garcia-Fructuoso, G., Mayoral, M., Sanmartí, F., Pons, F., 2014. Clinical Role of Subtraction Ictal SPECT Coregistered to MR Imaging and (18)F-FDG PET in Pediatric Epilepsy. J. Nucl. Med. Off. Publ. Soc. Nucl. Med. 55, 1099–1105. doi:10.2967/jnumed.113.136432

Pinard, E., Tremblay, E., Ben-Ari, Y., Seylaz, J., 1984. Blood flow compensates oxygen demand in the vulnerable ca3 region of the hippocampus during kainate-induced seizures. Neuroscience 13, 1039–1049. doi:10.1016/0306-4522(84)90287-2

Plant, R.L., Burns, D.H., 1993. Quantitative, Depth-Resolved Imaging of Oxygen Concentration by Phosphorescence Lifetime Measurement. Appl. Spectrosc. 47, 1594–1599.

Plum, F., Posner, J.B., Troy, B., 1968. Cerebral metabolic and circulatory responses to induced convulsions in animals. Arch. Neurol. 18, 1–13.

Pouliot, P., Tremblay, J., Robert, M., Vannasing, P., Lepore, F., Lassonde, M., Sawan, M., Nguyen, D.K., Lesage, F., 2012a. Nonlinear hemodynamic responses in human epilepsy: a multimodal analysis with fNIRS-EEG and fMRI-EEG. J. Neurosci. Methods 204, 326–340. doi:10.1016/j.jneumeth.2011.11.016

Pouliot, P., Truong, V.T., Zhang, C., Dubeau, S., Lesage, F., 2012b. Tight neurovascular coupling in a rat model of quasi-periodic interictal spiking using multispectral optical imaging. pp. 841203–841203–6. doi:10.1117/12.2000717

Prakash, N., Uhleman, F., Sheth, S.A., Bookheimer, S., Martin, N., Toga, A.W., 2009. Current Trends in Intraoperative Optical Imaging for Functional Brain Mapping and Delineation of Lesions of Language Cortex. NeuroImage 47, T116–T126. doi:10.1016/j.neuroimage.2008.07.066

Prasad, V., Semwogerere, D., Weeks, E.R., 2007. Confocal microscopy of colloids. J. Phys. Condens. Matter 19, 113102. doi:10.1088/0953-8984/19/11/113102

Prvulovich, E.M., Bomanji, J.B., 1998. The role of nuclear medicine in clinical investigation. BMJ 316, 1140–1146.

Quaranta, M., Borisov, S.M., Klimant, I., 2012. Indicators for optical oxygen sensors. Bioanal. Rev. 4, 115–157. doi:10.1007/s12566-012-0032-y

Rajadhyaksha, M., González, S., Zavislan, J.M., Anderson, R.R., Webb, R.H., 1999. In vivo confocal scanning laser microscopy of human skin II: advances in instrumentation and comparison with histology. J. Invest. Dermatol. 113, 293–303. doi:10.1046/j.1523-1747.1999.00690.x

Rajadhyaksha, M., Grossman, M., Esterowitz, D., Webb, R.H., Anderson, R.R., 1995. In vivo confocal scanning laser microscopy of human skin: melanin provides strong contrast. J. Invest. Dermatol. 104, 946–952.

Rasmussen, T., 1991. Tailoring of cortical excisions for frontal lobe epilepsy. Can. J. Neurol. Sci. J. Can. Sci. Neurol. 18, 606–610.

Rathakrishnan, R., Moeller, F., Levan, P., Dubeau, F., Gotman, J., 2010. BOLD signal changes preceding negative responses in EEG-fMRI in patients with focal epilepsy. Epilepsia 51, 1837–1845. doi:10.1111/j.1528-1167.2010.02643.x

Riegler, M., Castagliuolo, I., So, P.T., Lotz, M., Wang, C., Wlk, M., Sogukoglu, T., Cosentini, E., Bischof, G., Hamilton, G., Teleky, B., Wenzl, E., Matthews, J.B., Pothoulakis, C., 1999. Effects of substance P on human colonic mucosa in vitro. Am. J. Physiol. 276, G1473–1483.

Rizki, E.E., Uga, M., Dan, I., Dan, H., Tsuzuki, D., Yokota, H., Oguro, K., Watanabe, E., 2015. Determination of epileptic focus side in mesial temporal lobe epilepsy using long-term noninvasive fNIRS/EEG monitoring for presurgical evaluation. Neurophotonics 2, 025003–025003. doi:10.1117/1.NPh.2.2.025003

Rochefort, N.L., Konnerth, A., 2012. Dendritic spines: from structure to in vivo function. EMBO Rep. 13, 699–708. doi:10.1038/embor.2012.102

Roche-Labarbe, N., Zaaimi, B., Berquin, P., Nehlig, A., Grebe, R., Wallois, F., 2008. NIRS-measured oxy- and deoxyhemoglobin changes associated with EEG spike-and-wave discharges in children. Epilepsia 49, 1871–1880. doi:10.1111/j.1528-1167.2008.01711.x

Rowe, C.C., Berkovic, S.F., Austin, M.C., McKay, W.J., Bladin, P.F., 1991. Patterns of postictal cerebral blood flow in temporal lobe epilepsy: qualitative and quantitative analysis. Neurology 41, 1096–1103.

Roy, C.S., Sherrington, C.S., 1890. On the Regulation of the Blood-supply of the Brain. J. Physiol. 11, 85–158.17.

Rubart, M., 2004. Two-Photon Microscopy of Cells and Tissue. Circ. Res. 95, 1154–1166. doi:10.1161/01.RES.0000150593.30324.42

Rudd, N.C., Cannan, S., Bitziou, E., Ciani, I., Whitworth, A.L., Unwin, P.R., 2005. Fluorescence confocal laser scanning microscopy as a probe of pH gradients in electrode reactions and surface activity. Anal. Chem. 77, 6205–6217. doi:10.1021/ac050800y

Rumsey, W.L., Vanderkooi, J.M., Wilson, D.F., 1988. Imaging of phosphorescence: a novel method for measuring oxygen distribution in perfused tissue. Science 241, 1649–1651.

Russell, J.T., 2011. Imaging calcium signals in vivo: a powerful tool in physiology and pharmacology. Br. J. Pharmacol. 163, 1605–1625. doi:10.1111/j.1476-5381.2010.00988.x

Sakadžić, S., Mandeville, E.T., Gagnon, L., Musacchia, J.J., Yaseen, M.A., Yucel, M.A., Lefebvre, J., Lesage, F., Dale, A.M., Eikermann-Haerter, K., Ayata, C., Srinivasan, V.J., Lo, E.H., Devor, A., Boas, D.A., 2014. Large arteriolar component of oxygen delivery implies a safe margin of oxygen supply to cerebral tissue. Nat. Commun. 5, 5734. doi:10.1038/ncomms6734

Sakadzić, S., Roussakis, E., Yaseen, M.A., Mandeville, E.T., Srinivasan, V.J., Arai, K., Ruvinskaya, S., Devor, A., Lo, E.H., Vinogradov, S.A., Boas, D.A., 2010. Two-photon high-resolution measurement of partial pressure of oxygen in cerebral vasculature and tissue. Nat. Methods 7, 755–759. doi:10.1038/nmeth.1490

Sakadžić, S., Yuan, S., Dilekoz, E., Ruvinskaya, S., Vinogradov, S.A., Ayata, C., Boas, D.A., 2009. Simultaneous imaging of cerebral partial pressure of oxygen and blood flow during functional activation and cortical spreading depression. Appl. Opt. 48, D169. doi:10.1364/AO.48.00D169

Salomé, R., Kremer, Y., Dieudonné, S., Léger, J.-F., Krichevsky, O., Wyart, C., Chatenay, D., Bourdieu, L., 2006. Ultrafast random-access scanning in two-photon microscopy using acousto-optic deflectors. J. Neurosci. Methods 154, 161–174. doi:10.1016/j.jneumeth.2005.12.010

Sarikaya, I., 2015. PET studies in epilepsy. Am. J. Nucl. Med. Mol. Imaging 5, 416–430.

Sato, K., Nariai, T., Sasaki, S., Yazawa, I., Mochida, H., Miyakawa, N., Momose-Sato, Y., Kamino, K., Ohta, Y., Hirakawa, K., Ohno, K., 2002. Intraoperative intrinsic optical imaging of neuronal activity from subdivisions of the human primary somatosensory cortex. Cereb. Cortex N. Y. N 1991 12, 269–280.

Sato, T.R., Gray, N.W., Mainen, Z.F., Svoboda, K., 2007. The Functional Microarchitecture of the Mouse Barrel Cortex. PLOS Biol 5, e189. doi:10.1371/journal.pbio.0050189

Schridde, U., Khubchandani, M., Motelow, J.E., Sanganahalli, B.G., Hyder, F., Blumenfeld, H., 2008. Negative BOLD with large increases in neuronal activity. Cereb. Cortex N. Y. N 1991 18, 1814–1827. doi:10.1093/cercor/bhm208

Schulz, K., Sydekum, E., Krueppel, R., Engelbrecht, C.J., Schlegel, F., Schröter, A., Rudin, M., Helmchen, F., 2012. Simultaneous BOLD fMRI and fiber-optic calcium recording in rat neocortex. Nat. Methods 9, 597–602. doi:10.1038/nmeth.2013

Schummers, J., Yu, H., Sur, M., 2008. Tuned responses of astrocytes and their influence on hemodynamic signals in the visual cortex. Science 320, 1638–1643. doi:10.1126/science.1156120

Schwartz, T.H., 2005. The application of optical recording of intrinsic signals to simultaneously acquire functional, pathological and localizing information and its potential role in neurosurgery. Stereotact. Funct. Neurosurg. 83, 36–44. doi:10.1159/000085025

Schwartz, T.H., 2003. Optical imaging of epileptiform events in visual cortex in response to patterned photic stimulation. Cereb. Cortex N. Y. N 1991 13, 1287–1298.

Schwartz, T.H., Bonhoeffer, T., 2001. In vivo optical mapping of epileptic foci and surround inhibition in ferret cerebral cortex. Nat. Med. 7, 1063–1067. doi:10.1038/nm0901-1063

Schwartz, T.H., Chen, L.M., Friedman, R.M., Spencer, D.D., Roe, A.W., 2004. Intraoperative optical imaging of human face cortical topography: a case study. Neuroreport 15, 1527–1531.

Secomb, T.W., Hsu, R., Beamer, N.B., Coull, B.M., 2000. Theoretical simulation of oxygen transport to brain by networks of microvessels: effects of oxygen supply and demand on tissue hypoxia. Microcirc. N. Y. N 1994 7, 237–247.

Seyal, M., 2014. Frontal hemodynamic changes precede EEG onset of temporal lobe seizures. Clin. Neurophysiol. Off. J. Int. Fed. Clin. Neurophysiol. 125, 442–448. doi:10.1016/j.clinph.2013.09.003

Shain, W., Connor, J.A., Madelian, V., Martin, D.L., 1989. Spontaneous and beta-adrenergic receptor-mediated taurine release from astroglial cells are independent of manipulations of intracellular calcium. J. Neurosci. Off. J. Soc. Neurosci. 9, 2306–2312.

Sharan, M., Vovenko, E.P., Vadapalli, A., Popel, A.S., Pittman, R.N., 2008. Experimental and theoretical studies of oxygen gradients in rat pial microvessels. J. Cereb. Blood Flow Metab. Off. J. Int. Soc. Cereb. Blood Flow Metab. 28, 1597–1604. doi:10.1038/jcbfm.2008.51

Shariff, S., Suh, M., Zhao, M., Ma, H., Schwartz, T.H., 2006. Recent developments in oximetry and perfusion-based mapping techniques and their role in the surgical treatment of neocortical epilepsy. Epilepsy Behav. 8, 363–375. doi:10.1016/j.yebeh.2005.11.006

Sheth, S.A., Nemoto, M., Guiou, M., Walker, M., Pouratian, N., Hageman, N., Toga, A.W., 2004a. Columnar specificity of microvascular oxygenation and volume responses: implications for functional brain mapping. J. Neurosci. Off. J. Soc. Neurosci. 24, 634–641. doi:10.1523/JNEUROSCI.4526-03.2004

Sheth, S.A., Nemoto, M., Guiou, M., Walker, M., Pouratian, N., Toga, A.W., 2004b. Linear and Nonlinear Relationships between Neuronal Activity, Oxygen Metabolism, and Hemodynamic Responses. Neuron 42, 347–355. doi:10.1016/S0896-6273(04)00221-1

Shih, A.Y., Driscoll, J.D., Drew, P.J., Nishimura, N., Schaffer, C.B., Kleinfeld, D., 2012. Two-photon microscopy as a tool to study blood flow and neurovascular coupling in the rodent brain. J. Cereb. Blood Flow Metab. Off. J. Int. Soc. Cereb. Blood Flow Metab. 32, 1277–1309. doi:10.1038/jcbfm.2011.196

Shonat, R.D., Kight, A.C., 2003. Oxygen Tension Imaging in the Mouse Retina. Ann. Biomed. Eng. 31, 1084–1096. doi:10.1114/1.1603256

Shonat, R.D., Wachman, E.S., Niu, W., Koretsky, A.P., Farkas, D.L., 1997. Near-simultaneous hemoglobin saturation and oxygen tension maps in mouse brain using an AOTF microscope. Biophys. J. 73, 1223–1231. doi:10.1016/S0006-3495(97)78155-4

Sierra-Marcos, A., Carreño, M., Setoain, X., López-Rueda, A., Aparicio, J., Donaire, A., Bargalló, N., 2016. Accuracy of arterial spin labeling magnetic resonance imaging (MRI) perfusion in detecting the epileptogenic zone in patients with drug-resistant neocortical epilepsy: comparison with electrophysiological data, structural MRI, SISCOM and FDG-PET. Eur. J. Neurol. 23, 160–167. doi:10.1111/ene.12826

Siesjö, B.K., Plum, F., 1971. Cerebral energy metabolism in normoxia and in hypoxia. Acta Anaesthesiol. Scand. Suppl. 45, 81–101.

Siesjö, B.K., Wieloch, T., 1986. Epileptic brain damage: pathophysiology and neurochemical pathology. Adv. Neurol. 44, 813–847.

Simon, R.P., 1985. Physiologic consequences of status epilepticus. Epilepsia 26 Suppl 1, S58–66.

Slone, E., Westwood, E., Dhaliwal, H., Federico, P., Dunn, J.F., 2012. Near-infrared spectroscopy shows preictal haemodynamic changes in temporal lobe epilepsy. Epileptic Disord. Int. Epilepsy J. Videotape 14, 371–378. doi:10.1684/epd.2012.0535

Smith, L.M., Golub, A.S., Pittman, R.N., 2002. Interstitial PO(2) determination by phosphorescence quenching microscopy. Microcirc. N. Y. N 1994 9, 389–395. doi:10.1038/sj.mn.7800147

So, E.L., O'Brien, T.J., 2012. Peri-ictal single-photon emission computed tomography: principles and applications in epilepsy evaluation. Handb. Clin. Neurol. 107, 425–436. doi:10.1016/B978-0-444-52898-8.00027-6

Sokoloff, M.D., Plegue, M.A., Chervin, R.D., Barks, J.D.E., Shellhaas, R.A., 2015. Phenobarbital and neonatal seizures affect cerebral oxygen metabolism: a near-infrared spectroscopy study. Pediatr. Res. 78, 91–96. doi:10.1038/pr.2015.64

So, P.T., Dong, C.Y., Masters, B.R., Berland, K.M., 2000. Two-photon excitation fluorescence microscopy. Annu. Rev. Biomed. Eng. 2, 399–429. doi:10.1146/annurev.bioeng.2.1.399

Spencer, S.S., 1994. The relative contributions of MRI, SPECT, and PET imaging in epilepsy. Epilepsia 35 Suppl 6, S72–89.

Steinhoff, B.J., Herrendorf, G., Kurth, C., 1996. Ictal near infrared spectroscopy in temporal lobe epilepsy: a pilot study. Seizure 5, 97–101.

Stern, J.M., 2006. Simultaneous electroencephalography and functional magnetic resonance imaging applied to epilepsy. Epilepsy Behav. EB 8, 683–692. doi:10.1016/j.yebeh.2006.03.002

Strangman, G., Culver, J.P., Thompson, J.H., Boas, D.A., 2002. A quantitative comparison of simultaneous BOLD fMRI and NIRS recordings during functional brain activation. NeuroImage 17, 719–731.

Straub, S.V., Bonev, A.D., Wilkerson, M.K., Nelson, M.T., 2006. Dynamic inositol trisphosphate-mediated calcium signals within astrocytic endfeet underlie vasodilation of cerebral arterioles. J. Gen. Physiol. 128, 659–669. doi:10.1085/jgp.200609650

Suh, M., Bahar, S., Mehta, A.D., Schwartz, T.H., 2005. Temporal dependence in uncoupling of blood volume and oxygenation during interictal epileptiform events in rat neocortex. J. Neurosci. Off. J. Soc. Neurosci. 25, 68–77. doi:10.1523/JNEUROSCI.2823-04.2005

Sullivan, M.R., Nimmerjahn, A., Sarkisov, D.V., Helmchen, F., Wang, S.S.-H., 2005. In vivo calcium imaging of circuit activity in cerebellar cortex. J. Neurophysiol. 94, 1636–1644. doi:10.1152/jn.01013.2004

Svoboda, K., Denk, W., Kleinfeld, D., Tank, D.W., 1997. In vivo dendritic calcium dynamics in neocortical pyramidal neurons. Nature 385, 161–165. doi:10.1038/385161a0

Svoboda, K., Yasuda, R., 2006. Principles of Two-Photon Excitation Microscopy and Its Applications to Neuroscience. Neuron 50, 823–839. doi:10.1016/j.neuron.2006.05.019

Takano, T., Tian, G.-F., Peng, W., Lou, N., Libionka, W., Han, X., Nedergaard, M., 2006. Astrocyte-mediated control of cerebral blood flow. Nat. Neurosci. 9, 260–267. doi:10.1038/nn1623

Takasaki, K., Sabatini, B.L., 2014. Super-resolution 2-photon microscopy reveals that the morphology of each dendritic spine correlates with diffusive but not synaptic properties. Front. Neuroanat. 8, 29. doi:10.3389/fnana.2014.00029

Tanaka, S., Sako, K., Tanaka, T., Nishihara, I., Yonemasu, Y., 1990. Uncoupling of local blood flow and metabolism in the hippocampal CA3 in kainic acid-induced limbic seizure status. Neuroscience 36, 339–348.

Tarkin, J.M., Joshi, F.R., Rudd, J.H.F., 2014. PET imaging of inflammation in atherosclerosis. Nat. Rev. Cardiol. 11, 443–457. doi:10.1038/nrcardio.2014.80

Tenney, J.R., Duong, T.Q., King, J.A., Ferris, C.F., 2004. fMRI of Brain Activation in a Genetic Rat Model of Absence Seizures. Epilepsia 45, 576–582. doi:10.1111/j.0013-9580.2004.39303.x

Thompson, J.K., Peterson, M.R., Freeman, R.D., 2003. Single-neuron activity and tissue oxygenation in the cerebral cortex. Science 299, 1070–1072. doi:10.1126/science.1079220

Thornton, R., Laufs, H., Rodionov, R., Cannadathu, S., Carmichael, D.W., Vulliemoz, S., Salek-Haddadi, A., McEvoy, A.W., Smith, S.M., Lhatoo, S., Elwes, R.D.C., Guye, M., Walker,

M.C., Lemieux, L., Duncan, J.S., 2010. EEG correlated functional MRI and postoperative outcome in focal epilepsy. J. Neurol. Neurosurg. Psychiatry 81, 922–927. doi:10.1136/jnnp.2009.196253

Tokiwa, T., Inoue, T., Fujii, M., Ishizuka, S., Aou, S., Kida, H., Maruta, Y., Yamakawa, T., Nomura, S., Suzuki, M., Yamakawa, T., 2013. Penicillin-induced epileptiform activity elevates focal brain temperature in anesthetized rats. Neurosci. Res. 76, 257–260. doi:10.1016/j.neures.2013.05.001

Torres Filho, I.P., Leunig, M., Yuan, F., Intaglietta, M., Jain, R.K., 1994. Noninvasive measurement of microvascular and interstitial oxygen profiles in a human tumor in SCID mice. Proc. Natl. Acad. Sci. U. S. A. 91, 2081–2085.

Truccolo, W., Donoghue, J.A., Hochberg, L.R., Eskandar, E.N., Madsen, J.R., Anderson, W.S., Brown, E.N., Halgren, E., Cash, S.S., 2011. Single-neuron dynamics in human focal epilepsy. Nat. Neurosci. 14, 635–641. doi:10.1038/nn.2782

Vanderkooi, J.M., Maniara, G., Green, T.J., Wilson, D.F., 1987. An optical method for measurement of dioxygen concentration based upon quenching of phosphorescence. J. Biol. Chem. 262, 5476–5482.

Vazquez, A.L., Fukuda, M., Kim, S.-G., 2012. Evolution of the dynamic changes in functional cerebral oxidative metabolism from tissue mitochondria to blood oxygen. J. Cereb. Blood Flow Metab. Off. J. Int. Soc. Cereb. Blood Flow Metab. 32, 745–758. doi:10.1038/jcbfm.2011.198

Villringer, A., Planck, J., Stodieck, S., Bötzel, K., Schleinkofer, L., Dirnagl, U., 1994. Noninvasive Assessment of Cerebral Hemodynamics and Tissue Oxygenation during Activation of Brain Cell Function in Human Adults Using Near Infrared Spectroscopy, in: Vaupel, P., Zander, R., Bruley, D.F. (Eds.), Oxygen Transport to Tissue XV, Advances in Experimental Medicine and Biology. Springer US, pp. 559–565.

Vinogradov, S.A., Ceroni, P., Puntoriero, F., 2011. Porphyrin dendrimers as biological oxygen sensors. John Wiley & Sons.

Vulliemoz, S., Lemieux, L., Daunizeau, J., Michel, C.M., Duncan, J.S., 2010. The combination of EEG source imaging and EEG-correlated functional MRI to map epileptic networks. Epilepsia 51, 491–505. doi:10.1111/j.1528-1167.2009.02342.x

Wachowiak, M., Denk, W., Friedrich, R.W., 2004. Functional organization of sensory input to the olfactory bulb glomerulus analyzed by two-photon calcium imaging. Proc. Natl. Acad. Sci. U. S. A. 101, 9097–9102. doi:10.1073/pnas.0400438101

Wallois, F., Patil, A., Héberlé, C., Grebe, R., 2010. EEG-NIRS in epilepsy in children and neonates. Neurophysiol. Clin. Clin. Neurophysiol. 40, 281–292. doi:10.1016/j.neucli.2010.08.004

Walovitch, R.C., Hill, T.C., Garrity, S.T., Cheesman, E.H., Burgess, B.A., O'Leary, D.H., Watson, A.D., Ganey, M.V., Morgan, R.A., Williams, S.J., 1989. Characterization of technetium-99m-L,L-ECD for brain perfusion imaging, Part 1: Pharmacology of technetium-99m ECD in nonhuman primates. J. Nucl. Med. Off. Publ. Soc. Nucl. Med. 30, 1892–1901.

Wang, B., Xiao, J., Jiang, H., 2014. Simultaneous real-time 3D photoacoustic tomography and EEG for neurovascular coupling study in an animal model of epilepsy. J. Neural Eng. 11, 046013. doi:10.1088/1741-2560/11/4/046013

Wang, X., Lou, N., Xu, Q., Tian, G.-F., Peng, W.G., Han, X., Kang, J., Takano, T., Nedergaard, M., 2006. Astrocytic Ca2+ signaling evoked by sensory stimulation in vivo. Nat. Neurosci. 9, 816–823. doi:10.1038/nn1703

Wang, Z., Zhang, Z., Jiao, Q., Liao, W., Chen, G., Sun, K., Shen, L., Wang, M., Li, K., Liu, Y., Lu, G., 2012. Impairments of Thalamic Nuclei in Idiopathic Generalized Epilepsy Revealed by a Study Combining Morphological and Functional Connectivity MRI. PLOS ONE 7, e39701. doi:10.1371/journal.pone.0039701

Watanabe, E., Nagahori, Y., Mayanagi, Y., 2002. Focus diagnosis of epilepsy using near-infrared spectroscopy. Epilepsia 43 Suppl 9, 50–55.

Wichert-Ana, L., de Azevedo-Marques, P.M., Oliveira, L.F., Fernandes, R.M.F., Velasco, T.R., Santos, A.C., Araújo, D., Kato, M., Bianchin, M.M., Sakamoto, A.C., 2008. Ictal technetium-99 m ethyl cysteinate dimer single-photon emission tomographic findings in

epileptic patients with polymicrogyria syndromes: a subtraction of ictal-interictal SPECT coregistered to MRI study. Eur. J. Nucl. Med. Mol. Imaging 35, 1159–1170. doi:10.1007/s00259-007-0655-3

Williams, R.M., Piston, D.W., Webb, W.W., 1994. Two-photon molecular excitation provides intrinsic 3-dimensional resolution for laser-based microscopy and microphotochemistry. FASEB J. Off. Publ. Fed. Am. Soc. Exp. Biol. 8, 804–813.

Wilms, C.D., Eilers, J., 2007. Photo-physical properties of Ca2+-indicator dyes suitable for two-photon fluorescence-lifetime recordings. J. Microsc. 225, 209–213. doi:10.1111/j.1365-2818.2007.01746.x

Wilms, C.D., Schmidt, H., Eilers, J., 2006. Quantitative two-photon Ca2+ imaging via fluorescence lifetime analysis. Cell Calcium 40, 73–79. doi:10.1016/j.ceca.2006.03.006

Wilson, D.F., 1992. Oxygen dependent quenching of phosphorescence: a perspective. Adv. Exp. Med. Biol. 317, 195–201.

Wilson, D.F., Vinogradov, S.A., Grosul, P., Vaccarezza, M.N., Kuroki, A., Bennett, J., 2005. Oxygen distribution and vascular injury in the mouse eye measured by phosphorescence-lifetime imaging. Appl. Opt. 44, 5239–5248.

Wilt, B.A., Burns, L.D., Ho, E.T.W., Ghosh, K.K., Mukamel, E.A., Schnitzer, M.J., 2009. Advances in Light Microscopy for Neuroscience. Annu. Rev. Neurosci. 32, 435. doi:10.1146/annurev.neuro.051508.135540

Won, H.J., Chang, K.H., Cheon, J.E., Kim, H.D., Lee, D.S., Han, M.H., Kim, I.O., Lee, S.K., Chung, C.K., 1999. Comparison of MR imaging with PET and ictal SPECT in 118 patients with intractable epilepsy. AJNR Am. J. Neuroradiol. 20, 593–599.

Yaksi, E., Judkewitz, B., Friedrich, R.W., 2007. Topological reorganization of odor representations in the olfactory bulb. PLoS Biol. 5, e178. doi:10.1371/journal.pbio.0050178

Yang, X.-F., Schmidt, B.F., Rode, D.L., Rothman, S.M., 2010. Optical suppression of experimental seizures in rat brain slices. Epilepsia 51, 127–135. doi:10.1111/j.1528-1167.2009.02252.x

Yaroslavsky, A.N., Schulze, P.C., Yaroslavsky, I.V., Schober, R., Ulrich, F., Schwarzmaier, H.J., 2002. Optical properties of selected native and coagulated human brain tissues in vitro in the visible and near infrared spectral range. Phys. Med. Biol. 47, 2059–2073.

Yaseen, M.A., Srinivasan, V.J., Sakadzić, S., Wu, W., Ruvinskaya, S., Vinogradov, S.A., Boas, D.A., 2009. Optical monitoring of oxygen tension in cortical microvessels with confocal microscopy. Opt. Express 17, 22341–22350.

Zeng, H., Pizarro, R., Nair, V.A., La, C., Prabhakaran, V., 2013. Alterations in regional homogeneity of resting-state brain activity in mesial temporal lobe epilepsy. Epilepsia 54, 658–666. doi:10.1111/epi.12066

Zepeda, A., Arias, C., Sengpiel, F., 2004. Optical imaging of intrinsic signals: recent developments in the methodology and its applications. J. Neurosci. Methods 136, 1–21. doi:10.1016/j.jneumeth.2004.02.025

Zhang, C., Bélanger, S., Pouliot, P., Lesage, F., 2015a. Measurement of Local Partial Pressure of Oxygen in the Brain Tissue under Normoxia and Epilepsy with Phosphorescence Lifetime Microscopy. PLoS ONE 10, e0135536. doi:10.1371/journal.pone.0135536

Zhang, C., Bélanger, S., Pouliot, P., Lesage, F., 2015b. Measurement of Local Partial Pressure of Oxygen in the Brain Tissue under Normoxia and Epilepsy with Phosphorescence Lifetime Microscopy. PLoS ONE 10, e0135536. doi:10.1371/journal.pone.0135536

Zhang, C., Moeini, M., Lesage, F., 2017. Spatial landscape of oxygen in and around microvasculature during epileptic events. Neurophotonics 4, 010501–010501. doi:10.1117/1.NPh.4.1.010501

Zhang, X., Toronov, V.Y., Fabiani, M., Gratton, G., Webb, A.G., 2005. The study of cerebral hemodynamic and neuronal response to visual stimulation using simultaneous NIR optical tomography and BOLD fMRI in humans. Proc. SPIE-- Int. Soc. Opt. Eng. 5686, 566–572. doi:10.1117/12.593435

Zhao, M., Ma, H., Suh, M., Schwartz, T.H., 2009. Spatiotemporal dynamics of perfusion and oximetry during ictal discharges in the rat neocortex. J. Neurosci. Off. J. Soc. Neurosci. 29, 2814–2823. doi:10.1523/JNEUROSCI.4667-08.2009

Zhao, M., Nguyen, J., Ma, H., Nishimura, N., Schaffer, C.B., Schwartz, T.H., 2011. Preictal and ictal neurovascular and metabolic coupling surrounding a seizure focus. J. Neurosci. Off. J. Soc. Neurosci. 31, 13292–13300. doi:10.1523/JNEUROSCI.2597-11.2011

Zhao, M., Suh, M., Ma, H., Perry, C., Geneslaw, A., Schwartz, T.H., 2007. Focal increases in perfusion and decreases in hemoglobin oxygenation precede seizure onset in spontaneous human epilepsy. Epilepsia 48, 2059–2067. doi:10.1111/j.1528-1167.2007.01229.x

Zheng, K., Bard, L., Reynolds, J.P., King, C., Jensen, T.P., Gourine, A.V., Rusakov, D.A., 2015. Time-Resolved Imaging Reveals Heterogeneous Landscapes of Nanomolar Ca2+ in Neurons and Astroglia. Neuron 88, 277–288. doi:10.1016/j.neuron.2015.09.043

Zheng, Y., Martindale, J., Johnston, D., Jones, M., Berwick, J., Mayhew, J., 2002. A model of the hemodynamic response and oxygen delivery to brain. NeuroImage 16, 617–637.

Zijlmans, M., Huiskamp, G., Hersevoort, M., Seppenwoolde, J.-H., van Huffelen, A.C., Leijten, F.S.S., 2007. EEG-fMRI in the preoperative work-up for epilepsy surgery. Brain J. Neurol. 130, 2343–2353. doi:10.1093/brain/awm141

Zipfel, W.R., Williams, R.M., Webb, W.W., 2003. Nonlinear magic: multiphoton microscopy in the biosciences. Nat. Biotechnol. 21, 1369–1377. doi:10.1038/nbt899

Zonta, M., Angulo, M.C., Gobbo, S., Rosengarten, B., Hossmann, K.-A., Pozzan, T., Carmignoto, G., 2003. Neuron-to-astrocyte signaling is central to the dynamic control of brain microcirculation. Nat. Neurosci. 6, 43–50. doi:10.1038/nn980

Zubal, I.G., Spencer, S.S., Imam, K., Seibyl, J., Smith, E.O., Wisniewski, G., Hoffer, P.B., 1995. Difference images calculated from ictal and interictal technetium-99m-HMPAO SPECT scans of epilepsy. J. Nucl. Med. Off. Publ. Soc. Nucl. Med. 36, 684–689.